UiT The Arctic University of Norway

Faculty of Health Sciences
Department of Medical Biology

ATAD3 proteins in autophagy

Do ATAD3 proteins have a direct role in regulating autophagy

Nelsy Efundem Taboko

MBI3911: Masters thesis in Biomedicine, May 2020

Table of Contents

Abstract

ATPase Family AAA Domain -containing protein 3 (ATAD3) is a nuclear-encoded mitochondrial transmembrane protein encompassing three isoforms; ATAD3A, ATAD3B and ATAD3C. ATAD3 is involved in several cellular process and available data predict that ATAD3A and ATAD3B proteins may have potential roles in regulating autophagy and mitophagy. Preliminary data from our research group identified interactions between ATAD3A and ATAD3B with ATG8 proteins, p62, NDP52 and CALCOCO1. However, whether these interactions play any role in autophagy is not known. This study sought to characterise these interactions and evaluate their roles in autophagy or mitophagy. *In vitro* GST pulldown analysis together with autoradiography were used to probe the interaction between ATAD3 proteins and some autophagy-related proteins including LC3B, GABARAP, p62, NDP52 and CALCOCO1. Western blot analysis was employed to evaluate ATAD3A levels following starvation-induced autophagy, while immunostaining and confocal microscopy were used to assess ATAD3 colocalization with p62 and LC3B. Results showed that interaction between ATAD3 and LC3B and GABARAP is not mediated by a LIR motif. Instead, the interaction is dependent on the C-terminal ATPase domain. Likewise, the interaction with the autophagic receptors: p62, NDP52 and CALCOCO1 is mediated by the C-terminal region which has been reported to be embedded in the mitochondrial matrix. Moreover, ATAD3A is not degraded by starvation-induced autophagy; rather, its translation is upregulated.

Acknowledgments

My gratitude goes to Prof. Terje Johanesen for accepting me as a student into the MCRG and to all the members in the group for the warm welcome they offerd to me and their various contributions made inorder for this work to be a success.

A very special thanks to my main supervisor, Asso.Prof. Trond Lamark for all his scientific input, guideance and help offered during this study.

To Mireia Nager (PhD), (my co-supervisor) I say thank you for seeing me through the various task carried out in the laboratory.

Lastly, my appreciation goes to my lovely mother for her moral support and encouragements.

List of abbreviations

aa	Amino acid
ATAD3	ATPase Family AAA Domain -containing protein 3
ATAD3A	ATPase Family AAA Domain -containing protein 3 A
ATAD3B	ATPase Family AAA Domain -containing protein 3 B
ATAD3C	ATPase Family AAA Domain -containing protein 3 C
ALFY	Autophagic-linked FYVE protein
ATG	Autophagy-related proteins
ATG 5	Autophagy-related proteins 5
ATG 8	Autophagy-related proteins 8
ATG13	Autophagy-related proteins 13
ATG 14	Autophagy-related proteins 14
ATG 16	Autophagy-related proteins 16
Bnip3	B-cell lymphoma (BLC)2/adenovirus E1B19-kDa protein-interacting protein
BCL2L13	BCL2 like protein 13
CMA	Chaperon mediated autophagy
CALCOCO1	Calcium binding and coiled-coil domain 1
DMSO	Dimethyl sulfoxide
ER	Endoplasmic reticulum
FIP200	Focal adhesion kinase family interacting protein of 200kDa
FKBP8	FK 506 binding protein 8
FUNC1	Fun 14 domain containing 1
FYCO1	FYVE and coiled-coil domain autophagy adaptor 1
GABARAP	Gamma-aminobutyric acid receptor-associated protein
GABARAPL1	Gamma-aminobutyric acid receptor-associated protein like1
GABARAPL2	Gamma-aminobutyric acid receptor-associated protein like2
HTLV-1 Tax	Human T-cell lymphotropic virus type-1 Tax protein
LC3	Microtubule-associated protein 1A/1B-light chain 3
LIR	LC3 interacting region
NBR1	The neighbour of BRCA1 gen 1
NDP52	Nuclear dot protein 52kDa
NIX	Nip-like protein X
OPTN	Optineurin
P62	Sequestosome -1
P150	The yeast VPs15 homologue
PB1	Phox and Bpem 1
PLEKHM1	Pleckstrin homology domain-containing family M member 1
PI3K	Class III phosphatidylinositol-3 kinase
PINK-1	PTEN-induced kinase 1
SLRs	sequestosome -1-like receptors
TAX1BP1	Tax-1-binding protein 1
UBA	Ubiquitin associated binding domain

ULK1	The mammalian Unc-51 like autophagy activating kinase 1
Vps34	Vacoular protein sorting 34

List of tables

List of figures

Chapter 1

Introduction

1.1 Autophagy

1.1.1 Overview of autophagy

Autophagy is an evolutionary conserved catabolic process in eukaryotic cells for the degradation of cytoplasmic cellular constituents, such as damaged and superfluous organelles, microorganisms or protein aggregates in the lysosome (1-3). Besides basal autophagy that occurs continuously in cells to maintain cellular homeostasis, autophagy is also induced by cellular stresses such as nutrient starvation and intracellular pathogens (4). Autophagy plays a role in recycling nutrients in the cytosol during starvation for proper cell growth. In addition, autophagy is an important cytoprotective machinery which prevents toxic proteins from accumulating within the cell. It also plays a critical role in cellular immunity by eradicating invading micro-organisms (3).

Initially, autophagy was widely known to be a random non-selective and bulk degradation process during nutrient shortage to replenish nutrients in cells. However, recent studies have firmly established that this process is at least partially selective and highly regulated when it occurs in non-starved cells, where invading pathogens, damaged organelles and proteins are selectively degraded (5, 6). Different types of autophagy occur in mammalian cells namely: macroautophagy, chaperon-mediated autophagy (CMA), microautophagy. All forms entails lysosomal degradation of the sequestered cargo and recycling of released products into the cytosol (7). In microautophagy, the cytoplasmic cargo is taken up directly into the lysosome through lysosomal membrane invagination, while in CMA, soluble proteins with pentapeptide motifs are recognised by chaperones that subsequently deliver them to the lysosome through the lysosomal membrane translocation complex. Neither vesicles nor membrane invagination is required for CMA. Macroautophagy, commonly called autophagy, involves cargo recognition and engulfment in a double membraned vesicles called autophagosomes which subsequently fuse with lysosomes to degrade their contents (3, 7, 8).

1.1.2. Macroautophagy

Macroautophagy, hereby referred to as autophagy, is a multi-stage process that is orchestrated by a core autophagic proteins commonly known as autophagy-related proteins (ATG) (8, 9). These ATGs are conserved from yeast to mammals (9). In mammals, the mammalian autophagy-activating kinase 1(ULK1) protein kinase complex, comprising of ULK1, ATG13, ATG101 and focal adhesion kinase family interacting protein of 200kDa (FIP200) proteins regulates the initiation of autophagy by determining the site for the formation of the phagophore. Next is the nucleation phase, initiating the formation of a double membrane phagophore on the endoplasmic reticulum. Nucleation is mediated by the class III phosphatidylinositol -3-kinase (PI3K) (class III PI3K) complex, comprising the vacuolar protein sorting 34 (Vps34), ATG14, vacuolar protein sorting 15 (Vps15), and Beclin-1. Following activation of the PI3K complex by the ULK1 complex (10), PI3K phosphorylates phosphatidyl inositol (PI) to form phosphatidylinositol-3-phosphate (PI3P) on the membrane . The PI3P formed on the membrane triggers the recruitment of WIPI1-4 complex and ATG2 (11), which is necessary for the supply of lipids used for autophagosome biogenesis (12). Next, ATG8 is conjugated to phosphatidylethanolamine on the inner and outer membrane of the phagophore facilitating the elongation of the phagophore. This phase depends on the ATG12-ATG5 -ATG16 complex. Lastly, the phagophore encloses to form the mature autophagosome, which further fuses with the lysosome and its content is subsequently degraded by lysosomal acid hydrolases, **Figure 1** (2, 3, 13-15). Both selective and bulk autophagy commence by the formation a phagophore (13), selectivity is nonetheless conferred by the ability of the selective autophagic receptors to recognise and bind specific ubiquitinated cargo and dock it into the lipidated ATG8 conjugated within the growing double-membraned phagophore for lysosomal degradation (6, 13, 16). Therefore, both autophagic cargo receptor proteins and ATG8 proteins are necessary for cargo selection and degradation (8, 13). Different types of selective autophagy pathway exist, depending on the cargo sequestered for degradation. Examples can be seen in **Table 1.1** (8).

Table 1.1. Different selective autophagy pathway and their respective cargos

Selective autophagy pathway	Cargo
Aggrephagy	Protein aggregates
Ferritinophagy	Ferritin
Mitophagy	Mitochondria
Xenophagy	Pathogens including bacteria
ER-phagy	Endoplasmic reticulum

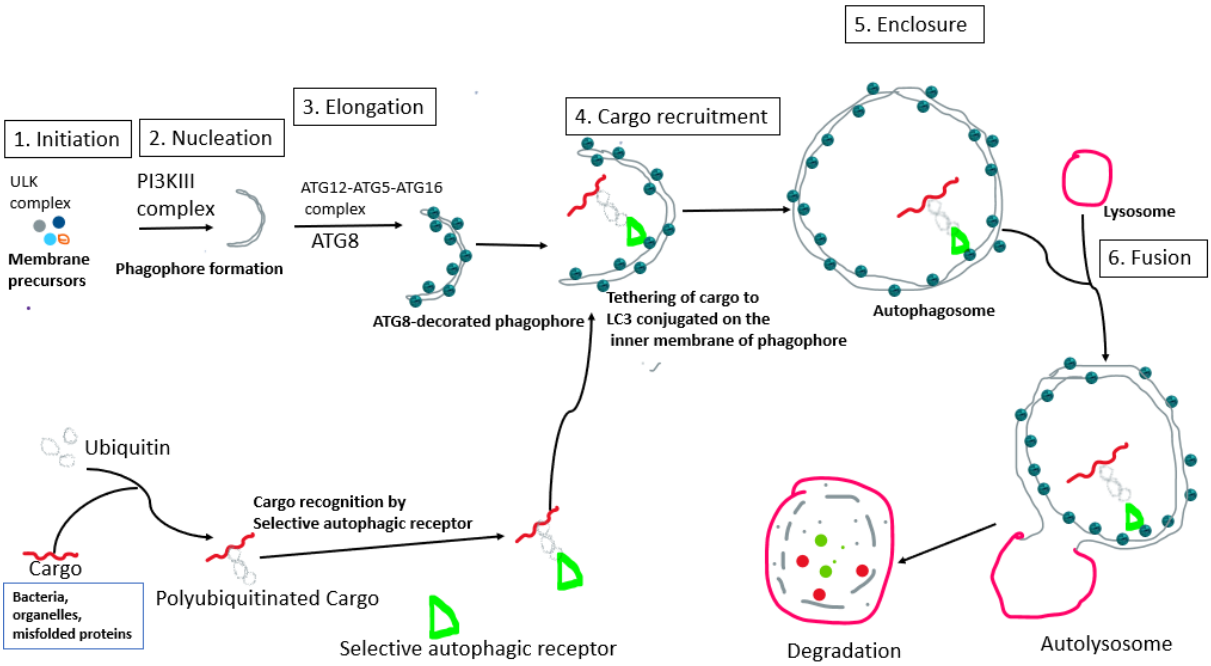

Figure1: **A schematic presentation of the stages of selective autophagy in mammals**.
Initiation: Activated ULK1 complex initiates formation of the phagophore. **Nucleation**: Initiation of phagophore formation**. Growth and Elongation**: phagophore grows, elongates and becomes decorated with lipidated ATG8. **Cargo recruitment**: selective autophagic receptor tether the selected cargo sequestered for degradation to the growing phagophore by binding to the lipidated LC3 in the inner membrane of the phagophore. **Enclosure**: phagophore matures and closes to form an autophagosome. **Fusion**: Autophagosome fuses with the lysosome to form an autolysosome which becomes degraded in the lysosome. The figure also presents a model on how the selected cargo is recruited to the growing phagophore.

1.1.2.1. Mitophagy

Mitophagy is the selective degradation of the mitochondria through autophagy. This process is necessary for the maintenance of mitochondrial homeostasis. Mitophagy also occurs in both yeast and mammals. ATG 32 is the mitophagy receptor for yeast, while an obvious mammalian homologue of ATG32 has not been identified. Although this process occurs both in yeast and mammals, the molecular mechanisms are not conserved. In mammals, two different pathways of mitophagy occurs: ubiquitination-mediated (commonly known as the PINK-parkin pathway of mitophagy) and ubiquitin independent (mitophagy-receptor-mediated) pathway (17). Ubiquitin-mediated mitophagy occurs when the mitochondria are depolarised. Following mitochondrial depolarisation, PINK1 (PTEN-induced putative kinas 1) accumulates on the mitochondrial surface and cause the recruitment of Parkin (an E3 ubiquitin ligase). The Parkin anchored on the surface of the mitochondria becomes phosphorylated by PINK1 resulting to

activation of its ubiquitin ligase activity (18). Parkin activation further promotes ubiquitination of other outer mitochondrial membrane (OMM) proteins, many of which are degraded by the proteasome. In addition ubiquitination of OMM also drives the recruitment of multiple autophagy receptors: sequestosome-1 (p62), optinerium (OPTN), nuclear dot protein 52kDa (NDP52), and Tax-1 binding protein 1 (TAX1BP1) to induce mitophagy (19, 20). While ubiquitin independent pathway involves mitophagy activation prior to mitochondrial depolarisation. This type of mitophagy is mediated by mitochondrial surface receptors such as Nip-like protein X (NIX), B-cell lymphoma 2 (BCL2)/adenovirus E1B19-kDa protein-interacting protein 3 (Bnip3), func 14 domain containing 1 (FUNC1), BCL2-like protein 13 (BCL2L13) and FK 506 binding protein (FKBP8) that recruit LC3. Their overexpression on the mitochondria induce mitophagy (21, 22).

1.1.3. Receptors of selective autophagy

Selective autophagy receptors (SARs) are proteins that recognise cargos. All SARs dock the sequestered cargo into the inner membrane of the phagophore through their interaction with the lipidated ATG8 that are already conjugated in the inner membrane of the growing phagophore (9, 16, 23). In mammals, the Sequestosome-1 like receptors (SLRs), comprising of p62, the related neighbour of BRCA1 gene 1 (breast cancer gene 1) (NBR1), OPTN, NDP52, TAX1BP1 (16, 23-25), are amongst the most studied SARs (25). The SLRs mediate selective autophagy by recognising the polyubiquitinated cargo and connect them to the autophagic machinery for degradation (3, 16, 23, 24). Typical of the sequestosome -1-like receptors, they can oligomerised into large structures and they contain an LC3 interacting region (LIR) motif and a ubiquitin binding domain which are necessary for their function as autophagic receptors (16). The ability of autophagic receptors to recognise ubiquitinated cargos is enabled by the non-covalent binding of the receptors to ubiquitin (already conjugated on proteins) through their ubiquitin binding domain (23, 24). Binding of the SLRs to the lipidated LC3B or another ATG8 family protein on the growing phagophore is dependent on its LIR motifs (16), which binds on the LIR docking pockets present in all ATG8 members (LC3/GABARAP). Thus, the LIR motif of the autophagic receptors is necessary for selective degradation of polyubiquitinated cargo (26). These receptors identify different cargo types within the cell, and each receptor can recognise more than one substrate, **Table 1.2** below.

Table 1.2: Mammalian sequestosome- 1-like receptors and their targeted substrates for sequestration

Autophagic Substrates/cargo	Sequestosome-1 like receptors
Mitochondria	OPTN, NDP52, TAX1BP1, p62,
Peroxisome	NBR1, p62
RNA granule disposal	NDP52, p62
Protein aggregates	P62, NBR1, OPTN
Bacteria	P62, OPTN, NDP52, TAX1BP1
Zymogen	P62
Viral capsid	p62
Midbody rings	P62 NBR1

Table adapted from Mancias *et al.*, 2016 and Terje *at al.*, 2020 (8, 9).

1.1.3.1. Sequestosome-1 (p62)

P62 is a 440-amino acid protein with several domains that enables it to interact with other autophagic markers and signalling proteins. Some of the main domains of p62 include: phox and Bpem1 (PB1) domain comprising of amino acid (aa) 21-103. The PB1 domain facilitates p62 dimerization and heterodimerisation with other PB1-containing proteins, the zz finger (aa 128-163), the TRAF6 binding region (aa 225-250), the LC3-interacting region (LIR) motif (aa 321-345), the Keap-interacting region (KIR, aa 346-359) and the ubiquitin-associated binding (UBA) domain (aa 386-440), (27). In addition the region between amino acid (aa) 170-221 have been shown to enhance its interaction with other proteins such as the autophagic-linked FYVE domain protein (ALFY), the human T-cell lymphotropic 1 Tax (HTLV-1 Tax) protein (28, 29) and LIM domain-containing protein Ajuba (30), **Figure 2**. Each p62 protein has a single LIR motif which becomes clustered when p62 oligomerises through its PB1 domain. Clustering of LIR motif increased the avidity of P62 for LC3B decorated on the membrane of the growing phagophore (6).

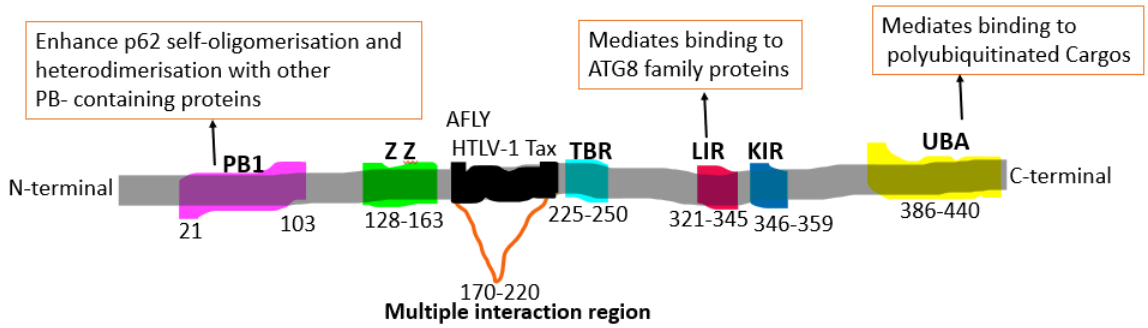

Figure 2: Domains of p62.
The figure highlights the various domains/motifs of p62. PB1, LIR and UBA are the three regions necessary for its interaction with other autophagic-related proteins. p62 forms dimers and heterodimers with other proteins through its PB1 domain. p62 interacts with polyubiquitinated cargos through its UBA domain and facilitates their selective degradation through autophagy by interacting with LC3B through its LIR motif.

p62 was originally termed sequestosome 1 (SQSTM1) due to its ability to form complex with ubiquitinated proteins in the cytoplasm (31). Initially, p62 was shown to function as the human selective autophagic receptor for ubiquitinated protein aggregates (32) and an autophagy substrate which is degraded alongside the ubiquitinated cargo. In which blockage of autophagic degradation resulted in cytoplasmic accumulation of p62 in the autophagosomes (16). Subsequent studies showed that p62 play a role in the degradation of different types of cargos including the mitochondria (33). During selective degradation of damaged mitochondria through the ubiquitin-dependent pathway, p62 is recruited following ubiquitination of the damage mitochondria by parkin(34, 35), which mediates ubiquitination-dependent clustering of damaged mitochondria (34) and final clearance of the mitochondria (35).

1.1.3.2. Nuclear dot protein 52kDa (NDP52)

NDP52 is the mammalian selective autophagy receptor for ubiquitin-decorated cytosolic bacteria (36) and mitochondria (37). NDP52 is involved in both Parkin-dependent (37) and parkin-independent mitophagy (38). NDP52 has an unconventional LIR motif that binds differentially to different ATG8 proteins (39) and a C-terminal zinc finger domains that facilitates its binding to the polyubiquitinated cargo (36, 38, 39). Its zinc finger domain has been shown to be absolutely required for its recruitment to the damage mitochondria during parkin-induced mitophagy (38). Moreover, NDP52 plays a role in the different stages of selective autophagy degradation of cargo beside cargo recognition. It mediates autophagosome biogenesis directly on the cargo, by recruiting the ULK1 complex to the polyubiquitinated cargo to initiate phagophore formation (38, 40). In a recent study carried by Vargas *et al*., 2019, it was demonstrated that NDP52's ability to initiate mitophagy is dependent on its interaction with ULK1 complex. Wherein NDP52 binds to the ULK1 complex through FIP200 (38). NDP52 also controls maturation of the autophagosome (40, 41) by interacting with the ATG8 (42).

1.1.3.3. Calcium binding and coiled-coil domain 1 (CALCOCO1)

Calcium binding and coiled-coil domain 1 (CALCOCO1) is a homologue of NDP52 (CALCOCO2) and TAX1BP1 also known as CALCOCO3, stemming from a common ancestral CALCOCO gene (43). Recently mass spectrometry proteome profiling analysis identified CALCOCO1 as a new autophagy associated protein in many cell lines and selective autophagic degradation of endoplasmic reticulum was impaired upon deletion of the CALCOCO 1 gene. CALCOCO1 interacts with the ATG8 proteins (44). Interestingly, a recent study in our research group showed that CALCOCO1 has a clear preference for the GABARAP

family and it is a selective autophagic receptor for endoplasmic reticulum degradation, (Nthiga et al., 2020, submitted to EMBO Journal). Nonetheless, unlike TAX1BP1 and NDP52 which are SLRs that interacts with ubiquitin, CALCOCO1 does not interact with ubiquitin. To date, little known concerning CALCOCO1 involvement in autophagy. Like its other homologues, it may have other roles in autophagy, in addition to ER-phagy.

1.1.4. Mammalian ATG8 and autophagosome formation

The human ATG8 family protein comprises of 2 sub-groups of proteins: the LC3 (LC3A, LC3B, LC3C) and gamma-aminobutyric acid receptor-associated protein (GABARAP) (GABARAP, GABARAP like-1, and GABARAP like 2) family proteins (26, 45). ATG8 family proteins are well known to be involved in the formation and maturity of the autophagosome and also regulate the size of the autophagosome formed (26). In addition, they also play a role in cargo recruitment, transport and fusion of the autophagosome with the lysosome (46). Eukaryotic cells depleted of ATG8 proteins had impaired autophagosome formation (13). During autophagosome biogenesis, the ATG8 proteins becomes lipidated and anchored to the outer and the inner membrane of the growing phagophore (9, 46), serving as scaffolds to recruit proteins to the phagophore membrane(47). ATG8 proteins on the inner membrane of the phagophore facilitate the recruitment and tethering of the sequestered cargo into the growing phagophore by directly interacting with the selective autophagic receptors. Whereas those on the surface of the autophagosome mediates the transport and fusion of the mature autophagosome with the lysosome by interacting with(FYCO1) (FYVE and coiled coil domain autophagy adaptor 1) and PLEKHM1 (pleckstrin homology domain-containing family M member 1) respectively (45). Specifically, LC3s serves as adaptors for cargo recruitment (9, 13), while the GABARAPs are essential for autophagosome formation (9). The ULK1 and PIK3 complexes that are necessary for initiation and formation of the phagophore binds preferentially to the GABARAP subfamily (47, 48).

Two conjugation reactions are necessary for the formation of autophagosomes. The first involves the conjugation of the ubiquitin like protein ATG12 to ATG5 to form an ATG12-ATG5 conjugate, which subsequently interact with ATG16L1 to form an ATG16L1 complex. This reaction is mediated by the E1-like ATG7 and E2-like ATG10 enzymes. The second reaction necessary for autophagosome formation is the lipidation of ATG8 proteins. Prior to ATG8 lipidation, the cytosolic ATG8 precursors (pro-ATG8) is proteolytically cleaved by ATG4 to form the I-form, (for example LC3-I) whose C-terminal glycine is exposed for possible conjugation with lipids. The I-form is next conjugated with phosphatidylethanolamine

to form the lipidated ATG8 also known as the II-form (such as LC3-II) attached on the phagophore memebrane (45). This lipidation reaction is mediated by ATG7, the E2-like ATG3, and the ATG16L1 complex. Similar to the SARs for example p62, LC3-II on the inner membrane of the autophagosome is also degraded alongside the cargo. Its level is however increased when degradation is impaired (45, 49). As such, LC3-II is also widely used to monitor autophagy activity (46). LC3-II has a smaller molecular mass than LC3-I and thus has a faster mobility on SDS PAGE than the LC3-I (49).

1.2. The ATPase Family AAA Domain -containing protein 3 (ATAD3)

1.2.1. Evolution and overview of the ATAD3 genes and proteins

ATPase Family AAA Domain -containing protein 3 (ATAD3) is a nuclear-encoded mitochondrial transmembrane proteins. The ATAD3 gene was initially found in the mitochondria of a mouse liver as a target gene for c-Myc (50-56). Based on the available genomic analysis, the ATAD3 genes are evolutionary highly conserved, present mainly in higher (multicellular) eukaryotes (50, 57), such as insects, plants, nematodes, amphibians, humans, rodents and birds (50). No ortholog exist in yeast nor prokaryotes. Plants have 3 isoforms of the ATAD3 genes resulting from polyploidy while a single copy of this gene is present in mouse (*Mus masculus*), rat (*Rattus norvegicus*), pig (*SUS scrofa*), cat (*Felis catus*), birds (*Gallus gallus*), fruit fly (*Drosophila*). Nonetheless, in humans and others primates the ancestral ATAD3 gene has evolved through duplication and gene deletion, giving rise to 3 isoforms (54). In humans, the 3 ATAD3 genes paralogs (ATAD3A, ATAD3B and ATAD3C) are located on chromosome 1 at 1p36.33 locus. ATAD3A is the primary form of the ATAD3 family gene, ATAD3B has a point mutation at the corresponding stop codon of ATAD3A while ATAD3C is the truncated version of the ATAD3 gene (50, 54, 58, 59), formed by the deletion of the conserved first 70 amino acid at the N-terminal of ATAD3A (60).

According to data gathered from NCBI, three transcript variants of human ATAD3A formed from alternative splicing has been described, namely; transcript variant 1 (NCBI Reference Sequence NM_018188.5), transcript variant 2 (NCBI Reference Sequence NM_001170535.3), transcript variant 3 (NCBI Reference Sequence NM_001170536.2). As such, 3 different ATAD3A protein isoforms of varying length are produced from these transcripts. Amongst the ATAD3A protein isoforms, isoform 1 (NCBI sequence reference NP 060658.3) constituting 634 amino acid (protein ID NP 001164006.1) is the longest and it is encoded by variant 1. While isoform 3 encoded by variant 3, is the shortest (57KDa, 507 amino

acid, NBCI Reference sequence NP_001164007.1). The second isoform has 586 amino acid with a molecular weight of 66kDa (NCBI Reference sequence NP_001164006.1). While the human ATAD3B also known as AAA-TOB3 has 2 transcript variants also produced by alternative splicing (54, 56). The identity of the 2 transcripts variant mRNA obtained from NCBI gene and nucleotide database includes: transcript variant 1 (NCBI reference sequence NM_031921.6), transcript variant 2 (NCBI reference sequence NM_001317238.2). These variants encode for different protein isoforms. The transcript variant 1 encodes for the human ATAD3B isoform AAA-TOB3I (NCBI reference sequence NP_114127.3). ATAD3B isoform AAA-TOB3I is the canonical protein with 648 amino acid and has a mass of 72KDa. While transcript variant 2 encodes for ATAD3B isoform AAA-TOB3s precursor with 602 amino acid (NCBI reference sequence NP_001304167.1). AAA-TOB3s precursor has a shorter N-terminus than the canonical isoform. The truncated-N terminal ATAD3C exist as a single mRNA variant (NCBI reference sequence NM_00103911.3), encoding for ATAD3C protein having 411 amino acid (NCBI sequence reference NP_001034300.2).

Just as the ATAD3 gene is conserved during evolution, the protein sequence of ATAD3 is also highly conserved during evolution, depicted by 39% similarities between the ATAD3 protein in human and that of the plant`s ortholog (54). Studies carried out on the expression pattern of these proteins in human and rodent cell lines revealed that ATAD3 proteins expression is tissue specific. ATAD3A is the most expressed and present in all the cells studied (50, 57), while ATAD3B is human specific, highly expressed specifically in pluripotent human embryonic stem cell, and down regulated in adult multipotent mesenchymal stem cells derived from adult bone marrow and in differentiated cells. ATAD3B is however re-expressed in cancer cells (59). The canonical ATAD3B protein (648 amino acid, mass 72KDa) is less expressed in most of the human cell lines as compared to ATAD3A (50, 57). Although ATAD3B is less expressed in cells, the canonical ATAD3B protein is highly expressed in the embryo brain and adult pituitary gland (U87 and U373 derived brain cell lines), head and neck carcinomas (50, 56). No analysis was done for the ATAD3C, due to lack of the appropriate antibody (50).

1.2.2. Structure and function of the domains of the human ATAD3 proteins

Biostatistical analysis studies carried out on the primary sequence of ATAD3A (586 amino acid, mass 66kDa) demonstrated that the N-terminal region ranges from 1-244 amino acid and the C-terminal (52, 57). ATAD3A is anchored in the mitochondrial inner membrane, with its C-terminal embedded in the matrix (51, 57), while the N-terminal makes interactions with the

mitochondrial outer membrane (57). Previously, it was uncertain whether the first 40 amino acids at the N-terminal extends to the cytosol or only interacts with the inner surface of the mitochondrial outer membrane (52, 57). Subsequently confocal images of mouse leydig tumour (MA-10) cells revealed that the protein is enriched in the mitochondrial-endoplasmic reticulum (ER) associated membranes (MAMs) (51). In an immunogold electron microscopy study, the N-terminal was detected at the contact sites of the mitochondrial inner and outer membranes in Hdh Q111 cells, whereas in HdhQ7 cells, the N-terminal of ATAD3A was detected in the cytosolic side of the outer membrane of the mitochondria (61). Thus, the N-terminal extends to the cytosol, however it is likely that the its localisation may be under regulation and not fix. The **Figure 3** below is a representative of the proposed models of ATAD3A topology.

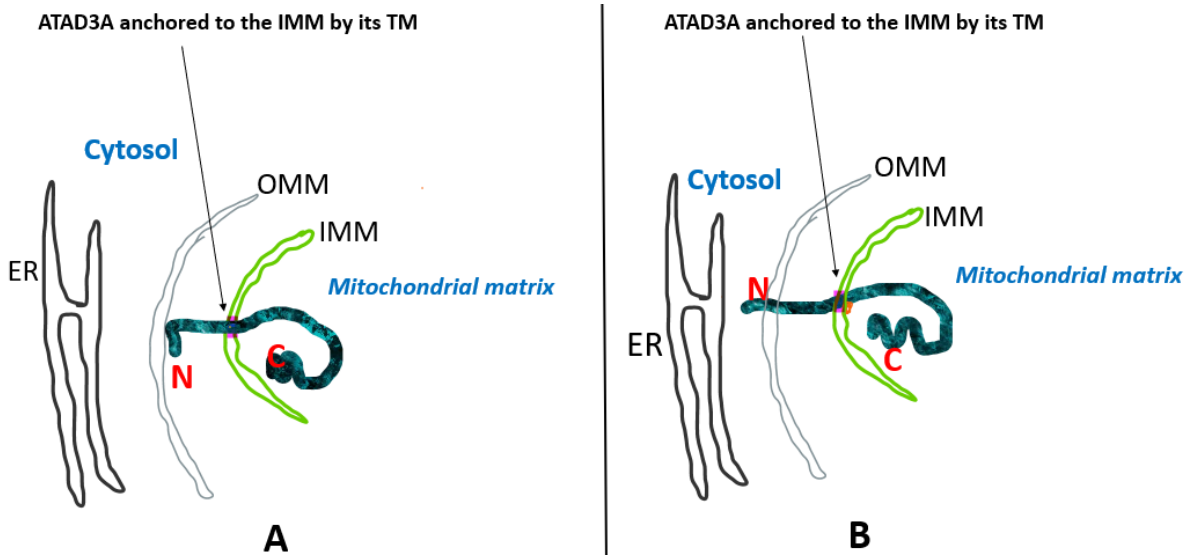

Figure 3: Representative models of ATAD3A topology. In both models (A and B), ATAD3A is anchored to the inner membrane of the mitochondria (IMM) by its transmembrane segment, with its C-terminal part embedded in the mitochondrail matrix. In model A, the N-teminal part makes interaction with the inner surface of the outer membrane of the mitochondria (OMM), while in B, the N-terminal part extends to the cytosol

The N-terminal of ATAD3 comprises of a proline-rich region (amino acid 18-27), 2 coiled-coil (CC) domains; the first CC domain which is rich in glutamine, ranges from the 85th amino acid to the 115th amino acid (54, 61), and the second CC domain ranging from the 180th amino acid to 220th. These CC domains are required for the oligomerisation of the protein (61). Unlike the N-terminal, the C-terminal of ATAD3A is embedded in the mitochondrial matrix

(52, 57, 62), and regulates the N-terminal interactions with the mitochondrial outer membrane through binding of ATP to the ATPase domain (57). The C-terminal part comprises of a putative transmembrane segments (TM) with the main one predicted to be close to the centre of the protein, ranging from the 247th -264th amino acid (52, 57), **Figure 4**. The TM mediates the attachment of ATAD3A on to the mitochondrial inter membrane (62). Adjacent to the TM, is a mitochondrial importing signal (MIS) sequence. ATAD3A do not have a canonical mitochondrial targeting sequence (52), its C-terminal is necessary for its mitochondrial targeting and import. Whereby, the TM and the mitochondrial import signal region cooperate to facilitate its import into the mitochondria (57). The C-terminal also contains the AAA+ ATPase core domain comprising the walker A and walker B motif residues (52, 57) which are the main motifs involved in ATP binding and hydrolysis respectively (54, 63). This C-terminal ATPase domain is very crucial for the proper functioning and stability of the ATAD3A proteins. The walker A motif of the ATPase domain has a phosphate-binding (P) loop (64), with a conserved sequence (-**G**352**PPGTGKTL**360-) in both human ATAD3A and ATAD3B. K358 is the site for interaction with ATP, and the K358 residue of ATAD3A is invariant in other homologues. (64). While the walker B has a conserved glutamate residue that mediates ATP hydrolysis. Mutation of the walker B glutamate inhibit ATP hydrolysis but not ATP binding (63).

Amongst the various forms of ATAD3 proteins expressed in humans, the structure/topology of ATAD3A protein has extensively been studied, while information regarding the other ATAD3 proteins isoforms is rare. Nevertheless, studies carried out on ATAD3B topology demonstrated that the conserved N-terminal domain of ATAD3B has the same localisation as ATAD3A, and it is also accessible to trypsin digestion (59). The canonical human ATAD3B (648 amino acid, 72kDa) and ATAD3A proteins are 93% similar in their primary sequence, with a slight difference in their C terminals, in which the C-terminal of ATAD3B is longer than ATAD3A (52, 54). The extended C-terminal region of ATAD3B has extra 62 amino acid sequence consisting of hydrophobic amino acids, cysteines residues (54, 59) as well as several potential sites for phosphorylation (54). Unlike their N-terminals, the C-terminal of both proteins have been shown to have different sub-cellular localisations(59). The extra C-terminal region of ATAD3B has putative transmembrane motif enrich with hydrophobic amino acids (52, 54), and it is positioned in the intermembrane space of the mitochondria (59).

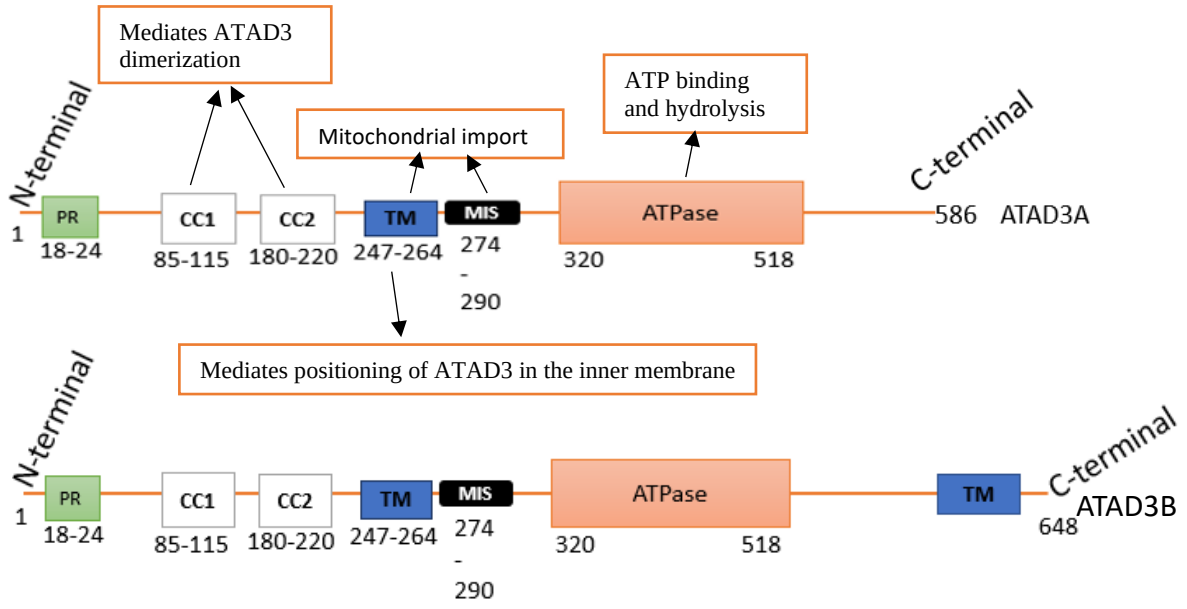

Figure 4: Domains of the ATAD3 proteins
Both ATAD3A and ATAD3B have a proline-rich region (PR), two coiled-coil (CC) domain that mediates self-dimerisation and heterodimerisation with other proteins, a transmembrane (TM) segment which enables ATAD3 to be attached to the mitochondrial inner membrane. Next to the TM region is the mitochondrial targeting signal sequence (MIS). The TM segment and MIS aid in mitochondrial import of ATAD3. Next to the MIS is the ATPase domain. ATAD3B has an extended C-terminal with an additional TM segment.

1.2.3. Functions of ATAD3 proteins

ATAD3 proteins are multifunctional mitochondrial ATPase that control mitochondrial dynamics and morphology (64), as well as other cellular processes which includes calcium homeostasis, apoptosis (57), mitochondrial DNA replication and stability, cell growth, cholesterol transfer and steroid biogenesis (57, 58, 64), mitochondrial-endoplasmic reticulum (ER) communication (50, 64), While ATAD3B has been reported to be a dominant negative of ATAD3A (59). This study will focus on the role of ATAD3 protein in the maintenance of mitochondrial homeostasis.

1.2.3.1. ATAD3 and Mitochondrial dynamics

Mitochondrial dynamics is a physiological process involving coordinated cycles of mitochondrial fission and fusion to maintain the shape, morphology, size, number and proper intracellular distribution of the mitochondria with in the cell (65). Mitochondria are double membrane organelles consisting of 4 compartments namely; the matrix, the inner membrane, intermembrane space, and the outer membrane (66, 67). The interactions that occur between the mitochondrial inner and outer membrane is essential for mitochondrial fusion and fission (mitochondrial dynamics). ATAD3A is an integral mitochondria protein which has been reported to be involved in mitochondrial dynamics by regulating the interactions between these

two membranes (57). In Hela and murine cells it was demonstrated that, ATAD3A also complex with mediators of mitochondrial fission; DRP1 and mediators of mitochondrial fusion such as mitofusins 1 and mitofusin 2 (68). While other co-immunoprecipitation studies in lung adenocarcinoma cell lines revealed an interaction between ATAD3A with mitochondrial fission protein dynamin-related protein 1 (DRP1) and mitochondrial fusion protein mitofusin 2 and optic atrophy 1 (OPA1) (58, 69). Thus, ATAD3A also regulates mitochondrial dynamics through its interaction with these proteins (58).

1.2.3.2. ATAD3 and mitochondrial morphology

Although ATAD3A and ATAD3B are involved in the regulation of mitochondrial network and shape, both have opposing effects. ATAD3A is necessary for the maintenance of mitochondrial morphology and content, (structural integrity), and total mitochondrial number within a cells (61, 64, 69). Down regulation of ATAD3A is associate with a decrease in total mitochondrial number and mitochondrial fragmentation (61, 68, 69). while overexpression of its ATPase deficient Walker A mutant incapable of binding ATP facilitates mitochondrial fragmentation (64). In addition, ATAD3A is vital for maintaining normal mitochondrial content and structural integrity. Studies carried out to evaluate the ultrastructure of the mitochondria in ATAD3 depleted skeletal muscle of mice using the transmission electron microscope showed that loss of ATAD3A altered the integrity of the cristae and also disrupted the contact between the cristae and the outer membrane (cristae junctions) (70). Likewise, same phenotype was observed in patients' fibroblast suffering from foetal neonatal cerebellar hypoplasia with biallelic mutation of ATAD3A (consisting of leu 406 Arg substitution) and a low expression of the 66kDa ATAD3A protein. Moreover, these patients also presented with a significantly smaller mitochondria that consist of a decreased cristae perimeter per mitochondrion (71). On the other hand, overexpression of ATAD3B promotes mitochondrial network fragmentation (57, 59) and also leads to a decreased in mitochondrial number in cells (72). While loss of ATAD3B in H1229 cells causes the mitochondria to be more filamentous (59).

1.2.3.3. ATAD3 regulates Mitochondrial DNA metabolism

Mitochondrial nucleoid proteins are proteins that interact with mitochondrial DNA. They play a role in organising and protecting the mitochondrial DNA (72), regulating transcription and mitochondrial protein synthesis (59). It has been suggested that ATAD3A may play a rule in mitochondrial DNA replication and maintains mitochondrial DNA integrity (72) and also regulates mitochondrial DNA metabolism by interacting with mitochondrial nucleoid proteins (59). The interaction between the mitochondrial nucleoid complex and

ATAD3A is mediated by the C-terminal of ATAD3A (59). Thus, distortion in the steady state of ATAD3A perturbs mitochondrial DNA maintenance (61). ATAD3B overexpression promotes ATAD3A destabilisation and distort mitochondrial DNA integrity. Different studies have shown that ATAD3B antagonises the action of ATAD3A in cells(59, 72), serving as a dormant negative of ATAD3A, to inhibit the interaction of ATAD3A with the mitochondrial nucleoid protein complexes including HSP60; a protein essential for stabilising mitochondrial DNA integrity (73). This inhibitory effect of ATAD3B on ATAD3A is enhanced by the formation of ATAD3A/ATAD3B heterodimers when the C-terminal of ATAD3B and ATAD3A interacts. Heterodimerisation between the 2 isoforms causes a change in ATAD3A C-terminal environment and consequently induces cleavage at the C-terminal of ATAD3A. Thus, formation of heterodimers between the 2 isoforms abrogates the association of ATAD3A to the nucleoid proteins, hence distorting the integrity of mitochondrial DNA (59).

1.2.3.4. ATAD3 proteins and autophagy

Mutations leading to a loss of function of ATAD3A have been associated with upregulated autophagy activities. Patient's fibroblast with R528W mutant ATAD3A were reported to have an increased mitophagy (58), while p62 levels were constitutively low in those expressing the walker A mutant (G355D) deficient of its ATPase activity (64). Moreover, ATAD3A knockdown or silencing with resveratrol in uterine cervical cancer (SKG-1) cells increased the number of autophagosomes, in which some autophagosomes had encapsulated mitochondria (74). Further studies identify ATAD3A as a regulator of the ubiquitin-dependent mitophagy in hematopoietic progenitor cells. In which ATAD3A interacts with proteins involved in the transport of proteins across the mitochondria (TOM40; translocase of outer mitochondrial membrane 40 homolog and TIM 23; translocase of the inner membrane 23) to facilitate mitochondrial import and subsequent processing of PINK1. Depletion of ATAD3A resulted to accumulation of PINK1 outside the mitochondria and finally mitophagy (21). On the other hand, studies on the involvement of ATAD3B in autophagy are rare. However, a recent study carried out by Heo *et al*., 2019, to identify possible OMM proteins that are ubiquitinated by parkin using proximity biotinylation experiments with OPTN or TAX1BP1, ATAD3B was identified amongst other proteins (20).

1.3. Aim of study

Several resident mitochondrial proteins have been shown to regulate mitophagy by recruiting and/or interacting with ATG8 proteins, and SLRs such as p62 NDP52, TAX1BP1 and OPTN (75, 76). Based on data available, it appears ATAD3 proteins have potential roles in

regulating autophagy and mitophagy (20, 64). Recently it was shown in our group that ATAD3 proteins interact with ATG 8 family proteins, p62, NDP52 and CALCOCO1 (not published). This study was thus aimed at evaluating if ATAD3 proteins have a regulatory role in recruiting these autophagy proteins during stress to induce mitophagy.

1.3.1. Objectives of the study:

I. To characterise the interactions of ATAD3A and ATAD3B with p62, NDP52 CALCOCO1 and the human ATG8 proteins.
II. To assess the co-localisation of ATAD3A and ATAD3B with p62 and LC3B in cells.
III. To evaluate autophagic degradation of ATAD3A and ATAD3B.
IV. To determine the relevance of the identified interactions in the process of autophagy or mitophagy.

Chapter 2

Materials and Methods

2.1 Materials

Table 2.1 List of vectors

Vectors	Promoter	Selective marker	Purpose	Source
pDest-myc C1 gateway expression vector	Human CMV promoter for mammalian expression of protein, and T7 promoter for *in vitro* translation	Ampicillin resistance gene	-Expression of myc-tagged proteins in Hela cells. -Expression of myc-tagged proteins *in vitro*	Lamark *et al.*, 2003 (77)
pDest15 gateway expression vector	T7 promoter	Ampicillin resistance gene	Expression of GST-fusion proteins in E coli	Invitrogen
pDest-FLP-EGFP-C1	Human cytomegalovirus (CMV) promoter	Hygromycin resistance gene	Inducible expression of EGFP-tagged proteins in Flp-in Hela cells	Alemu *et al.*, 2012 (48)
pGEX-2T	Tac promoter	Ampicillin resistance gene	Expression of GST protein in E coli	Amersham
pDONR221 gateway cloning vector		Kanamycin resistance gene	Production of entry clones	Invitrogen

The different plasmids used were made from different vectors types depending on the purpose:

Table 2.2: The following plasmids were used in this study

Plasmids	Type of plasmid	Purpose	Source
pDest15-LC3A	Gateway expression clone	Production of GST-LC3A proteins	Pankiv et *al.*, 2007 (78)
pDest15-LC3B	Gateway expression clone	Production of GST-LC3B proteins	Pankiv *et al.*, 2007 (78)
pDest15-LC3C	Gateway expression clone	Production of GST-LC3C proteins	Kirkin *et al.*, 2009 (79)
pDest15-GABARAP	Gateway expression clone	Production of GST-GABARAP proteins	Pankiv *et al.*, 2007 (78)
pDest15-GABARAPL1	Gateway expression clone	Production of GST-GABARAPL1 proteins	Pankiv *et al.*, 2007 (78)
pDest15-GABARAPL2	Gateway expression clone	Production of GST-GABARAP L2 proteins	Pankiv *et al.*, 2007 (78)

pDest15-LC3B F52A	Gateway expression clone	Production of LDS mutant GST-LC3B protein	Kirkin *et al*., 2009 (79)
pDest15-GABARAP Y49A	Gateway expression clone	Production of LDS mutant of GST-GABARAP proteins	mutugi 2019
pGEX-2T	Expression vector	Product of GST proteins	
pDest15 p62	Gateway expression clone	Production of GST-p62 protein	Abudu et al., 2019
pDest15 p62 ΔPB1	Gateway expression clone	Production of mutant GST-p62 protein without the PB1domain	Abudu et al., 2019
pDest15 p62 Δ 123-170	Gateway expression clone	Production of mutant GST-p62 protein without amino acid 123-170	Abudu et al., 2019
pDest15 p62 Δ171-256	Gateway expression clone	Production of mutant GST-p62 protein without amino acid 171-256	Abudu et al., 2019
pDest15 p62 Δ257-370	Gateway expression clone	Production of mutant GST-p62 protein without amino acid 257-370	Abudu et al., 2019
pDest15 p62 Δ371-385	Gateway expression clone	Production of mutant GST-p62 protein without amino acid 371-385	Abudu et al., 2019
pDest15 p62 ΔUBA	Gateway expression clone	Production of mutant GST-p62 protein without the UBA domain	Abudu et al., 2019
pDest15 NDP52	Gateway expression clone	Production of GST-NDP52 protein	Abudu et al., 2019
pDest15 CALCOCO1	Gateway expression clone	Production of GST-CALCOCO 1	Mutugi *et al*., 2020
pDest-*myc* ATAD3A	Gateway expression clone	Production of *in vitro* translated ^{35}S-myc ATAD3A protein -	Nthiga 2018
pDest-myc ATAD3B	Gateway expression clone	Production of *in vitro* translated ^{35}S-myc ATAD3B protein	Nthiga 2018
pDest-myc ATA3B Δ1-50	Gateway expression clone	Production of *in vitro* translated ^{35}S-myc ATAD3B protein without 1-50 amino acid	Nthiga 2018
pDest-myc ATA3B Δ 50-320	Gateway expression clone	Production of *in vitro* translated ^{35}S-myc ATAD3B protein without amino acid 50-320	Nthiga 2018
pDest-myc ATA3B Δ321-518	Gateway expression clone	Production of *in vitro* translated ^{35}S-myc ATAD3B protein without amino acid 321-518	Nthiga 2018
pDest-myc ATAD3B 1-224	Gateway expression clone	Production of *in vitro* translated ^{35}S-myc	This study

		ATAD3B protein with 1-224 amino acid	
pDest-myc ATAD3B 1-320	Gateway expression clone	Production of *in vitro* translated ^{35}S-myc ATAD3B protein with 1-320 amino acid	This study
pDest flp-in EGFP ATAD3B	Gateway expression clone	Inducible expression of EGFP-tagged ATAD3B in Hela cells	Nthiga 2018
pDest flp-in EGFP ATAD3B	Gateway expression clone	Stable transfection of cells	Nthiga 2018
pDest-myc ATAD3B1-518	Gateway expression clone	Production of *in vitro* translated ^{35}S-myc ATAD3B protein with 1-518 amino acid	This study

Table 2.3: List of primers used in this study

Primer Sequence (5' to 3')	Description
Reverse primer 5'-gccagccgtcctgatctactccaagacggtct-3' **Forward primer** 5'-agaccgtcttggagtagatcaggacggctggc-3'	Site directed mutagenic primer to insert a stop codon at S225 of ATAD3B
Reverse primer 5'-gccctccgtcagccgctagacctccgagcactt-3' **Forward primer** 5'-aagtgctcggaggtctagcggctgacggagggc-3'	Site directed mutagenic primer to insert a stop codon at 519 of the ATA3B
forward primer ggggacaagtttgtacaaaaaagcaggctccaccatgttagtccagcctggaagc **reversed primer** ggggaccactttgtacaagaaagctgggtctacctagcgacctccgagcacttc	Attb-flanged ends primers for the amplification of the ATPase domain with attb end for gateway cloning
T7 primer	Primer for forward sequencing of pDest-myc plasmids
Sp6 primer	Primer for reverse sequencing of pDest-myc plasmids
M13 forward sequencing	Primer for forward sequencing of pDONR221 plasmids

Table 2.4: List of equipment used in this study

Name	Manufacturer	Purpose
Sonics vibra cell ^{TM} USA		Sonication of cell lysate
AccuBlock ^{TM} Digital Dry Bath	labnet international, Inc	Boiling samples for electrophoresis
M-26 Transilluminator	BioDoc-it ^{TM} imaging system	Imaging of DNA and Coomassie stained SDS-PAGE gels

U/V visible spectrophotometer	Medinor Produkcer medispec III	Measure bacterial optical density during GST- fusion protein production
FUJIFILM BAS- 5000	FUJIFILM	Autoradiography
Fuljifilm Bas cassette 2025	Fuljifilm	Image developer
Nanodrop® spectrophotometer ND-1000	Saveen Werner	Measurement of plasmid concentration
Avanti® J-26 XP centrifuge	Beckman Coulter®	Harvesting of bacteria cells
Model 583 gel dryer	Bio-Rad	Drying of gels
PCR analyser		Thermal cycling
T-75 tissue culture flask		Tissue culturing
Cell counter	Bio-rad	Seeding of cells
Confocal microscope LSM800	ZEISS	Fluorescence microscopy
Imagequant LAS 4000	GE Healthcare	Western blot analysis
Protein transfer analyser	GE Healthcare	Western blot analysis
CLARIOstar® plus Microplate reader	BMG Labtech	Measurement of total protein concentration of cell lysate
96 well plates	Falcon	
35x10cm plate		Cell culture
6 well culture plates		
24 well culture plates		
15mls falcon tubes		
50ml falcon tubes		
Rotator		
Mixer		

Table 2.5: The following chemicals were used in this study

Reagents	Manufacturer	Purpose
Glutathione sepharose beads	GE Healthcare	Extraction of GST-fusion proteins from crude lysate
Unstained protein standard	Biolabs In New England	Protein electrophoresis
TNT® T7 quick coupled transcription/translation protein system + ^{35}S methionine	Promega	*In vitro* translation of radio-labelled proteins
isopropyl β-D-1-thiogalactopyranoside (IPTG)		Induction of protein expression in E coli with T7 polymerase
N N N` N` - tetramethylethylenediamine (TEMED)	Sigma	Preparation of the separating and stacking gel for SDS-PAGE
GenElute™ plasmid Miniprep kit	Sigma-Aldrich	Purification of plasmid DNA from recombinant *E coli* DH5α strain culture
Quikchange site-directed mutagenesis kit	Agilent Technologies	Mutagenesis
Fetal bovine serum		Cell culture

Penicillin and streptomycin solution		Cell culture
Nitrocellulose membrane		Blotting of proteins
Pierce™ BCA protein assay kit	Thermo scienctific	Measurement of total protein concentration in cell lysate
Phusion®high fidelity DNA polymerase	BioLab	Amplification of the ATPAse domain of ATAD3B
GelRed® dye	Biotium	Staining of DNA
Bafilomycin A1		Block lysosomal degradation
Bigdye 3.1	Sekvenslab UiT	DNA sequencing
Cycloheximide 62µg/ml		Inhibit protein synthesis
Doxycycline 1µg/ml		Turn on ATAD3 gene expression in stable cells
Hygromycin 200µg/ml		Selection of stable cell lines
Blasticidin S HCL 10µg/ml		Generation of stable cell lines
SuperSignal™ western blot substrate	ThermoFisher Scientific	HRP Western blot detection
Gateway™Bp clonase™ II enzyme mix recombination kit	ThermoFisher Scientific	Production of pDON221 ATAD3B 320-518
Gateway™ LR clonase™ II enzyme mix recombination kit	ThermoFisher Scientific	Production of pDest-myc ATAD3B 320-518

Table 2.6: Cloning host and cell lines used in the study

Host	Purpose
Standard BL21 (DE3) competent *E coli* cells	Production of the recombinant ATG 8 family proteins fused to GST
soluBL21 (DE3) competent *E coli* cells	Expression of the recombinant (p62, NDP52, CALCOCO1) proteins fused to GST
DH5α (DB3-1) competent *E coli* cells	Cloning host for propagation of the plasmids
Flp-In T-Rex Hela cells	

Table 2.7: Growth Media used in this study

Name	Purpose
LB agar plates with 100µg/ml ampicillin or Kanamycin	Cloning of bacteria with pDest vector
LB media supplemented with 100µg/ml ampicillin	Set up overnight bacterial culture
Yeast extract-tryptone (2xYT) media supplemented with100µg/ml ampicillin	Production of GST-fusion proteins in bacteria

Dulbecco`s Modified Eegle`s medium with Low glucose and L-glutamine, sodium bicarbonate	Cell culture
Hanks balanced salt solution Modified with sodium bicarbonate	Nutrient starvation media used to induce autophagy in cells
S.O.C media	Bacterial transformation

Table2.8: Antibodies, florescence stains used in this study

Name	Dilution/purpose	Manufacturer	Animal source
Anti-ATAD3A (H00055210-D01)	1:100 (IF) 1:1000 (WB)	Abnova	Rabbit
Anti-tom20 (F-10) Sc-17764	1:400 (IF)	Santa cruz	Mouse
Anti-p62 (GP62-C)	1:2000 (IF)	PROGEN	Guinea pig
P62 #610833	1:1000 (WB)	BD Biosciences	Mouse
Anti-LC3B(0231-100/LC3-5)	1:1000 (IF)	Nanotools	Mouse
Anti-LC3B (nb100-2220)	1:1000 (WB)	Novus	Rabbit
Anti-beta actin (A 2066)	1:1000 (WB)	Sigma	Rabbit
Anti-NRF2 (ab62382)	1:1000 (WB)	Abcam	Rabbit
Anti-biotin HRP linked antibody	1:2000 (WB)	Cell signaling technology	Rabbit
Anti-GFP (ab290)	1:1000 (WB)	Abcam	Rabbit
Anti-myc (#2276)	1:1000 (WB) 1:200 (IF)	Cell signalling technology	Mouse
Alexa flour® 488 anti-rabbit	1:500 (IF)	Invitrogen	Goat
Alexa flour®555 anti - mouse	1:500 (IF)	Invitrogen	Goat
Alexa flour®647 ant-guinea pig	1:500 (IF)	Invitrogen	Goat
DAPI	1.4000 (IF)		

IF = immunofluorescence, WB = western blotting

Table 2.9: list of Restriction enzymes used in this study

Name of enzyme	Reference number
Dpn 1	R0176L
Proteinase K	25530049

Table 2.10: list of Buffers, solutions and stains used in this study

Name	Composition	Purpose
1x Phosphate buffer saline (PBS)	1ml of 100% PBS 99ml of distilled water	Washing
1x PBS-T (1L)	100ml of 10 x PBS 0.1% Tween-20	Western blotting

	Distilled water to 1L	
0.1%Triton X-100	1ml 10%triton X-100 90ml distilled water	Permeabilization of cells for immunostainings
10% Triton x-100	10ml 100%triton-100 90 ml distilled water	Cell lysis during GST tagged protein extraction
Lysis buffer (200ml)	10ml 1M TrisCl pH = 8 (final conc 50mM) + 25ml 2M NaCl (final conc 250mM) 165ml distilled water	Bacterial cell lysis
Bacterial Cell lyse solution (4ml)	3.85ml of lysis buffer + 140µl lysozyme (10mg/ml) + 4 µl 1MDithiothreitol (DTT) + 8 µl Ethylenediaminetetraacetic acid (EDTA)	Lysis of bacteria during protein purification
NETN buffer (200ml)	4ml of 1M Tris-Cl $P^{H}8$ 10ml of 2M NaCl 1m of 100% Nonidet P (NP) -40 400µl of 0.5M EDTA 2ml of 0.1M EGTA Add dH_2O to 200ml	GST Pull down
4x concentration buffer (1L)	60.55g Tris-base +4g SDS + dH2O to 1L pH adjusted to 6.8 with HCl	Preparation of the stacking polyacrylamide gel for SDS-PAGE
10%Ammonium persulfate (APS)	1g ammonium persulphate in 10ml of distilled water	Preparation of the separating and stalking gel for SDS-PAGE
TEMED		
4x separating buffer(1L)	181.65g Tris-base + 4g SDS + dH2O to 1L, pH adjusted to 8.8 with HCl	Preparation of the separating gel for SDS-PAGE
Running buffer (5L)	15g Tris-base + 75g glycine + 5g SDS + dH2O to 5L	Running of the electrophoresis
Sample/loading buffer	4 parts of 2x (SDS 2-mercaptoethanol) + 1 part DTT	Sample preparation for SDS-PAGE
Gel-Fixing solution (1L)	400ml methanol (final conc 40%) + 100ml acetic acid (final conc 10%) + 500ml dH2O	Fixing of proteins in the gel and washing away the components of the running buffer on the gel
Coomassie blue staining solution	Stock 1g of Coomassie blue dye + 100ml of deionised water	Staining of proteins bands in the polyacrylamide gel
De-stain solution 1 (1L)	500ml methanol + 10ml acetic acid + dH2O to 1L	First de-staining of the stained electrophoresis gel to

		removal of background stains on the gel
De-stain solution 2 (1L)	50ml methanol + 70ml acetic acid + dH20 to 1L	Second de-staining of electrophoresis gel
1X SDS buffer100ml	5ml of 1M Tris-HCL PH 7.4 10ml of 20% SDS 20ml of 50% glycerol d H20 to 100ml	Harvesting of mammalian cultured cells
20x minigel buffer	193.76g Tris-HCL, 27.22g sodium acetate 14.9g EDTA Distilled water 2 Litres Adjust pH to 8 with acetic acid	Agarose gel electrophoresis
Ponceau S stain solution (1L)	1g ponceau S, 50ml acetic acid, distilled water to 1L	Protein visualisation after transfer to a nitrocellulose membrane
Transfer buffer (1L)	Tris 300nM, methanol 20%, SDS 0.05%, Glycine 300nM	Western blotting
TE buffer 100ml	Tris 10mM, pH8 EDTA pH8 1mM	Cloning, agarose gel electrophoresis
Cutsmart buffer		Restriction digestion
4% paraformaldehyde		Fixation of cells
5x sequencing buffer		Plasmid sequencing
Methanol		Permeabilization of cells
Goat serum		Blocking of unspecific binding in during immunofluorescence
DAPI		Immunofluorescence

2.2 Methods

2.2.1. Agarose gel electrophoresis

Agarose gel electrophoresis separates DNA fragments on the bases of their size/mass and was used to analyse the size of PCR fragments and purified plasmids. To prepare a 1% agarose gel, 0.5g of agarose crystals was dissolved in 50ml of diluted minigel buffer (20x), followed by boiling in the microwave to enable the agarose dissolve. The gel was heated in pauses while swirling to allow even distribution of heat. Heating was continued until the solution became clear with no agarose crystals seen in the flask. After cooling to about 60^{o}C, the gel was casted into a gel casting tray with a comb fitted in the tray to create loading wells. Following solidification of the gel, the comb was removed and the gel tray containing the solidified agarose gel was placed into the electrophoresis chamber. The electrophoresis buffer was filled

with the running buffer which enhances the movement of the DNA along the gel from the negative to the positive electrode. To enable visual monitoring of DNA migration along the gel during electrophoresis, 1ul of 6x DNA gel loading dye was added the plasmids and the total volume was made up to 6ul using TE buffer. The prepared samples were subsequently loaded into the wells together with a ladder (DNA fragments) of known molecular weight. After loading the samples, the electrophoresis was run at 95mA for 1 hr 30 min. The applied current enabled the movement of the DNA molecules. After the run, the gel was removed and stained with a fluorescent nucleic acid dye; GelRed® for 1 hour to enhance visualisation of the DNA under the UV light.

2.2.2. Bacterial transformation

Bacterial transformation is a method used for introducing plasmids into bacteria, and plasmids were transformed into competent *E. coli* to produce recombinant GST fusion proteins or for cloning purposes. In our research group, there are different strains of competent *E coli* bacteria prepared with calcium chloride to enhance binding of plasmid DNA to the bacterial wall and stored at -70^{o}C. Each strain of *E coli* is transformed based on the purpose. Hence, during transformation of the competent *E coli* bacteria, the bacteria stored at -70^{o}C were thawed on ice. Next, 50µl of the competent bacteria was put in a new Eppendorf tube and 2µl of the plasmid DNA added. The bacteria were incubated with the plasmids on ice for about 20 minutes to allow the DNA plasmids to bind on the cell wall. Afterwards, the bacteria were heat shocked for 2 minutes at 37^{o}C to create pores on the membrane that facilitates bacterial uptake of the plasmids that were already resting on the cell membrane. Following heat shocking, the bacteria were cooled for 2 minutes on ice to enhance recovery of the bacteria. The bacteria were then briefly grown for 1 hour in 300µl prewarmed antibiotic-free SOC media to allow the bacteria commence the expression of the plasmid with the antibiotic resistant gene. The bacteria were further plated on an LB plate containing ampicillin or kanamycin (antibiotics) for the plasmid selection and incubated overnight at 37^{o}C. A subculture was made from a single colony of bacteria from the LB plate.

2.2.3. Isolation and Purification of Plasmids DNA from bacteria cultures using GenElute™ plasmid Miniprep kit

This method of plasmid isolation and purification involves alkaline lysis of bacteria, followed by the binding of plasmid DNA onto a silica membrane in the presence of high salt, washing and elution of the bound DNA (80). Overnight bacterial cultures were harvested by centrifugation at 13000g for 1 minute and the supernatant discarded. The recombinant DNA

plasmids in the bacterial pallet were purified using the GenElute^{TM} plasmid Miniprep kit (Sigma-Aldrich) based on the manufacturer`s procedure, whereby the harvested bacterial culture was first resuspended in ribonucleases (RNAase) solution to enhance the degradation of RNA molecules. The resuspended bacterial cells were then lysed and bacterial chromosomal DNA or proteins precipitated with a neutralisation solution. Next, the precipitate was separated by centrifugation for 10 minutes, after which the cleared solution was transferred onto a prepared silica-based binding column and centrifuged. The column was washed once to remove the remaining contaminants. The washed DNA plasmid was then eluted from the binding column.

2.2.4. Measuring purity and concentration of the plasmid DNA

Nana drop 1000D spectrophotometer (Saveen Werner) was used to measure the concentration and evaluate the purity of the isolated plasmids. The analyser measures DNA concentration based on the absorbance of the UV-visible light by the DNA at an optical density (OD) of 260nm. The nucleic acid application in the nanodrop software was used for the measurements. Sample measurements were done following the manufacturer`s procedure. The elution buffer (2µl) was first run as the blank after which DNA concentration was measured from 2µl of plasmid DNA. The concentration and purity ratios of each sample were automatically calculated by the nano drop soft wear. The purity of the plasmids was assessed by evaluating the A_{260}/A_{280} and A_{260}/A_{230}ratios. An A260/A280 ratio between 1.8-1.9 was considered a pure DNA, ratio above 2 indicated the presence of RNA, while ratios lower that 1.8 indicated the presence of contaminants and proteins which absorbs at or near 280nm. A 260/A230 between 1.8-2.2 was considered a pure DNA, and below 2 indicated the possible presence of contaminants which absorbs at 230nm (81).

2.2.5. Polymerase chain reaction

Polymerase chain reaction (PCR) is an *in vitro* technique used to make multiple copies of a specific DNA segment from a sample containing this segment (parent DNA). PCR or a PCR-based cycling reaction was used for site-directed mutagenesis and for amplifying a cDNA fragment for BP cloning using the Gateway cloning system (Invitrogen). The components of a PCR technique includes: a forward primer, a reverse primer, parent DNA template, a thermal stable DNA polymerase, free nucleotides RNase free water and 10x reaction buffer (82). The PCR reaction begins with an initial heating for 2 minutes at 95^{o}C to initially denature the double stranded DNA and boost activation of the polymerase enzyme, followed by repeated thermal cycles for 18-35 cycles, depending on the purpose. The steps/conditions per thermal cycle

include: Denaturation of the parent DNA at a temperature of 95^{o}C for 30 seconds to produce single stranded DNA, followed by annealing of the primers to the separated strands for 1minute and extension of the complementary DNA strands at 72^{o}C by DNA polymerase. The extension temperature is polymerase specific, while the time of extension depends on the size of the DNA fragment being amplified (the PCR product) and its usually 1min/1kb. At the end of the last cycle, there is a final extension step for 5min or longer at 72^{o}C to allow the complete synthesis of many uncompleted amplicon or fill-in additional adenine residues to the 3` ends in all PCR products with the case of *Taq* polymerase. at the end of the final extension, the PCR reaction is terminated by chilling the mixture to 4^{o}C (82).

2.2.6. Plasmids and plasmid construction:

Most plasmids used in this study were obtained from the research group's plasmid archives (**Table 2.1)**. Nonetheless, a few were made during this study using site-directed mutagenesis or gateway cloning. The **Figure 5 and 6** below is a map of some of the plasmids used in this study

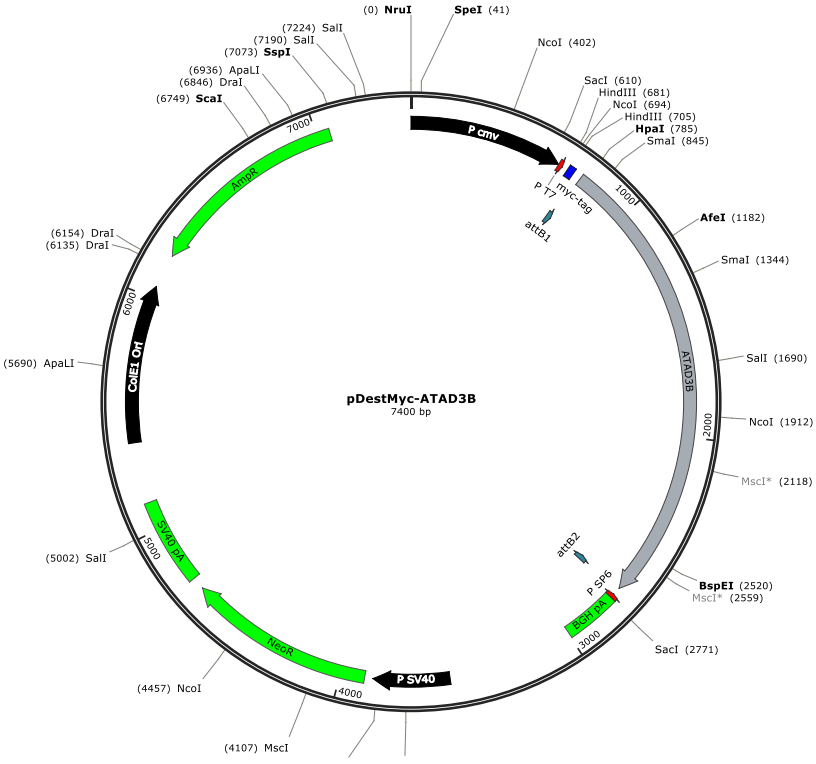

Figure 5: Diagram showing the map of pDestMyc-ATAD3B plasmid. pDest-Myc is the vector backbone, ATAD3B is the inserted gene (grey), Myc is the fusion tag (blue) and it is inserted N terminal of the inserted gene. Ampicillin (AmpR) is the selection marker.

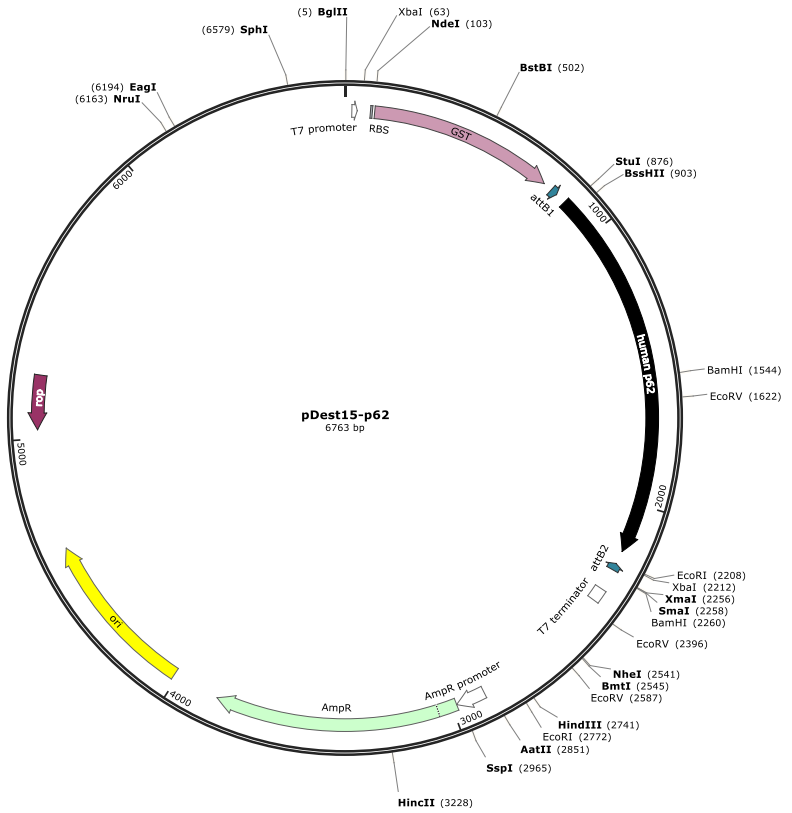

Figure 6: Diagram showing the map of pDest15-p62 plasmid. pDEST15 is the vector backbone, p62 is the inserted gene (black), GST is the fusion tag (purple) and it is inserted N terminal of the inserted gene. Ampicillin (AmpR) is the selection marker (green). The origin of replication depicted in yellow

2.2.6.1. Site-directed Mutagenesis

Site directed mutagenesis is a polymerase chain reaction (PCR) method to induce mutation on specific nucleotides of a plasmid (83). In this study, this method was used to make mutant plasmid constructs having an early stop codon at the nucleotides of interest. Hence, in light of these, forward and reverse mutagenic DNA primers (oligonucleotides) that induced early termination codons at the desired sites on the ATAD3B genes were designed using QuickChange Primer design program (https://www.agilent.com/store/primerDesignProgram.jsp) **Table 2.3**. The mutant DNA of interest was produced using the Quikchange site-directed mutagenesis kit based on the manufacturer procedure. In which case the reaction components, DNA plasmid and the primers were mixed together (**Table 2.11**).

Table 2.11: Reaction components for site-directed mutagenesis

Reaction components	Quantity (25ul total vol)
10x reaction buffer	2.5µl
DNA template	30ng
Forward primer 10µM	1.3 µl
Reverse primer 10µM	1.3 µl
DMSO	0.5 µl
dNTP 10mM	0.5 µl
Pfu polymerase	0.5 µl
RNase free water	To make a total volume of 25 µl

The pfu polymerase was the last component to be added into the mixture, in order to prevent degradation of the primers by the enzyme. Dimethyl sulfoxide (DMSO) was used for optimisation of the reaction. Following mixing of the reaction components, a PCR was setup using the following program in **Table 2.12**.

Table 2.12: PCR program used for site directed mutagenesis

Steps	**Duration**
1. Initial heating at 95^{o}C	2min
2. Denaturation at 95^{o}C	30 sec
3. Annealing at 58-65^{o}C (depends on the Tm of the primers used)	1min
4. Extension by pfu polymerase at 72^{o}C	2min/kb
5. Final extension at 72^{o}C	10min
6. Reaction termination	4^{o}C

After the initial heating for 2 minutes (**step 1**), step 2-4 were repeated 18 times, followed by a final extension for 10 minutes (**step 5**) and termination of the reaction (**step 6**). The PCR products were subsequently incubated with 1µl Dpn 1 endonucleases enzyme for 1hour at 37^{o}C to digest parental methylated and hemi-methylated DNA present in the PCR products. Next, competent DH5 alpha bacteria were transformed with the mutagenic plasmids to make multiple copies of the plasmids. Overnight cultures were set up from a single colony and the plasmids were purified from the bacteria using GenElute^{TM} plasmid Miniprep kit. The size of plasmids were then analysed by agarose gel electrophoresis. Plasmids with corresponding sizes were sent for sequencing at the UiT's Medical Genetics facility. Sequencing results were analysed using the BioEdit program to evaluate if the desired mutation was inserted. **Figure 7** below shows the summary of the steps involved to construct a site-directed mutagenic plasmid.

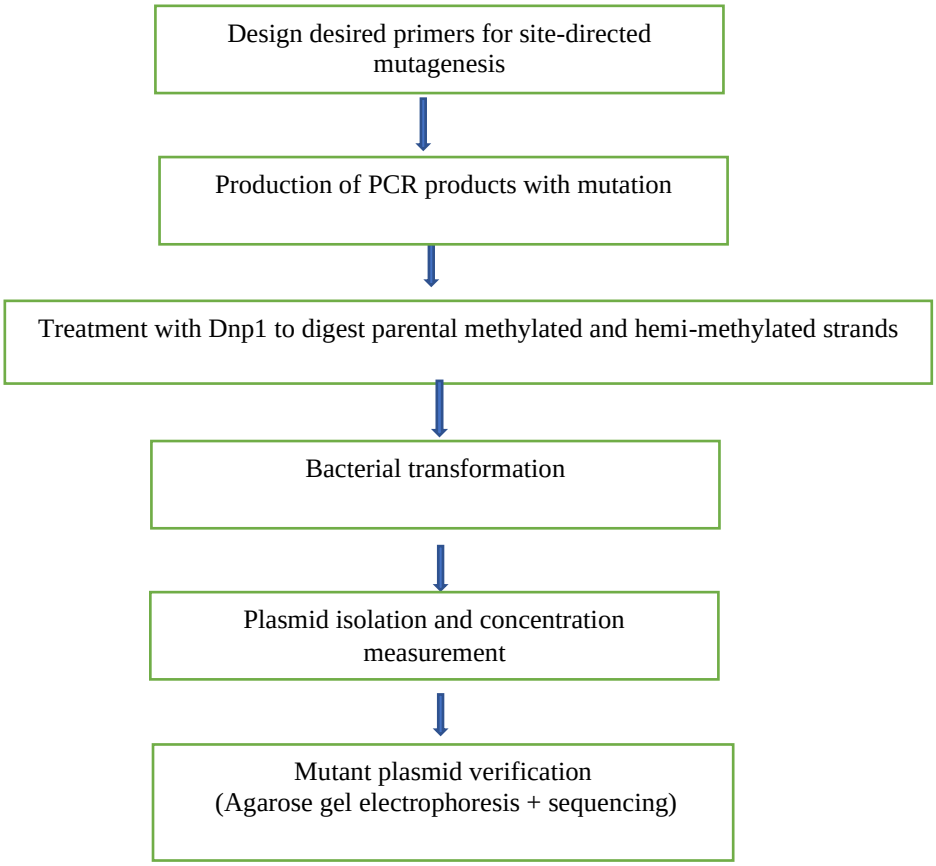

Figure 7: **A flow chart for the summary of the steps to make site-directed mutagenic constructs**

2.2.6.2. Construction of gateway clones by gateway recombination cloning system (Invitrogen)

Gateway cloning allows DNA fragments to be easily inserted into a vector or be transferred from one vector into another by site-directed recombination (84). The gateway system depends on two types of recombination; the BP reaction using the BP clonase recombination system and the LR reaction using the LR clonase recombination system. Described below is the protocol for PCR amplification and purification of a cDNA fragment with flanking attB sequences, followed by a BP reaction where the cDNA fragment is inserted into the DONOR vector pDONR221.

PCR amplification and purification of cDNA fragment with flanking attB sequences

Primers with attB-flanked ends (***att***- recombination sequence) targeted for the amplification of the cDNA fragment of interest were designed using the using the OligoPerfect Primer Designer program on Thermo Fisher scientific (https://apps.thermofisher.com/apps/oligoperfect/#!/design). The DNA fragment was amplified

using phusion® high fidelity polymerase kit from New England BioLabs *inc*, according to the manufacturer`s procedure. The reaction components included

Table2.13: Reaction components for DNA amplification by phusion® high fidelity polymerase

Reaction components	Volume (total volume 20 µl)
5x Phusion buffer	4µl
DNA template	50ng
Forward primer 10µM	1µl
Reverse primer 10µM	1µl
dNTP 10mM	0.4 µl
DMSO	0.5 µl
phusion® high fidelity polymerase	0.3µl
RNase free water	To 20µl mark

Following mixing of the components, a PCR was setup, beginning with an initial heating for 30 seconds. The DNA fragment was amplified through 34cycles of thermal cycling reactions comprising of step 2 to 4 as indicated in **Table 2.14** below. The extension time was allowed for 30 seconds, since the size of the region to be amplified on the parent DNA is about 600bp. DMSO was added to the reaction mixture to optimise the reactions to achieve a higher yield of the amplicon. The reaction was terminated at by decreasing the temperature to 4^{o}C

Table 2.14: PCR program used for DNA fragment amplification

Steps	Duration
1. Initial heating at 98^{o}C	30sec
2. Denaturation at 98^{o}C	30 sec
3. Annealing at 65^{o}C (depends on the Tm of the primers used)	15sec
4. Extension by pfu polymerase at 72^{o}C	30sec
5. Final extension at 72^{o}C	10min
6. Reaction termination	4^{o}C

After the PCR amplification, the amplicons were cleaned up using GenElute™ PCR clean up kit as per the manufacturer`s procedure to remove any form of impurities. During this clean-up process, separation columns were prepared to enhance the binding of the DNA to the column. After which the DNA was pre-incubated with a binding solution to enhance its binding to the prepared column. The pre-incubated DNA was then put in the separation column and centrifuged at a very high speed for 1 min. The bound DNA is washed and dried. The DNA was then eluted, and its concentration measured using nanodrop. Next, an agarose gel

electrophoresis was done to verify that the expected amplicon was obtained by evaluating its size. Secondly, an agarose gel electrophoresis was done to further purify the amplicon from the left-over impurities. All the pre-cleared DNA fragment with 644bp was then ran on a 2% agarose gel at 95mA. The gel was stained with 1ul GelRed® for 1 hour to increase visualisation of the bands. Next, a band with a size corresponding to the expected size (slightly above the 500bp band of the ladder) was excised, chopped into tiny pieces and put in a column prewashed with Tris-EDTA (TE) buffer. DNA was extracted by centrifuging at 21000g for 10 minutes at 4ºC. The TE buffer was used to prepare the column because it enhances DNA solubility and protects it from degradation during centrifugation.

Production of an entry clone by a gateway BP clonase recombination

In a Gateway BP recombination reaction, the BP recombinase enzyme recombines the attB sites of a PCR fragment or expression clone with the attP sites of a Gateway donor vector, swapping the gateway cassette with the selected fragment to produce an entry clone flanked by attL sites. This recombination reaction is unidirectional as attB1 recombines with attP1 and attB2 recombines with attP2 (85). This method was used in this study to insert the purified cDNA fragment into the gateway cloning vector pDONR221. In the BP reaction, 150ng of the pDONR221 vector, 150ng of the amplified DNA, and 2µl BP clonase enzyme were mixed and incubated for 1hr at 25ºC. The BP recombination reaction was terminated by degrading (digesting) the BP clonase with proteinase K for 10 minutes at 37ºC. Competent DH5 alpha *E coli* bacteria strain was subsequently transformed with the BP clonase recombination product, and overnight cultures prepared from single colonies of bacteria. Plasmids were then isolated and purified using the gene elute miniprep kit, followed by DNA sequencing to verify the sequence of the amplified DNA fragment obtained. The BioEdit software was used to analyse the sequenced plasmid.

2.2.7. Sodium Dodecyl Sulfate-Polyacrylamide Gel Electrophoresis (SDS-PAGE)

In SDS-PAGE, proteins are separated based on their sizes (molecular mass) via an electric current. Polyacrylamide gels used in SDS-PAGE consist of a stacking and a separating gel. The stacking gel concentrates the proteins before they enter the separating gel, while the separating gel separates the proteins based on their size. In this study, SDS-PAGE was used to test the yields of GST fusion proteins after immobilization on glutathione sepharose beads and analyse proteins after GST pulldown assays or western blot experiments. The acrylamide concentration used were 4% for the stacking gel and 8% 10%, 14% or 16% for the separating gel (depending

on the molecular weight of the proteins being analysed). The gels were prepared by mixing water with 4x separating buffer or 4x stacking buffer (¼ the total volume required), and acrylamide added to the required final concentration. Gels were polymerised with a final concentration of 0.01% Ammonium persulfate (cross linking agent) and 0.15% N,N,N',N'-tetramethylethylenediamine (catalyst). The separating gel was first prepared and casted into the assembled electrophoresis cassette. The cassette was filled with deionised water prior to polymerisation to remove unwanted air bubbles present in the gel and completely level the surface of the gel. The gel was then allowed to polymerise for 10 minutes. The stacking gel with a lower concentration of acrylamide was prepared and casted over the separating gel. A comb was inserted into the stacking gel to create loading wells after the gel polymerises. Next, protein samples to be tested on the SDS-PAGE was prepared by boiling them with 10µl sample buffer (**Table 2.9**) at 100^{o}C for 5 minutes to fully denature the proteins. The samples were cooled and loaded into the wells of the gel. The cassette containing the gel was mounted into the electrophoretic chamber. The chamber was subsequently filled with the running buffer, connected to a running tap and an electric current applied at 20 mA per gel for 1 hour. The electric current enabled migration of the proteins through the gel from the negative to the positive terminal. After electrophoresis, subsequent processing of the gel also depended on the purpose.

2.2.8. Protein -protein interaction studies

The interaction between all the ATAD3 constructs and autophagic markers were evaluated by performing in vitro GST pulldown assays. In order to do this, three main steps were done. Firstly, the GST-fusion proteins were produced in bacteria and immobilised on glutathione sepharose beads. Secondly, ^{35}S methionine radiolabelled ATAD3 constructs were synthesised *in vitro,* using methionine-free reticulocyte (Promaga). Lastly, binding of the radiolabelled *in vitro* synthesised proteins to the immobilised GST-fusion protein were tested by *in vitro* GST pulldown assays followed by SDS-PAGE to enable detection of the co-precipitated radiolabelled proteins by autoradiography.

2.2.8.1. Bacterial expression and immobilization of recombinant GST-proteins

E coli is one of the most used host to produce recombinant proteins due to the fact that it is inexpensive, fast growing and give a high yield of protein (86, 87). Nonetheless, *E coli* as a bacterial system do not have all the necessary enzymatic machinery necessary for post-translational modifications as well as protein folding, and it is often prone to metabolic burden resulting from high protein expression (88). Thus, this makes *E coli* limited in expressing

soluble biological functional proteins which results in the formation of inclusion bodies of the proteins due to misfolding of the proteins. As such, genetically engineered *E coli* strains have been produced to improve protein solubility *in vivo*, for example the soluBL21(DE3) strains of *E coli* is being used to facilitate the production of cytoplasmic proteins that are prone to aggregate formation when expressed in the standard *E coli* DE3 strains. Similarly, fusion partners such as maltose binding protein (MBP), His-tag, NusA and GST are used to enhance solubility of the protein expressed. These fusion partners also facilitate the purification of these proteins from the whole cell lysate (86, 88).

In this study, the autophagic related proteins were produced and extracted as GST-fusion proteins. The bacterial strain *E. coli* BL21 was used for production of GST, while the bacterial strains *E coli* BL21 (DE3) and *E coli* soluBL21 (DE3) were used to produce the other GST-fusion proteins. The different bacterial strains expressing the various proteins of interest with GST tag were streak on an LB agar plate containing 100µg ampicillin. A colony of each bacteria were used to produce overnight culture in 5ml of LB media with ampicillin at 37^{o}C on a shaker. The overnight culture was transferred to a 100ml 2xYT agar (having a higher nutrient content than the LB media) and allowed to grow while bacterial growth was being monitored by measuring the absorbance at an optical density (OD) of 600. At an absorbance between 0.6-0.9, protein production was induced with 0.5mM isopropyl β-D-1-thiogalactopyranoside (IPTG). Upon induction of protein synthesis, the bacteria were transferred to room temperature to reduce the formation of recombinant protein aggregates, which is mostly favoured under higher temperatures (86, 88). The bacteria were then allowed to grow at room temperature for 4hrs to allow protein synthesis. The bacteria expressing the GST-fusion proteins were harvested by centrifuging at 4^{o}C for 10min at 5000rpm.

In order to purify the GST-fusion proteins from the harvested bacteria, the bacterial cell wall and membrane were ruptured. The harvested bacteria were chemically and enzymatically lysed by adding 4ml of the lysis solution containing lysosome, EDTA, DTT, Tris-CL, NaCl (**Table2.9**). Lysozyme is an enzyme that disrupts the bacterial cell wall by degrading the glycosidic bond of the crosslinked peptidoglycan. Tris-HCl was included to alter the pH of the cell membrane, thereby making it more prone to break. DTT served as reducing agent that prevents intramolecular and intermolecular disulphide bonds formation, and EDTA was used as a protease inhibitor to protect the GST-fusion proteins from proteolytic degradation during the purification process (89). The mixture (bacteria + cell lysis solution) was then resuspended and incubated on ice for at least 20min to allow cell wall disruption by the enzyme, before

adding 140ul of 10% Triton X-100 which ruptures the bacterial cell membrane. The lysate was subsequently frozen overnight at -70°C followed by thawing on ice and sonication the next day. The sonication was done on ice in 3 repeats for 30 seconds each at a pause of 10 seconds, and was done to physically lyse the bacteria (89).

Following bacterial lysis, the lysate was centrifuged at 13000g for 10 minutes at 4°C and the pellets discarded. Next, glutathione sepharose beads were used to isolate and immobilize the GST-fusion proteins from the mixture of proteins in the suspension. The glutathione sepharose beads and the suspension were incubated on a rotator for 1 hour at 4°C. Purification of GST-fusion proteins was based on the binding affinity of the GST to glutathione. After the incubation, the mixture was centrifuged and the supernatant discarded, leaving the GST-fusion protein attached to the glutathione sepharose beads. Beads were washed 3x with PBS and the 4th wash with NETN buffer. The GST-fusion proteins were resuspended in NETN buffer with protease inhibitor to prevent easy degradation of protein during long term storage. Protein identification as well as their level of protein expression (abundance) was detected using SDS-PAGE (**Figure 8**). Images of the stained gels were taken using UV transilluminator.

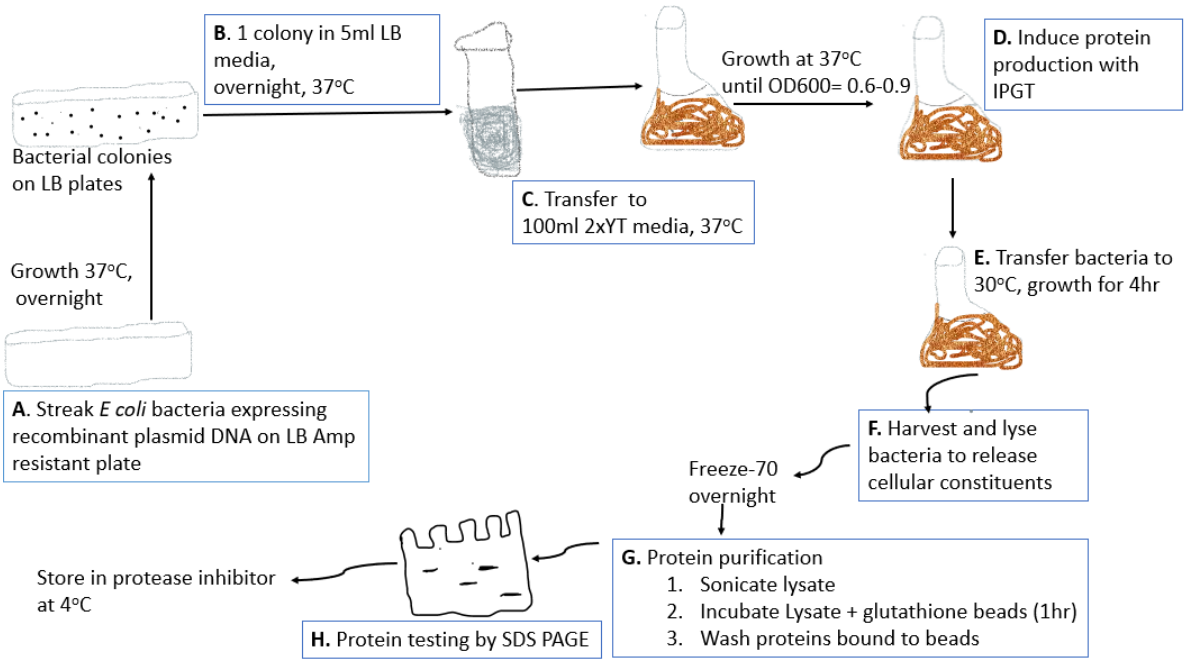

Figure 8: A schematic presentation of the steps in the production of GST-fusion proteins. Steps from streaking of *E coli* bacteria expressing the plasmid of interest on the LB plate to testing of the extracted proteins.

2.2.8.2. In vitro synthesis of ^{35}Sradiolabelled proteins

Recombinant ATAD3A and its C-terminal have reported difficult to be produce in a functional state in bacteria (90), as such these proteins were produced *in vitro* using the rabbit reticulolycte system (Promega). In this system, proteins are produced from plasmid DNA, that is first transcribed by T7 polymerase and then translated by ribosomes present in the reticulocyte lysate. The pDest-Myc vector used to make the ATAD3 constructs, has a T7 promoter (immediately upstream of the Myc-tag sequence) to which the T7 polymerase binds to and initiate transcription. The plasmids (250ng/µl each per reaction) were *in vitro* transcribed and translated in the presence of radiolabelled ^{35}S (methionine), T7 polymerase and a TNT® T7 reticulocyte Lystate system without methionine. 10µl of the *in vitro* translated radiolabelled ^{35}S-myc-tagged radiolabelled proteins or mutant proteins were pre-cleared for 30 minutes at 4^{o}C by incubating with 10 µl empty glutathione sepharose beads and 100 µl of NETN buffer supplemented with EDTA free protease inhibitor. Preclearing was done to remove any non-specific binding, and the protease inhibitor added during preclearing of the proteins was to prevent digestion of the proteins.

2.2.8.3. GST-pulldown assay

It is an *in vitro* method used in this study to test for the interaction between *in vitro*-synthesised proteins and GST-fusion proteins immobilised on glutathione sepharose beads. In each experiment, the amount of beads were adjusted to secure that approximately equal amounts of the different GST-fusion proteins were added. Beads with immobilized GST fusion proteins were mixed with *in vitro* translated ^{35}S-methionine labelled proteins and then incubated on rotation at 4^{o}C for 1 hour and subsequently washed 5 times to remove unbound proteins. The GST-fusion proteins complexes were eluted from the glutathione beads by adding the sample buffer (4 parts of 2x SDS loading buffer and 1 part of DTT) and fractionated by 10%-14% SDS-PAGE, depending on the size of proteins. At the end of the electrophoretic run, gels were fixed for 10 minutes and stained with Coomassie blue overnight to visualize the GST fusion proteins. The gel was de-stained in a de-stain solution 1 for 1 hour and de-stain solution 2 for 1 hour and images for the GST-proteins taken using M-26 Transilluminator. After which gels were dried using model 583 gel dryer. Samples were ran with a 10% input of the *in vitro* translated protein as a control. ^{35}S-methionine labelled proteins on the gel were detected by autoradiography (**Figure 9**), in which images were developed using Fuljifilm Bas-MS 2025 imaging plate and analysed using a FUJIFILM BAS-5000 analyser. Images were taken at a resolution of 100 and 16 bit. Detection by autoradiography enabled the quantification of the binding capacity of the

in vitro translated radiolabelled proteins to the GST-fusion proteins, based on the radioactive signal produced per pull down reaction (91). The quality, reproducibility and consistency of the NETN buffer used for the pulldown was controlled during each batch of pull-down reaction by loading a GST-fusion protein washed trice with the NETN buffer. The percentage binding was estimated by calculating the relative average signal per band.

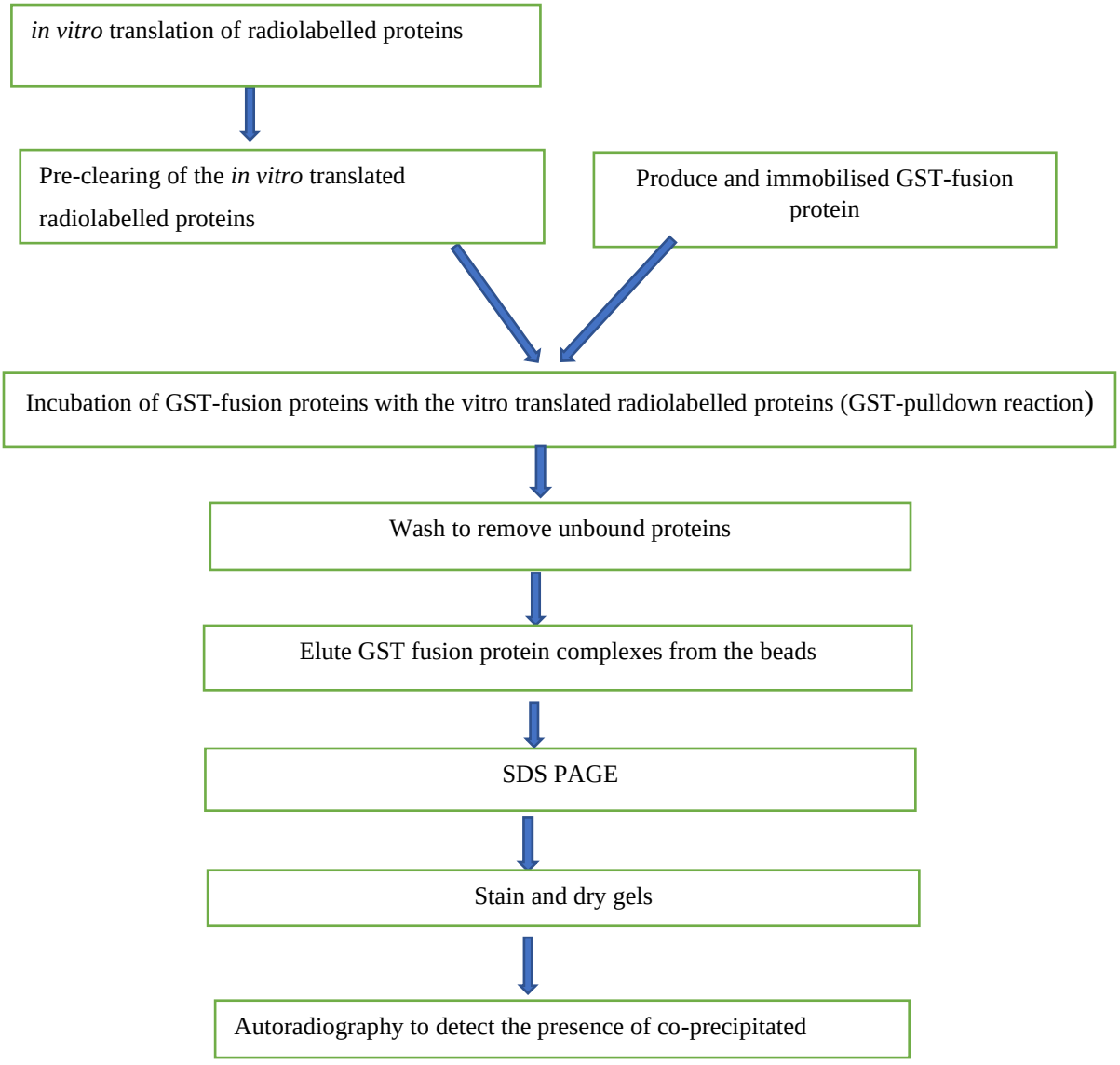

Figure 9: A flow chart showing a summary of the steps in testing for the protein-protein interactions *in vitro*.

2.2.9. Mammalian Cell culturing and maintenance

Mammalian cell culture refers to the process of growing human cells *in vitro* in a flask or dish (92). This technique is used for cytogenetic, biochemical, molecular and diagnostic studies. During cell culturing, adherence to aseptic techniques that prevent contamination and loss of cells is required for a long-term maintenance of the cell's viability (93). In this study, Flp-in T-Rex Hela cells were cultured in T75 flask. Cell growth media were prepared by supplementing Dulbecco`s Modified Eegle`s medium (DMEM) (low glucose and L-glutamine) with 10% fetal bovine serum (FBS) to enhance growth and 1% penicillin and streptomycin antibiotic to avoid microbial growth. Cell were kept alive and growth maintained by passing 10% of the cells twice per week. Cell passage involves detaching of the cultured cells from the surface of the current culturing vessels and subsequent transfer of a subset of the cells into a new culture vessel (94, 95). The frequency of cell passage depends on the growth rate of individual cells (95). Cells were checked microscopically to monitor growth and viability of cells.

During cell passaging, the prepared cell culture media and trypsin were prewarmed by placing them in the incubator at 37^{o}C for a few minutes. The media bottles, culturing flask, falcon tubes and pipette tips were sterilised with ethanol before placing them into an alcohol-cleaned hood to avoid contamination. The culturing media was suctioned out from the cells and cells were gently washed once with 1X PBS. Next, the cells were treated with trypsin and placed in the inhibitor for 3 minutes to detach them from the surface of the flask. After the cells have fully been detached, the trypsin was neutralised by adding 5ml of growth media. Cell suspension were later transferred into 15ml falcon tubes and centrifuged at 1000g for 3min. Supernatant was discarded, and pellets resuspended in 1ml culture media. 100µl of the resuspended cells were transferred into a new culturing flask containing 10ml of fresh growth media to provide fresh nutrients to cells and keep them healthy (95). Cells were gently mixed to allow even distribution of cells and placed in the incubator at 37^{o}C in 5% carbon dioxide for further propagation.

2.2.10. Cell transfection

Transfection is a method by which foreign/exogenous DNA are introduced into cells to make genetically modified cell (96, 97). Genetic materials can either be transiently introduced into the cell for a shorter period or stably introduced into the host genome which are being passed onto the progeny during cell division (97). This experimental tool enables the function and regulation of a gene and protein to be studied in cells (96, 97). In this study, both transient

and stable transfection were done. The flp-in T-rex Hela cells were transiently transfected with pDest-myc plasmids, while pDest flp-in plasmids were used for stable transfection. In both types, metafectene® Pro was used to enhance uptake of the plasmids into the cells.

2.2.10.1. Transient transfection of cells

3 x10^5cells/ml were seeded in a 6 well plate and allowed to grow in 2ml complete growth media for 16-24hrs. Cells in each of the wells were transfected with 2ng of the plasmid. Thus, to transfect a single well, 2ng of the plasmids were added in a 15ml falcon tube containing 200µl of serum-free Dulbecco`s Modified Eagle`s medium with low glucose and L-glutamine. Next, 4ul of metafectene was added to the plasmid in the tube. The mixture was incubated for 30min to allow the plasmid and metafectene to form a complex. The mixture was then gently added to the seeded flpn T-Rex Hela cells. The plate was slowly swirled to facilitate even distribution of the complexes within the well. Cells were grown for 24hrs at 37^{o}C in 5% carbon dioxide.

2.2.10.2. Stable transfection and generation of stable cell lines

Stable transfection was used to establish a stable cell lines for inducing over expression of our protein of interest. In contrast to transient transfection, for stable transfection, 1 x10^5 cells/ul were seeded in each well in a six well plate and the cells were transfected with either 1ng of pDest flp-in EGFP ATAD3A or 1ng of pDest flp-in EGFP ATAD3B. The cells in one of the wells served as a control and were not transfected. Forty-eight hours following transfection, the media was changed and all cells (in wells containing transfected cells and wells without transfected cells) were washed twice with 1x phosphate buffer saline (1x PBS). After which the cells expressing the pDest flp-in EGFP plasmids were selected by treating the cells (both transfected and control) first with 200µg/ml hygromycin and 10ug/ml blasticidin S HCL. Selection was done for about 14 days during which all the cells in the control well died. After which, the surviving stable cells in the other wells were grown in normal growth media for 24hrs and subsequently treated them 300µg/ml of hygromycin and 15ug/ml of Blasticidin S HCL for 4 days to further select cells that have a higher expression of the plasmid. The flp-in system enables stable expression of recombinant proteins in mammalian cells. This system allows the induction of gene expression in the presence of an inducer such as tetracycline or doxycycline under the control of the human CMV promoter (98). Following selection of cells stably expressing the plasmids, EGFP-tagged protein expression was induced using 1µg/ml of doxycycline and detected using confocal imaging and western blots. Some of the cells were freeze- stocked in 10%DMSO in FBS.

2.2.11. Cell harvesting

Cell harvesting and lysis are crucial for the study of the complexity of intracellular processes. Depending on the analysis following cell lysis, different methods of cell harvesting are used. In this study a detergent based lysis was used, which involves incorporation of the detergent in the cell membrane, formation of pores within the membrane followed by complete lysis of cells (99). Here, SDS was used as detergent to lyse cells and also to denature the released proteins. During harvesting of cells, cells were taken out of the incubator and the growth media aspirated. After which the adherent cells were washed three times with 1x PBS. Next, adherent cells were detached and lysed by adding 75ul of 1x SDS buffer (**table 2.10**). A plastic cell scrapper was used to scrape out cells from the surface and the viscous suspension transferred into an Eppendorf tube. The solution was later boiled at 100^{o}C to completely denature the proteins. Boiling of the sample was terminated when the solution had completely lost their viscosity. Lysates were stored at -20^{o}C for further analysis (100).

2.2.12. Total protein quantification by Pierce™ BCA Protein Assay

This is a colorimetric semi-endpoint method that detects and measures protein concentration using bicinchoninic acid (BSA). During the BCA assay, proteins in solution reduces the Cu^{2+} to Cu^{+} ion in an alkaline medium. The Cu+ ions further chelates with BCA to form a purple colour that is being detected. Protein concentration is quantified based on the intensity of the purple colour formed. The higher the intensity of the colour formed the greater the total protein concentration. In this study, the BSA assay was used to measure total protein concentration in order to estimate approximately equal amount of total proteins in the different experimental cell lysates. All measurements were done based on the manufacturer procedure. After harvesting cells with 1x SDS buffer, samples were diluted 10 times and aliquoted into the 96 well microplate. Protein standards of varying concentrations ranging from 2-0.025µg/ml were prepared with the same harvesting buffer (1x SDS buffer) and aliquoted into the 96 well microplate. The harvesting buffer was also used as the blank. The Cu^{2+} working reagent was prepared as per the manufacturer guide. Following preparation of the working reagent, samples and standards were incubated with the working reagent at 37^{o}C for 30 minutes, and absorbance read at 562nm using CLARIOstar® plus Microplate reader. All samples and standards were ran in duplicates. The mean value of the duplicates per sample/standard was determined. Next, a standard curve of mean absorbance value of the standards versus their respective concentrations was generated. The concentration of each test sample was interpolated from the standard curve generated based on the mean absorbance value of each sample. The final concentration of each

sample was determined by multiplying the values obtained from the curve by 10 (the dilution factor).

2.2.13. Western blotting analysis

Western blotting is an immunological detection method used detect the presence and abundance of the proteins of interest in the whole cell lysate after fragmentation of the proteins in the cell lysate by SDS-PAGE. After measurement of total protein concentration, approximately 20µg of the total protein in each sample were boiled for 10 minutes with 2x loading buffer containing DTT to enhance proper denaturation of the tertiary structure the proteins before running samples on SDS PAGE. Samples were loaded on the gel alongside a stained protein ladder and a biotinylated ladder. Different percentages; ranging from 8-16% of thick gels were made, depending on the molecular mass of the protein to be detected. The gel was ran at 30mA/gel for 1hour. Next, the proteins in the gel were then electro-transferred to a nitrocellulose membrane to enhance exposure of the proteins for easy accessibility by the antibodies. The transfer was done for 15min at 13A and 25V using 1x transfer buffer. One of the precautions taken during preparation of the sandwich for the transfer, was getting rid of air bobbles which could interfere with the transfer of proteins from the gel to the membrane. After transfer of proteins, the membrane was washed in distilled water for 10 minutes to remove debris before staining with Ponceau S stain to visualised if proteins were properly transferred onto the membrane. Possible unspecific binding of the primary antibody to other proteins was blocked by incubating the membrane with 5% blocking milk in PBS-T for 30 minutes. The blocked membrane was then washed in PBS-T for 10min and incubated overnight at 4^{o}C with the appropriate primary antibody against the specific protein. The next day, the membrane was washed with PBS-T to remove unbound antibodies and incubated with HRP-labelled secondary antibodies directed against the primary antibody and anti-biotin directed against the biotinylated ladder. Another washing was done 3 times for 10min each to remove unbound secondary antibody. Membrane was then incubated with HRP-superSignal^{TM} West Pico PLUS chemiluminescent substrate, which binds to the HRP-labelled secondary antibody. The substrate was prepared based on the manufacturer instructions. Protein detection was done by chemiluminescence using Imagequant LAS 4000 LAS (**figure 10)**. The intensity of each band was quantified using Image J.

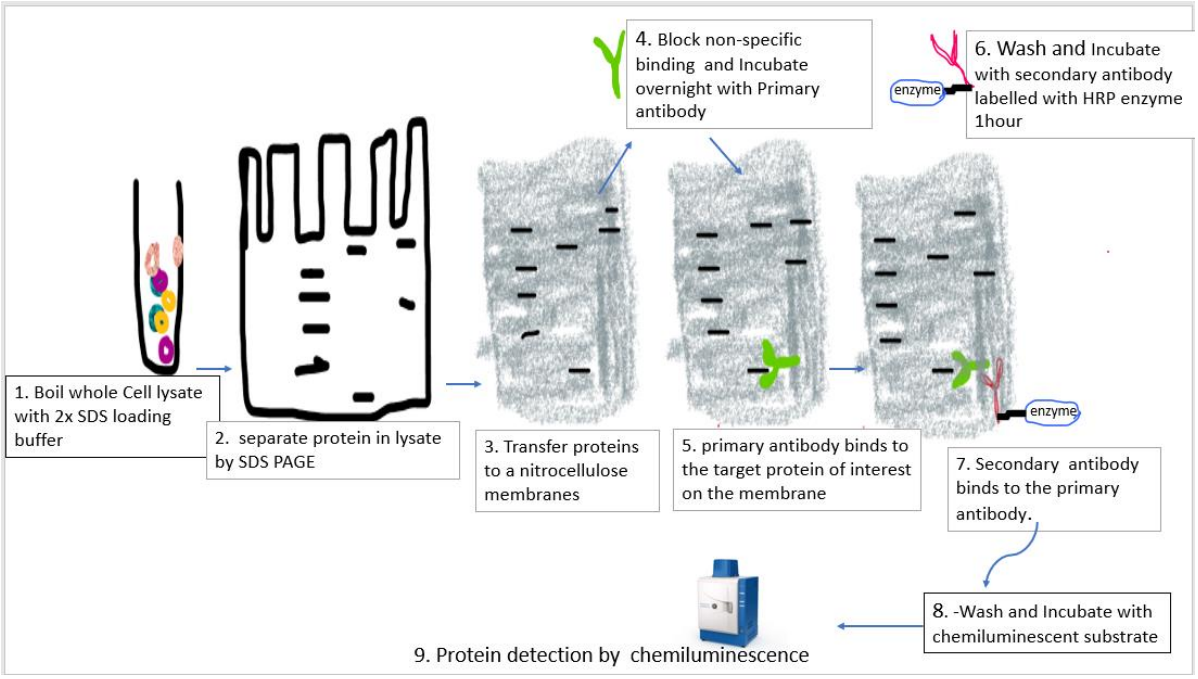

Figure 10: A schematic presentation of the procedure used for the detection of protein in a cell lysate. Steps from sample preparation for SDS PAGE to protein detection by chemiluminescence

2.2.14. Immunofluorescence and confocal microscopy

Immunofluorescence is a method used to detect the cellular localisation and distribution of a molecule/protein by using a specific antibody directed against the target protein of interest (101, 102). During immunofluorescence analysis of cells, confocal microscope is used for the visualisation of the protein-antibody complexes through immunofluorescence from the fluorophore-conjugated secondary antibodies targeted against the primary antibody (101). For immunofluorescence analysis, approximately $1x10^5$ cells/ml were seeded on coverslips placed in a 24 well falcon plate and allowed to grow for 48 hours. Cells were immediately fixed with 4% paraformaldehyde after removal of cell culture media to preserve cellular morphology and integrity. In order to establish which fixation is better for retaining the cellular distribution and staining pattern of the proteins and maintaining the morphology of the mitochondria, 2 types of fixation conditions were made: fixation at room temperature with 4% paraformaldehyde and fixation at 37^{o}C with pre-warmed 4% paraformaldehyde. After fixation, cells were permeabilised to sufficiently disrupt the cell membranes in order to enhance access of the antibodies into subcellular locations and ensure their access to the epitope of the proteins (102, 103). As such, ice-cold methanol and 0.1% of Triton x-100 were used to permeabilised the cells in order to evaluate which is a better permeabilization reagent for the protein of interest. The permeabilised cells were later washed three times with 1x PBS and nonspecific binding of the primary antibody to other cellular components were blocked, by incubating the cells with 3%

goat serum in PBS for 1hr. Following blocking of unspecific binding, the proteins of interest were immunolabeled by incubating the cells with the respective primary antibodies for an hour. Unbound primary antibodies were washed away, and the cells were further incubated for another 1 hour with fluorescent-tagged secondary antibodies directed against the primary antibody (**Table 2.8).** Moreover, control cells were stained only with the secondary antibody to assess for any nonspecific binding of the secondary antibodies. The nuclei were also stained with DAPI (102). Coverslips with seeded cells were mounted on slides using mowiol. Images were taken using ZIESS LSM800 confocal microscopy using oil immersion objective 60x.

Table 2.15: Pre-staining conditions tested used in cells

Different experimental conditions tested	Cell Fixation	Cell permeabilization
1	Room temperature with 4% paraformaldehyde	Ice cold methanol
2	37^{o}C with pre-warmed paraformaldehyde	Ice cold methanol
3	37^{o}C with pre-warmed paraformaldehyde	0.1% triton x-100 in PBS

Chapter 3

Results

3.1. Characterising the binding between ATAD3A and ATAD3B and autophagy related proteins

In this study, the human ATAD3B isoform 1 comprising of 648 amino acids (NCBI protein ID NP_114127.3) and the human ATAD3A isoform 2 comprising of 586 amino acid (NCBI protein ID NP 001164006.1) were used. Available data have demonstrated that ATAD3 proteins may be involved in the regulation of autophagy and mitophagy (20, 64). Recent studies in the group on co-immunoprecipitation experiments using CALCOCO1 stably expressed in HEK293 cells as bait, followed by mass spectrometry to identify the interacting partners, revealed that endogenous ATAD3A and ATAD3B interacts with CALCOCO1. Furthermore, this study suggested that CALCOCO1 may function as a selective autophagy receptor (Nthiga *et al*., 2020, submitted to EMBO Journal). Subsequent *in vitro* assays also supported a binding between CALCOCO1 and full length ATAD3A and ATAD3B, while other preliminary experiments also showed interactions of ATAD3A and ATAD3B with p62, NDP52, and the human ATG8 proteins (LC3A LC3B, LC3C, GABARAP, GABARAP like 1, GABARAP like 2) (data not published). As a result, several deletion constructs of ATAD3B were made but were never used. From these findings, it was hypothesised that ATAD3 proteins may have a direct role in regulating autophagy or mitophagy. Consequently, this study was geared to characterise these interactions, and to evaluate if the interaction was essential for either the degradation of ATAD3 itself by autophagy, or for the proposed role of ATAD3 in regulating autophagy or mitophagy.

3.1.1. ATAD3 proteins binds directly to the ATG8 proteins

To verify the observed interactions of ATAD3A and ATAD3B with human ATG8 (hATG8) proteins, GST pulldown analysis were done. Each hATG8 protein was produced as GST-fusion proteins in *E coli* and extracted on beads as baits, while ATAD3A (isoform 2) and ATAD3B (isoform 1) were *in vitro* translated using the reticulocyte lysate system and ^{35}S methionine. Next, a GST pulldown assay was done to test for binding. Protein complexes were eluted from beads and separated by SDS-PAGE, GST and GST-ATG8 proteins were detected by Coomassie blue staining, while the co-precipitated radiolabelled ATAD3 proteins were detected by autoradiography. Based on *in vitro* GST pulldown analysis followed by autoradiography, it was revealed that radiolabelled ATAD3A and ATAD3B directly interacts

with the ATG8 proteins *in vitro.* Both proteins exhibited a stronger interaction with GST-ATG8 proteins than with GST (negative control), indicating a specific interaction. By quantifying the percentage binding capacity, it was revealed that ATAD3A binds slightly stronger than ATAD3B. In addition, ATAD3A and ATAD3B showed a similar binding pattern to the ATG8 family, where both binds better to GABARAP like-1 followed by GABARAP and LC3A **(Figure 11B),** which is contrary to what has been reported for most ATG8 interacting partners like members of the ULK1 complex and ATAG13 that binds stronger to GABARAP, GABARAP L1, GABARAPL2 and LC3C (45).

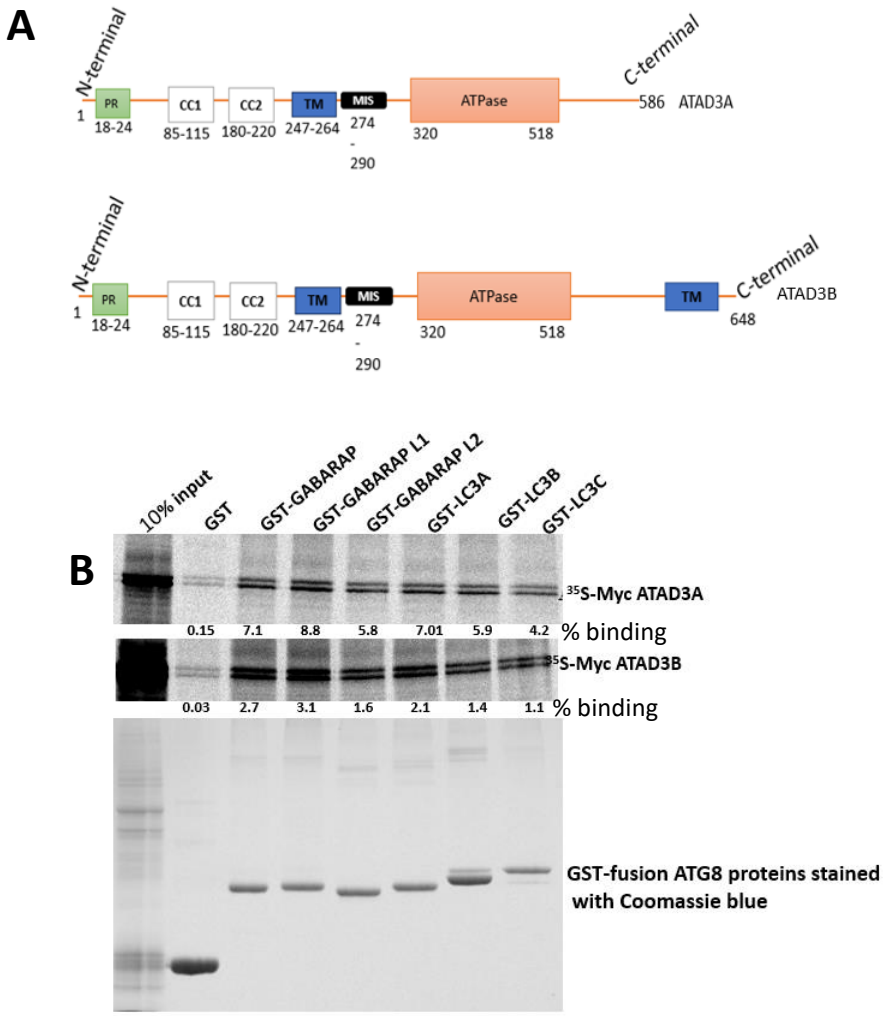

Figure 11: **Human ATAD3A and ATAD3B interact with ATG8 proteins *in vitro***.

A. Presentation of the various domains/motifs of ATAD3A and ATAD3B.

B. *In vitro* GST pulldown assay conducted to test for the interaction between *in vitro* translated ^{35}S radiolabelled ATAD3A and ATAD3B full length and GST-tagged human ATG8 proteins. GST-tagged ATG8 proteins were produced from *E coli* and immobilised on beads as baits. ATAD3 proteins were radioactively synthesised using Rabbit reticulocyte system and ^{35}S methionine. GST-fusion proteins and radiolabelled ATAD3A or ATAD3B incubated. Following pulldown, proteins were washed, eluted and separated through SDS-PAGE. Coomassie brilliant blue stains was used to visualise GST and the GST-fusion proteins on the gel. The co-precipitated radiolabelled myc-ATAD3A and myc-ATAD3B were detected by autoradiography. Numbers on each band lane represent % binding of ATAD3A or ATAD3B to the respective GST-fusion proteins.

3.1.2. The ATPase domain of ATAD3B is necessary for its interaction with GABARAP and LC3B

Only ATAD3B mutant constructs were used to map the region of the protein necessary for the binding because both ATAD3A and ATAD3B have very similar sequences. In addition, the ATAD3B isoform used has 62 additional amino acid in its C-terminal which might confer an additional biochemical property to ATAD3B (52, 54). Considering that ATG8 proteins are localised mainly in the cytosol, it was hypothesised that the region of ATAD3B that extends to the cytosol may be responsible for its binding. In this regard, a construct without the extended C-terminal part (^{35}S myc-ATAD3B 1-518) was made by inserting an early stop codon at A519 using site-directed mutagenesis. ^{35}S myc-ATAD3B 1-518 together with other available deleted and N-terminal truncated mutants of ATAD3B were *in vitro* translated and tested against full length GST-LC3B and GST-GABARAP on beads, in order to map out the domain that mediates its binding to the hATG8 family proteins **(Figure 12A)**. Hence, the following deleted and truncated ATAD3B mutants were used **(Figure 12B)**:

- ^{35}S-myc ATAD3B Δ1-50 with out the first 50 amino acid of the N-terminal,
- ^{35}S-myc ATAD3B Δ50-320 which lacks the coil-coil region, the transmembrane region and the MIS,
- ^{35}S-myc ATAD3B Δ321-518 which lacks the ATPase domain.
- ^{35}S-myc ATAD3B 1-518 without the last C-terminal 130 amino acid

Following *in vitro* GST pulldown analysis, quantifying the % binding per mutant construct demonstrated that deletion of the different regions affected the binding of ATAD3B to the LC3B and GABARAP, making a precise conclusion challenging. However, the greatest loss of binding capacity was observed upon deletion of the ATPase domain, in which the amount of ATAD3B mutant captured during the GST pulldown reaction got reduced by approximately 80% (**Figure 12B and 12C)**. Thus, suggesting that the interaction of ATAD3B with LC3B and GABARAP might be mediated by the ATPase domain that is embedded in the mitochondrial matrix. To further show that the ATPase domain mediates this interaction, gateway cloning method was used to make a pDest-myc ATAD3B (320-518) construct consisting of only the ATPase domain of ATAD3B. Nonetheless, construction of the plasmid was unsuccessful because the entry clone (pDONR ATAD3B 320-518) produced by BP reaction was out of frame, thus could not be used to produce the expression clone pDest-myc ATAD3B (320-519).

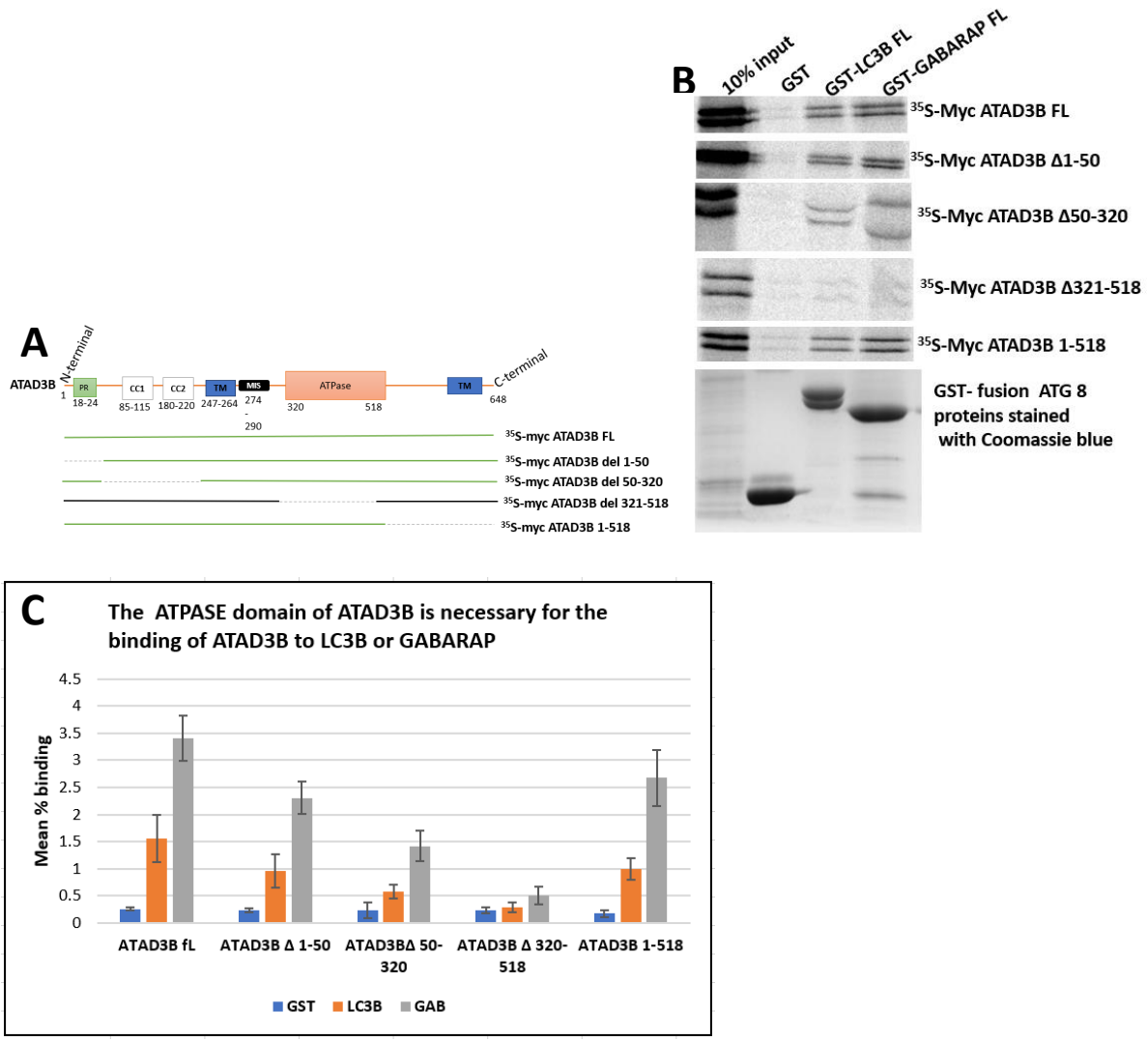

Figure 12: The ATPase domain of ATAD3B is required for its interaction with GABARAP and LC3B.

A. A presentation of the domain architecture of ATAD3B. The various deleted and truncated ATAD3B mutant constructs were used during GST pulldown assays to map its interaction with LC3 and GABARAP are shown. The broken lines represent regions of ATAD3B deleted and the construct with no binding is indicated in black.

B. GST pulldown analysis to map the region of ATAD3B necessary for its binding to the LC3 and GAGABRAP. ATAD3B mutant proteins were radioactively synthesised *in vitro* using rabbit reticulocyte system and ^{35}S methionine and tested for binding to the GST-LC3B and GST-GABARAP on beads by performing *in vitro* GST pulldown assay. After which proteins were washed, eluted from beads and fragmented on SDS PAGE. GST, GST-LC3B and GST-GABARAP were detected by Coomassie blue stain. The bound ATAD3B proteins detected by autoradiography.

C. A bar chart illustrating the mean percentage binding of the different ATAD3B constructs to GST, LC3B and GABARAP obtained from more than 3 biological replicates. After quantification of the signal intensity per band in the autoradiograph, the expected intensity per a single reaction volume was obtained by multiplying input signal by the reaction volume of the *in vitro* translated protein used. Next, the % binding capacity of each construct was calculated by dividing the signal intensity of the constructs (from each band) by that of the expected intensity per a single reaction volume, multiplied by 100%. Each bar on the chart present the mean values of more than 3 biological replicates.

3.1.3. The binding of human ATAD3 proteins to LC3B and GABARAP is not LIR dependent

Previous studies have shown that most of the main autophagic adaptors have a LIR motif that binds to the LDS of the ATG8 family proteins. In which mutating the LDS of the ATG8 prevents the interaction. (45). Thus, it was hypothesised that, binding of the ATAD3 proteins to the ATG8 proteins could also be LIR dependent. To test whether ATAD3A and ATAD3B also have a LIR motif which enables them to bind to the LIR docking site on the human ATG8 proteins, a single member from the LC3 subfamily and GABARAP subfamily with mutated LIR docking site incapable of binding proteins with LIR motif were used. Hence, GST-LC3B F52A and GST-GABARAP Y49A whose LDS has been mutated were produced from *E coli* and tested against full length *in vitro* translated radiolabelled ATAD3A and ATAD3B. It was observed that mutation at the LDS did not abrogate the binding of LC3B and GABARAP to ATAD3A and ATAD3B. Therefore, it implies that this interaction is not dependent on a LIR motif. **Figure 13.** As seen with p62 used as a positive control, results not shown.

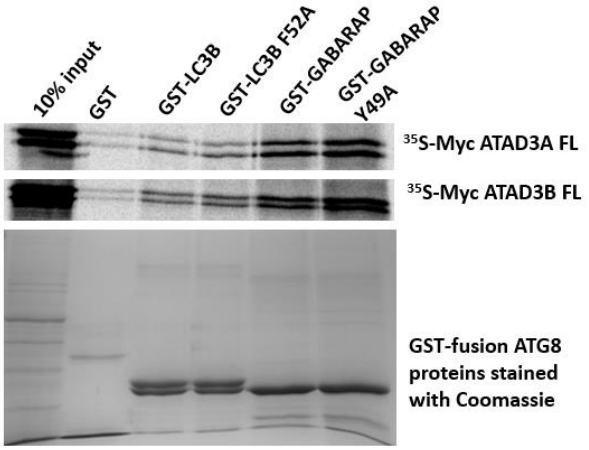

Figure 13: The interaction of the human ATAD3 proteins with GABARAP and LC3B to is not LIR dependent. *In vitro* GST pulldown assay was performed between GST-tagged LDS mutant of GABARAP and LC3B, wildtype of GABARAP and LC3B against full length ^{35}S radiolabelled *in vitro* translated ATAD3B and ATAD3A. Protein complexes were eluted from beads and separated on SDS PAGE. GST-ATG 8 proteins visualised with Coomassie blue stain, while radiolabelled ATAD3B and ATAD3A were detected by autoradiography.

3.1.4. The ATAD3 proteins interacts directly to p62, NDP52 and CALCOCO1 and strongest to NDP52.

As seen with the ATG8 above, similar experiments were also done to study the interaction between the ATAD3 proteins and p62, NDP52, and CALCOCO1. *In vitro* GST pulldown analysis between ATAD3 protein with p62, NDP52, and CALCOCO1 revealed a

direct interaction. Both ATAD3A and ATAD3B bind strongest to NDP52. However, ATAD3B exhibited a stronger binding capacity to p62, NDP52 and CALCOCO1 than ATAD3A. **(Figure 14B)**. Although *in vitro* GST pulldown revealed a direct interaction between ATAD3 proteins and p62, NDP52 and CALCOCO1, one of the setbacks in this method was to produce abundant and a biological functional GST-proteins from *E coli* which was sometimes challenging especially with CALCOCO1.

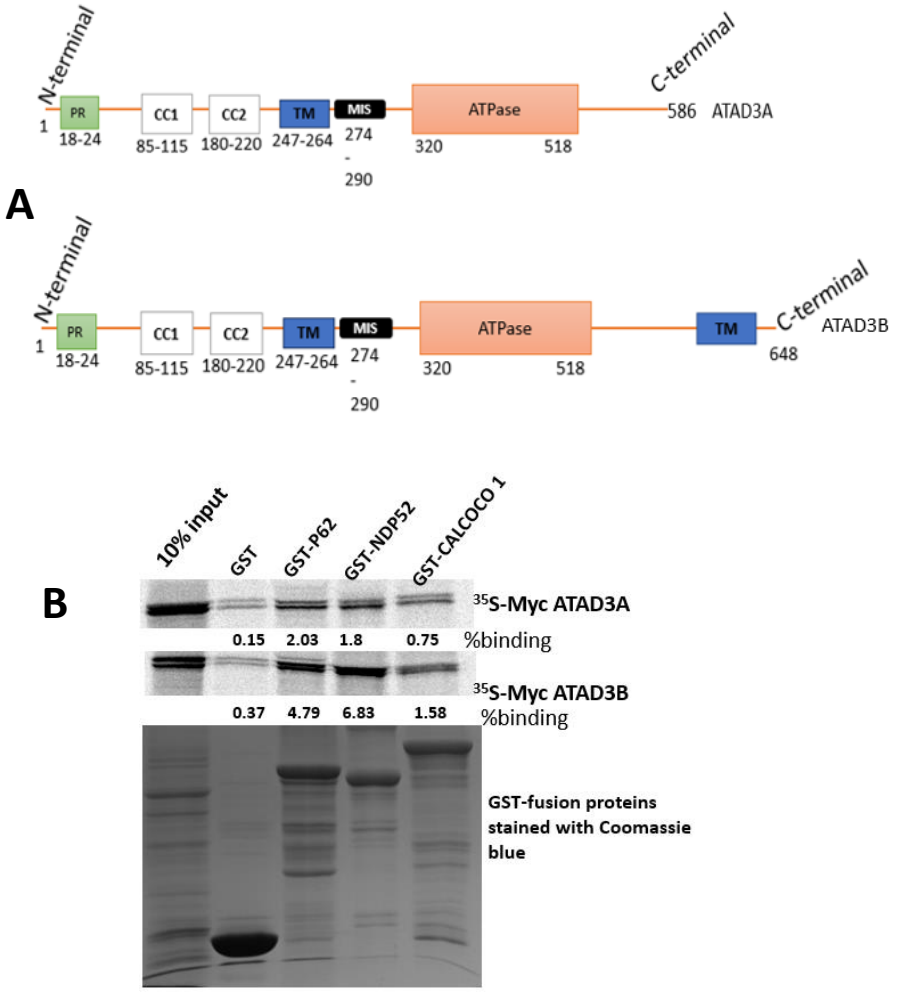

Figure 14: **Human ATAD3 proteins binds directly to p62, NDP52 and CALCOCO1 *in vitro*.**

A. Presentation of the various domains/motifs of ATAD3A and ATAD3B.

B. A GST pulldown analysis done between *in vitro* translated radiolabelled myc-ATAD3A / myc-ATAD3B and GST-p62, GST-NDP52, GST-CALCOCO1. GST-fusion proteins were produced from *E coli* and extracted on beads as baits. ATAD3B proteins were radioactively synthesised using Rabbit reticulocyte system and ^{35}S methionine. Both GST-proteins and radiolabelled ATAD3A or ATAD3B incubated. After incubation, proteins were washed, eluted from beads and fragmented on SDS PAGE. GST, GST-p62, GST-NDP52, and GST-CALCOCO1 were detected by Coomassie blue stain. The captured radiolabelled myc-ATAD3A and ATAD3B were detected by autoradiography. Numbers on each lane represents % binding of ATAD3A and ATAD3B to GST and the respective GST-tagged fusion proteins.

3.1.5. The C-terminal part of ATAD3B mediate the binding of ATAD3B to P62, NDP52 and CALCOCO1

Considering that p62, NDP52 and CALCOCO1 localise mainly in the cytosol, it was hypothesised that the region of ATAD3B that extends to the cytosol may be responsible for its binding to p62, NDP52 and CALCOCO1. Thus, to verify this, the N-terminal truncated ATAD3B without the first 50 amino acid (ATAD3B Δ50) and the C-terminal truncated ATAD3B (ATAD3B 1-518) without the last 130 amino acids were tested (**Figure 15A)**. Surprisingly, it was observed that deletion of the first 50 amino acid at the N-terminal rather increased the binding intensity of ATAD3B to p62 and NDP52 but not with CALCOCO1 (**Figure 15B and 15C)**, while about 20% reduction of the binding capacity was observed with the C-terminal truncated ATAD3B 1-518 (**Figure 15C**). Indicating that this part of the protein is not responsible for the interaction. To further evaluate the segment of ATAD3B that facilitates this interaction, ATAD3B Δ320-518 (ΔCC, ΔMIS), ATAD3B Δ50-320 (Δ ATPase) were tested (**Figure 15A**). These deleted constructs showed a reduced binding affinity to the receptors especially with NDP52. (**Figure 15B and 15C)**. Thus, based on all these results gathered, it was suggested that, the peptides in the C-terminal part and not the N-terminal might be involved in the interaction between ATAD3B with p62, CALCOCO1 and NDP52. In this regard, two N-terminal constructs ^{35}S myc-ATAD3B 1-224 and ^{35}S myc-ATAD3B 1-320 were made using site-directed mutagenesis and tested. As predicted, ^{35}S myc-ATAD3B 1-224 without any of the C-terminal amino acid completely loose interaction with the GST-p62, GST-NDP52, and GST-CALCOCO1 while a slight binding was observed with ^{35}S myc-ATAD3B 1-320, which have some amino acid residues of the C-terminal (**Figure 15B and 15C).** Moreover, it was observed that, by aligning ATAD3B 1-225, ATAD3B 1-320, ATAD3B 1-518, the binding capacity of ATAD3B gradually increases. Which clearly show that the C-terminal part mediates the binding of ATAD3B to these proteins. Another interesting observation was that, CALCOCO1 and NDP52 were similarly affected by the deletions (50-320, and 320-518). This might be because they are homologues with similar domain architecture.

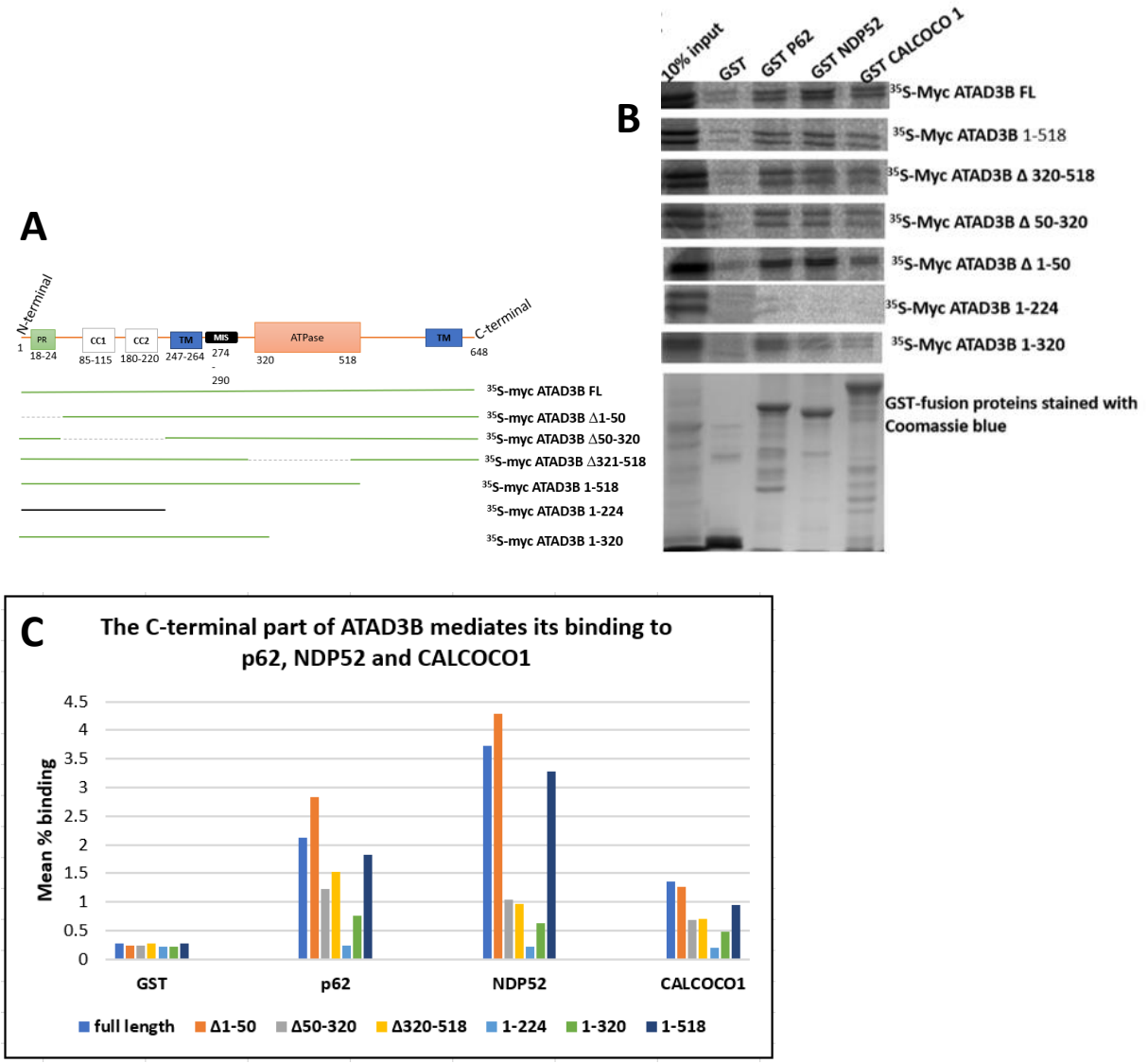

Figure 15: The C-terminal part of ATAD3B contribute its binding to p62, NDP52 and CALCOCO1.

A. A presentation of the domain architecture of ATAD3B. The different truncated and deleted ATAD3B constructs used to map out the region of ATA3DB that contributes for its binding to p62, NDP52, and CALCOCO1. Broken lines indicate deleted regions of the constructs. The construct that loose binding to the GST-fusion proteins is presented in a black colour.

B. The ATAD3B N-terminal construct (1-224) is unable to bind to full length GST-p62, GST-NDP52, GST-CALCOCO1. ATAD3B mutant proteins were radioactively synthesised *in vitro* using rabbit reticulocyte system and ^{35}S methionine and tested for binding to the GST-p62, GST-NDP52, GST-CALCOCO1 by performing *in vitro* GST pulldown assay. After which proteins were washed, denatured and fragmented on SDS PAGE. GST, GST-p62, GST-NDP52, and GST-CALCOCO1 were detected by Coomassie blue stain. The bound ATAD3B proteins detected by autoradiography.

C. A bar chart presenting the mean percentage binding capacity of each ATAD3B constructs to GST, p62 NDP52 and CALCOCO1. After quantification of the signal intensity per band in the autoradiograph, the expected intensity per a single reaction volume was obtained by multiplying input signal by the reaction volume of the *in vitro* translated protein used. Next, the % binding capacity of each construct was calculated by dividing the signal intensity of the constructs (from each band) by that of the expected intensity per a single reaction volume, multiplied by 100%. Each bar on the chart present the mean values of more than 3 biological replicates.

Table 3.1: Standard deviation values of in vitro GST pulldown analysis of ATAD3B constructs with GST proteins

	GST	GST-p62	GST-NDP52	GST-CALCOCO1
Full length ATAD3B	0.098021	1.248382	2.158008	0.558794
Δ1-150 ATAD3B	0.082989	1.064816	2.480899	0.753089
Δ50-320 ATAD3B	0.240388	1.235233	1.049759	0.685641
Δ320-518 ATAD3B	0.092254	0.70743	0.362551	0.233432
1-244 ATAD3B	0.162012	0.128321	0.147402	0.129163
1-320 ATAD3B	0.191628	0.188514	0.21008	0.132403
1-518 ATAD3B	0.154943	0.517608	1.500982	0.449111

3.1.6. p62 interacts with ATAD3B and ATAD3A through the region between the 171th - 256th amino acid residues of p62

To further delineate the domains of the autophagic receptors that facilitates their interaction with the human ATAD3 proteins, GST-p62 and its mutant constructs were used since it is the primary and most studied autophagic receptor (104). In light of this, a GST pulldown between deletion constructs of GST-p62 were used against full length ATAD3B and ATAD3A. The following GST-P62 mutants were used (**Figure16A**):

- GST-P62 ΔPB1
- GST-p62 Δ123-170
- GST-p62 Δ171-256
- GST-p62 Δ257-370
- GST-p62 Δ371-385
- GST-p62 ΔUBA

It was observed that the GSTp62 Δ171-256 mutant could not pulldown both full lengths *in vitro* translated radiolabelled ATAD3A and ATAD3B. Hence, indicating that the region between amino acid 171-256 of p62 is required for interaction with ATAD3A and ATAD3B. GST protein served as a negative control while PINK1 served as a positive control (**Figure 16B**).

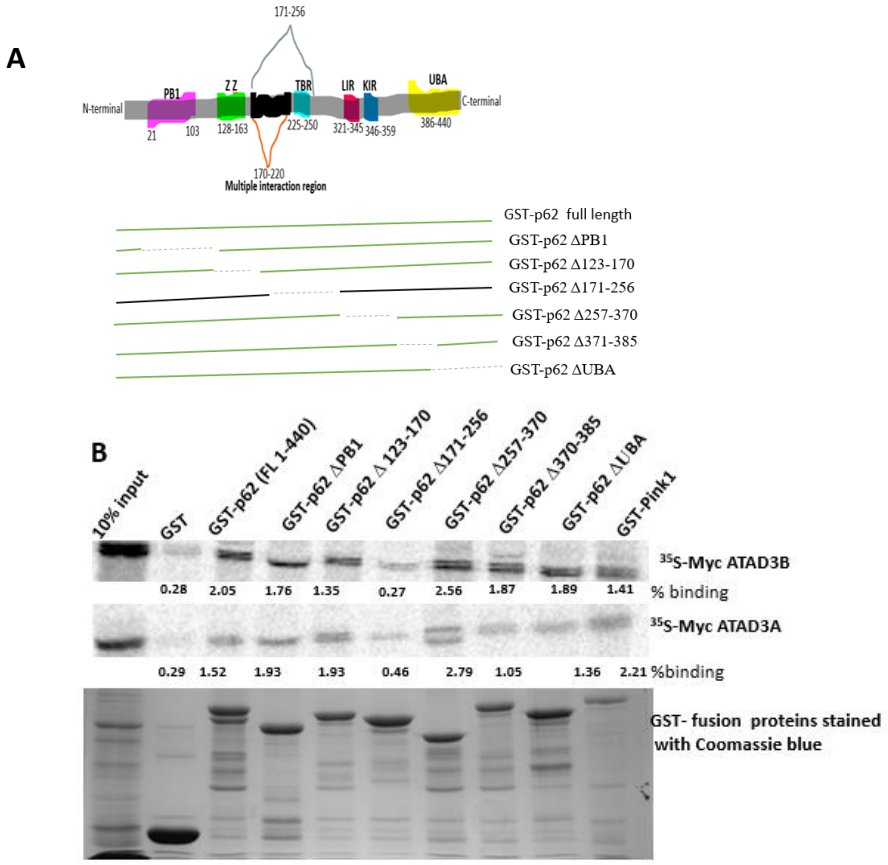

Figure16: The region between 171-256 amino acid in p62 mediates its interaction with the ATAD3 proteins.

A. Domain architecture of p62. The following mutants constructs of p62 were used to map out the region of p62 that contributes for its binding to ATAD3A and ATAD3B. Broken lines indicate deleted regions of p62. The construct that loose binding to the ATAD3 proteins is presented in a black colour.

B. Both ATAD3A and ATAD3B binds to the same amino acid region (171-256) of p62**.** *In vitro* GST pulldown analysis was conducted between *in vitro* translated radiolabelled ATAD3A and ATAD3B (full length) against GST, GST-p62 constructs (full lengths and deletion constructs). GST and GST-p62 constructs were visualised with Coomassie blue stain (lower panel) while the radiolabelled myc-ATAD3A/ATAD3B were detected by autoradiography. The numbers below each band represents the % binding between the GST-p62 and ATAD3A/ATAD3B.

3.2. Endogenous ATAD3A does not colocalise with endogenous p62 and LC3B under normal growth conditions

Due to the direct interaction observed between the ATAD3 proteins and the autophagy markers, the next objective was to determine whether endogenous ATAD3 proteins colocalise with these autophagy related proteins in cells under normal physiological conditions. p62 and LC3B were the protein of choice because they are the most studied autophagy markers (46, 49, 78). However, the colocalization of only endogenous ATAD3A with endogenous LC3B and p62 was tested because the available antibody for ATAD3B tested was not good. Hence, to assess for the colocalization of endogenous ATAD3A with p62 and LC3B, the subcellular

localisation of endogenous ATAD3A in these cells was first assessed. Flp-in Hela cells were used to for this purpose. The cells were seeded on a coverslip in a 24 well plate and allowed to grow to confluence. Next, cells were washed, fixed, permeabilised and the proteins immuno-stained. Different pre-staining conditions were tested to evaluate which is suitable for ATAD3A staining. Subcellular localisation was assessed by co-immunostaining ATAD3A and TOM20 (a marker of the mitochondrial outer membrane) and visualising with the confocal microscopy to check for any possible colocalization between the 2 proteins, TOM20 stained red and ATAD3A stained green. A control was done by staining cells with just the secondary antibody to check for non-specific binding by the secondary antibody, while DAPI was used to stain of the cell nucleus. ATAD3A colocalised with TOM20 producing a greenish-yellow colour when both colours were merged (**Figure 17)**. This indicates the presence of ATAD3A in the mitochondria of the Hela cells used. This result obtained is in line with other studies that had demonstrated the localisation of ATAD3A in the mitochondria of cells (52, 57, 62). No green or pink dots were seen in cells stained with just the secondary antibody, indicating there was no unspecific binding of the secondary antibody. Amongst the different method tested, fixation at 37^{o}C with prewarmed 4% paraformaldehyde followed by permeabilization with 0.1% triton x100 appeared to be the proper pre-staining conditions for microscopic analysis ATAD3A, as more colocalization between endogenous TOM20 and ATAD3A were seen and the proteins retained the normal staining pattern (**Figure 17**).

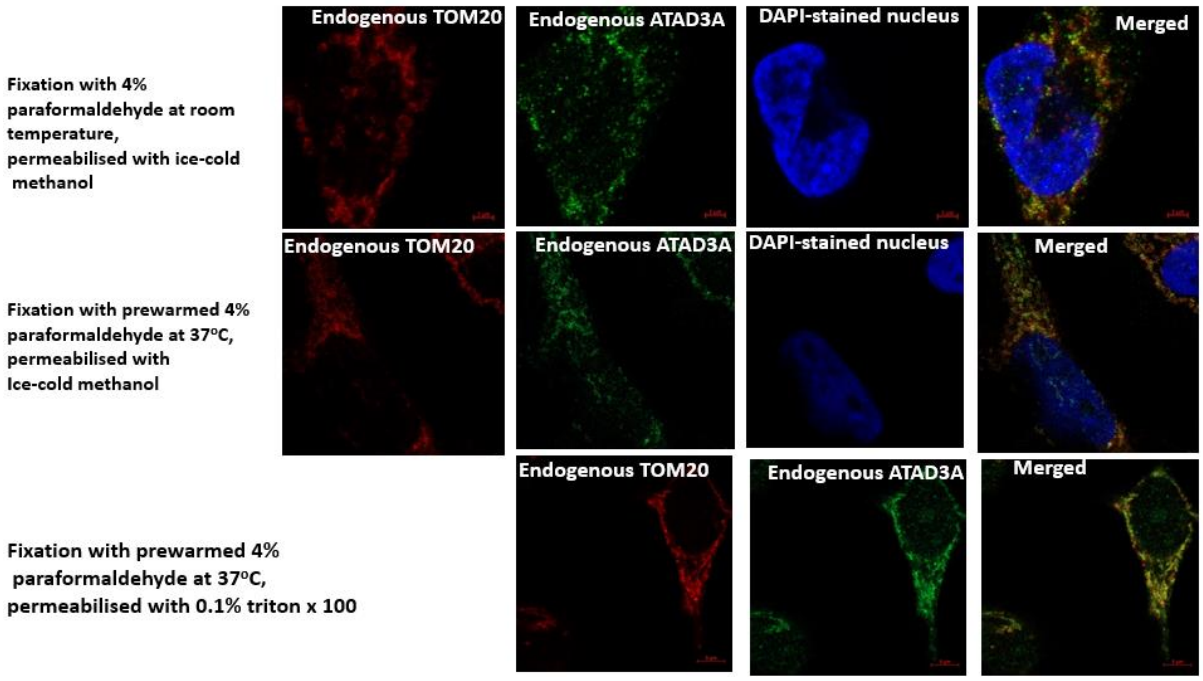

Figure 17: Endogenous ATAD3A localises in the mitochondria of flp-in Hela cells. $1x10^5$ flp-in Hela cells were seeded on coverslips in 24well plates and allowed to grow overnight. Cells were fixed with 4% paraformaldehyde at 37°C or at room temperature and permeabilised with either ice-cold methanol or 0.1% triton x 100. Cells were co-immunostained for endogenous TOM20 (red) and ATAD3B(green). The nucleus stained with DAPI. Slides mounted and images taken by Ziess LSM 800 confocal microscope. Areas of colocalization appears as yellow in the merged images. The scale bar represents 5μm

Following determination of the subcellular localisation of ATAD3A in Flp-in Hela cells, endogenous P62 and LC3B were co-stained with endogenous ATAD3A without any prior cell treatments to detect if these proteins colocalise with ATAD3A in cells under normal conditions. No colocalization was seen when endogenous ATAD3A was co-stained with endogenous p62 and LC3B, see **Figure 18A and B** below.

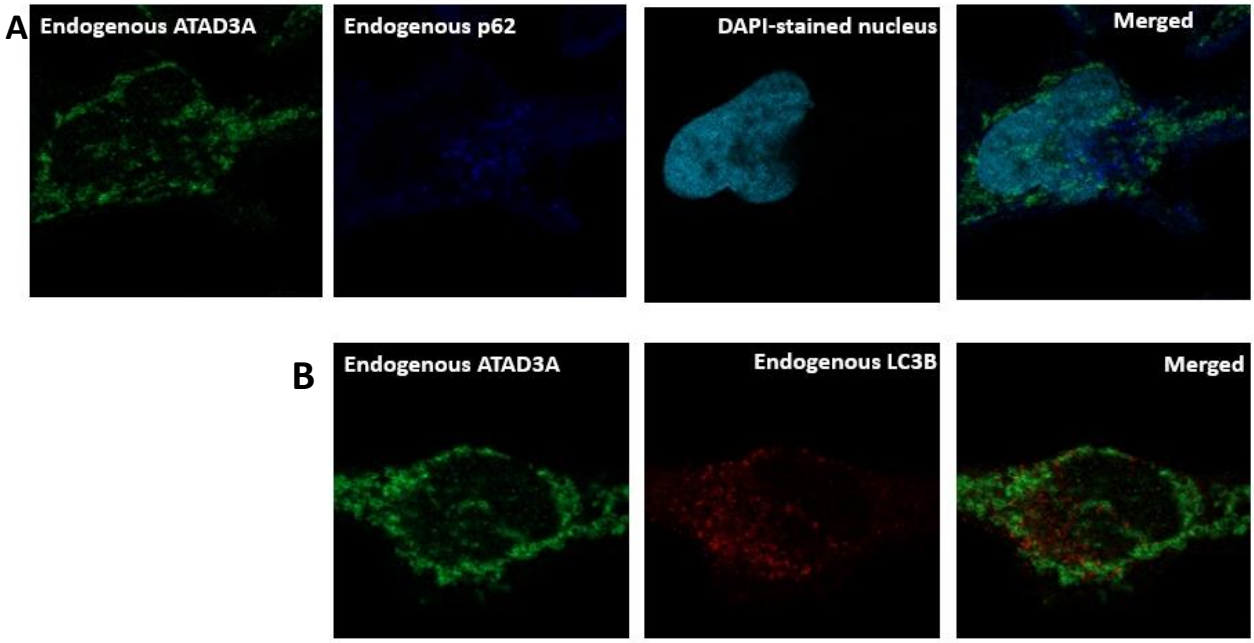

Figure 18. Endogenous ATAD3A does not colocalised with endogenous p62 and LC3B in flp-in Hela cells under normal conditions. $1x10^5$ flp-in Hela cells were seeded on coverslips in 24well plates and allowed to grow overnight. Cells were fixed with prewarmed 4%paraformaldehyde at 37ºC and permeabilised with 0.1% triton-x 100. **(A)** cells co-immuno-stained with anti p62 and anti-ATAD3A antibody, nucleus stained with DAPI. **(B)** cells co- immune-stained with anti-LC3B and anti-ATAD3A antibody. Slides mounted and images taken by Zeiss LSM 800 confocal microscope. p62: blue, ATAD3A: green, LC3B: red.

3.3. ATAD3A is not degraded by starvation-induced autophagy

The next objective was to determine whether ATAD3 proteins are degraded by autophagy by evaluating the effect of starvation-induced autophagy on the levels of endogenous ATAD3 proteins. However, the autophagic degradation of only endogenous ATAD3A was assessed due to lack of a good antibody for ATAD3B. It is well known that autophagic degradation is experimentally induced *in vivo* when cells are starved from nutrient availability for longer hours, and the rate of degradation increases proportionally with the duration of starvation. Also, considering that autophagy is a lysosomal dependent degradation pathway, bafilomycin A1 (a lysosomal inhibitor) is used to experimentally block autophagosomes degradation in cells (105). Therefore, to assess the autophagic degradation of ATAD3A, cells were seeded in a 6 well plate and allowed to grow near confluent, after which cells were either left untreated, treated with bafilomycin A1 for 6hrs, starved for 6 hours to induced autophagic degradation, or starved for 6 hours and treated with bafilomycin A1, to inhibit the autophagic degradation. P62 and LC3-II are autophagy substrates that are degraded by autophagy (16, 45, 46), thus the levels of p62 and LC3-II proteins were detected as controls degraded by autophagy while beta-actin was included as loading control (**Figure 19**). Similar to Shuijie and colleagues

in 2014 (50), 2 bands of the ATAD3 proteins with a corresponding mass of 66kDa and 72kDa was observed following western blot analysis using anti-ATAD3A antibody. Also, Bogenhagen *et al*., 2008 had previously reported 2 bands of ATAD3 proteins in Hela; one abundant and a less abundant slightly higher protein, which they initially assumed to be ATAD3B (106). However, it became clear that the less abundant ATAD3 detected is the phosphorylated form of ATAD3A (50). So, after 6hrs of starvation, a small noticeable increase in the level of endogenous ATAD3A was observed, unlike p62 and LC3II (used as a control) whose levels decreased upon autophagy induction and increased when autophagic degradation was inhibited with bafilomycin A1 (**Figure19)**. Thus, endogenous ATAD3A is not degraded in response to starvation.

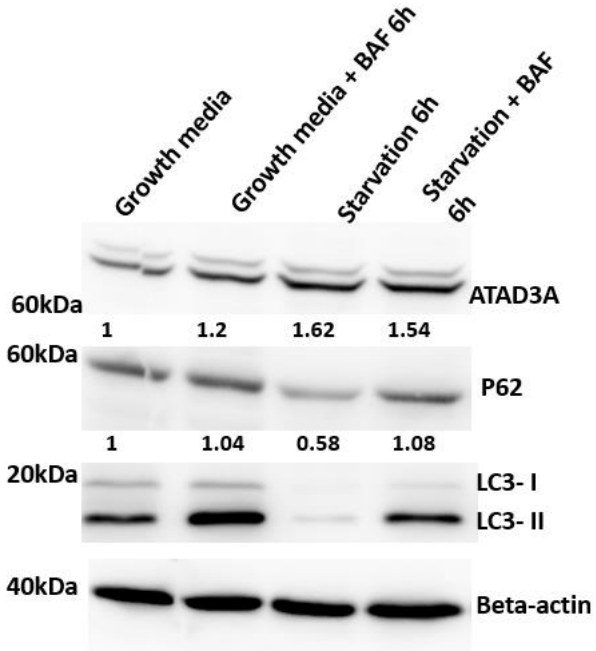

Figure 19: Endogenous ATAD3A is not degraded during starvation-induced autophagy. 3 x 10^5flp-in Hela cells were seeded in a 6-well plate and allowed to grow overnight in growth media. The cells were either left untreated, treated with 200nM bafylomycin A1 (BAF) for 6 hours, starved for hours with or without 200nM/ml bafilomycin A1 (BAF). Cells were later harvested and western blot analysis done to evaluate endogenous levels of ATAD3A, p62, LC3-I, LC3-II and beta-actin. Image J was used to quantify the signal intensity of each band. Next, the signal intensity per band of endogenous ATAD3A and p62 were normalised to that of their respective beta actin, by dividing intensity of the ATAD3A/p62 by that of beta-actin. These normalised ratios were used to determine the relative values of endogenous ATAD3A and p62 per experimental condition with respect to their expreimental control (growth media). The number below each band represent the various estimimated relative values of ATAD3A and p62.

3.3.1. Translation of ATAD3A is upregulated during starvation-induced autophagy

The small increase in the level of endogenous ATAD3A seen after 6 hours of nutrient starvation brought up the question whether the levels of ATAD3A in cells is upregulated during starvation-induced autophagy. Hence, to answer this question, a time chase analysis of 24-hour nutrient starvation of the cells was done. It was observed that, the level of ATAD3A consistently increased during nutrient starvation and in a time dependent manner, p62 served as the biological control (**Figure 20A and 20B)**.

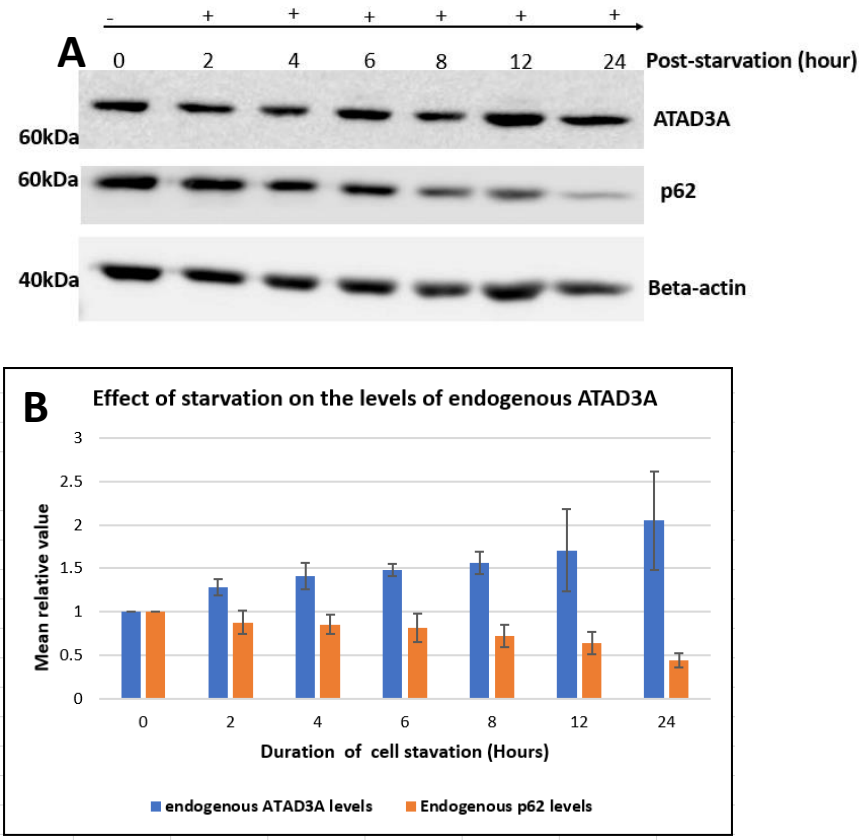

Figure 20: Endogenous ATAD3A levels increase upon nutrient starvation.

A. Western blot analysis of the level of endogenous ATAD3A (p62 used as experimental control) at different time points during a 24-hour starvation of flp-in Hela cells. 3 x 10^5 cells were seeded in 35mm culture plates and allowed to grow near confluence. Cells were washed with 1x PBS, growth media replace with HBSS (starvation media). Control cells without starvation were harvested with 1x SDS buffer at the start of the time course (t = 0), starved cells were harvested with 1x SDS buffer at different time point; 2hr, 4hr, 6hr, 8hr, 12hr and 24hrs. Total protein concentration of lysate measured and approximately 20ng of protein in each lysate loaded for analysis.

B. A bar chart showing the mean relative value of endogenous ATAD3A and p62 during a 24-hour nutrient starvation in flp-in Hela cells. Image J was used to quantify the signal intensity of each band. Next, the signal intensity per band of endogenous ATAD3A and p62 were normalised to that of their respective beta actin, by dividing intensity of the ATAD3A/p62 by that of beta-actin (the loading control). These normalised ratios were used to determine the relative values of endogenous ATAD3A and p62 per duration(hour) of starvation with respect to the e control (t=0), each bar represents the mean of the relative values obtained.

Similarly, Hsin-Yuan Fang *et al*., in 2010 had reported that ATAD3A expression in lung adenocarcinoma cells(LADC) increases during serum starvation in a dose and time dependent manner, but this increase was not associated with increase levels of ATAD3A mRNA level (69). Upregulation of proteins in cells might be due to increase synthesis or impared degradation. Increased synthesis of a proteins in cells is enhanced either by increase mRNA transcription or by translational activation (107). Given that Hsin-Yuan Fang and colleauges did not report any increase in ATAD3A mRNA transcription when cells were starved (69), it was proposed that increased ATAD3A levels in Hela cells seen during starvation might be due to translational activation. To test this hypothesis, cells were starved and translation of ATAD3A inhibited by treating the starved cells with 62µg/ml cylohexamide in ethanol; a translational inhibitor that inhibits protein synthesis in eukaryotes by prventing translational elongation (108). Thus, cells were either treated with 62µg/ml cylohexamide in ethanol, starved for 4 / 8 hours with or without 62µg/ml cyclohexamide in ethanol. As predicted, the levels of ATAD3A slightly decreased consistently (repeatedly), upon treatment of starved cells with cyclohexamide. Thus, indicating that translation of ATAD3A is upregulated during starvation-induced autophagy. The nuclear factor erythriod 2- related factor 2 (NRF2) has been shown to have a half life less than 30 minutes following treatment of HL60 (leukemia) cells with 100µg/ml with cyclohexamide (109), thus it was used as a biological control (**Figure 21).**

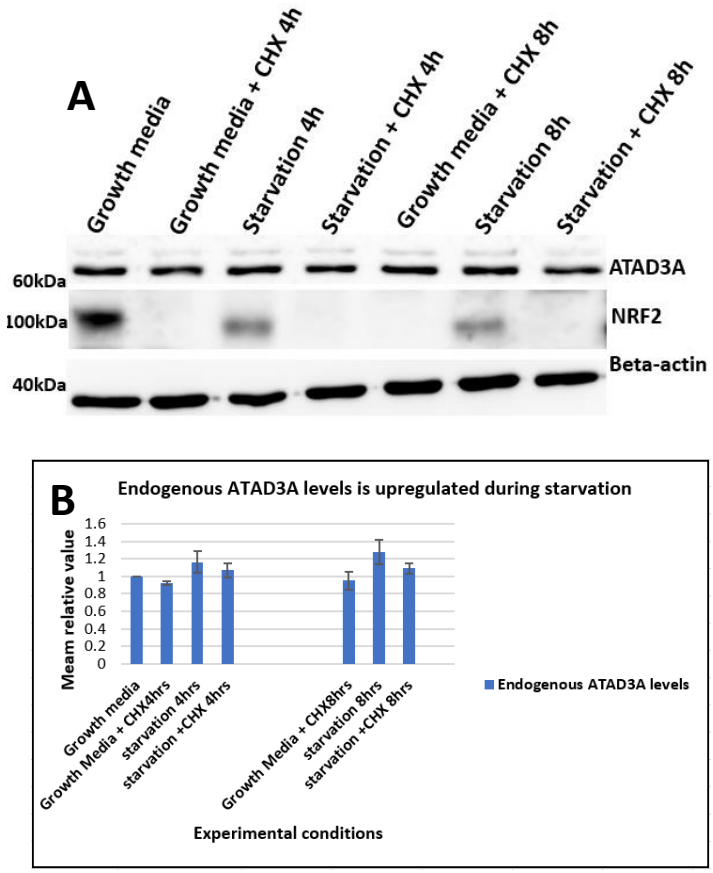

Figure 21: Endogenous ATAD3A translation is activated during nutrient starvation.

A. 3 x 10^5 flp-in Hela cells were seeded in a 35mm plate and allowed to grow overnight in growth media. The cells were either left untreated, treated with 62.5µg/ml cyclohexamide (CHX) for 4 or 8 hours, starved for 4 or 8 hours with or without 62.5µg/ml cyclohexamide (CHX). Cells were later harvested, and approximatly 20ng of the total protein was analyse by western botting to evaluate endogenous levels of ATAD3A. NRF2 served as biological control while beta actin was used as the loading control.

B. A bar chart showing the mean relative value of endogenous ATAD3A. Image J was used to quantify the signal intensity of each band. Next, the signal intensity per band of endogenous ATAD3A were normalised to that of their respective beta actin, by dividing intensity of the ATAD3A by that of beta-actin. These normalised ratios in each treatment condition were used to determine the relative values of endogenous ATAD3A with respect to that of the untreated cells (growth media). Each bar represents the mean of the relative values obtained.

3.4.Myc-tag and not EGFP tag is suitable for overexpression of tagged ATAD3A in the mitochondria

The lack of colocalisation seen between ATAD3A with p62 and LC3B poses a question on the physiological relevance of their interaction seen *in vitro*. Thus, the next step was to analyse the effect of ATAD3B or ATAD3A overexpression on the autophagy process as well as the mitochondria, and also evaluate the effect each specific mutation of ATAD3 proteins has on its its interaction partner, the mitochondria and the turnover of autophagy process by producing cells that can stably expressed these proteins upon induction. The ATAD3 constructs

used to generate the stable cell lines were fused to an EGFP tag because it enables the ATAD3 proteins to be visualised in cells without the use of antibodies. Stable expression of EGFP-ATAD3 were made using the Flp-in T-Rex system. Based on this system, EGFP-tagged ATAD3 expression in the cells was under the control of tetracyclin/doxycycline-inducible CMV promoter present in the pDest-Flp-in vector.

Hence, inorder to generate cells stably expressing ATAD3, Flp-in Hela cells were transfected with either pDest-Flp-in EGFP ATAD3A or pDest-Flp-in EGFP ATAD3B plasmids. After transfection, cells expressing the plasmids were selected with 200µg/ml hygromycin and 10ug/ml blasticidin S HCL for 14 days. Unfortunatly, the cells transfected with the ATAD3B plasmids did not survive following treatment with hygromycin and blasticidin. This could be because the plasmid which confers hygromycin rersistance to the cells was not intergrated into the cell's genome, resulting in cell dead. As a result, only the effect of ATAD3A overexpression could be analysed here.

To test the effect of ATAD3A overexpression on autophagic flux, the expression of EGFP-tagged ATAD3A protein was induced for 16-24hrs using 1µg/ml doxycycline in some of the cells. After which the EGFP-tagged ATAD3A induced cells were either untreated, starved for 6 hours to induced autophagic degradation or starved for 6 hours with 200nM/ml bafilomycin A1 to block the induced autophagy. Controls were run without induction of EGFP-tagged ATAD3A expression but treated as their test counterparts. Levels of p62 and LC3 were detected to evaluate autophagy flux. Western blot analysis revealed that, in normal growth media, the levels of p62, LC3 I and LC3 II in cells with induced EGFP-tagged ATAD3A expression consistently and significantly increased as compared to p62 and LC3 I levels in cells whose ATAD3A expression was not induced ($p=0.003$, $p=0.02$, $p=0.028$ respectively) (**Figure 22A and 22B).** Thus**,** indicating an increase/upregulation of autophagic activity in the EGFP-tagged ATAD3A induced cells. Moreover, p62 levels decreased by approximately 50% upon induction of autophagy in cells with induced EGFP-tagged ATAD3A expression, while cells without induction of EGFP-tagged ATAD3A expression had about 25% deduction in the levels of p62 when autophagy was activated (**Figure 22C)**. Collectively, results demonstrated that cells with induced EGFP-tagged ATAD3A overexpression had an increase autophagic flux.

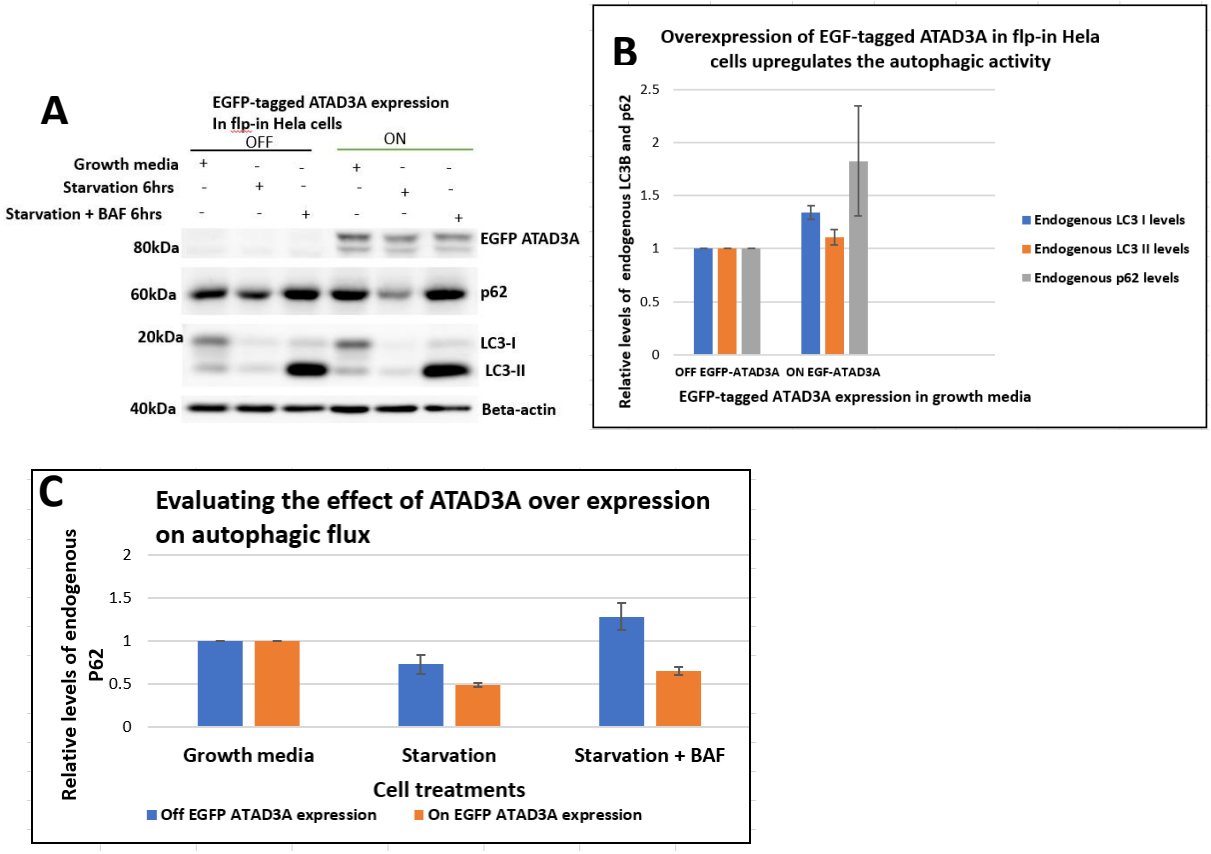

Figure 22: Overexpression of GFP- tagged ATAD3, induces increase autophagic flux in flp-in Hela cells

A. Western blot analysis of endogenous p62, LC3-I, LC3-II in EGFP-ATAD3A induced and non-induced flp-in Hela cells. EGFP-ATAD3A induced and non-induced flp-in Hela cells were either left untreated, starved for 6hours or starved for 6 hours with 200nM/ml bafilomycin A1 treatment. Cell harvested, total protein concentration measured and about 20ng of the total protein per lysate analysed. Beta-actin is the loading control.

B. A bar showing the levels of endogenous p62, LC3 I and LC3 II in EGFP-ATAD3A induced flp-in Hela cells relative to that in EGFP-ATAD3A non-induced flp-in Hela cells in growth media. Image J was used to quantify the signal intensity of each band. Next, the signal intensity per band of endogenous p62, LC3-I and LC3-II were normalised to that of their respective beta actin, by dividing intensity of each protein by that of beta-actin. These normalised ratios were used to determine the relative values of endogenous p62, LC3-I and LC3-II in EGFP-ATAD3A induced cells with respect to the non-induced flp-in Hela cells, each bar represents the mean of the relative values obtained. student's t test (p62 p=0.003), (LC3-I p=0.02), (LC3-II p=0.03)

C. A bar showing the effect of EGFP-ATAD3A overexpression on autophagic flux. EGFP-ATAD3A induced or non-induced cells were left untreated, starved for 6 hours or starved for 6 hours with 200ng/ml bafilomycin A1. P62 levels were detected, and p62 band signal intensity were normalised to that of their respective beta actin (loading control). Normalised ratios were used to determine the relative values of endogenous p62.

Based on these observations from western blot analysis, confocal images were taken to check if EGFP-tagged ATAD3A had the expected subcellular localisation pattern, and to evaluate whether EGFP-tagged ATAD3A colocalises with endogenous p62 and LC3B. In this regard, EGFP-tagged ATAD3A expression was turned on, cells were left untreated, starved treated with bafilomycin A1. The cells were subsequently fixed, permeabilised, immuno-stained and observed microscopically. Confocal imaging revealed that EGFP-tagged ATAD3A did not retain the normal ATAD3A staining pattern. (**Figure 23A and 23B)**. In addition, confocal imaging revealed more positive p62 dots in cells whose EGFP-tagged ATAD3A expression was induced **(Figure 23A)**, however the data was not quantified. Furthermore, there was no colocalization seen between EGFP-tagged ATAD3A with p62 and LC3B even when the cells were starved for 6 hours in the presence of bafilomycin A1 (**Figure 23A and 23B)**.

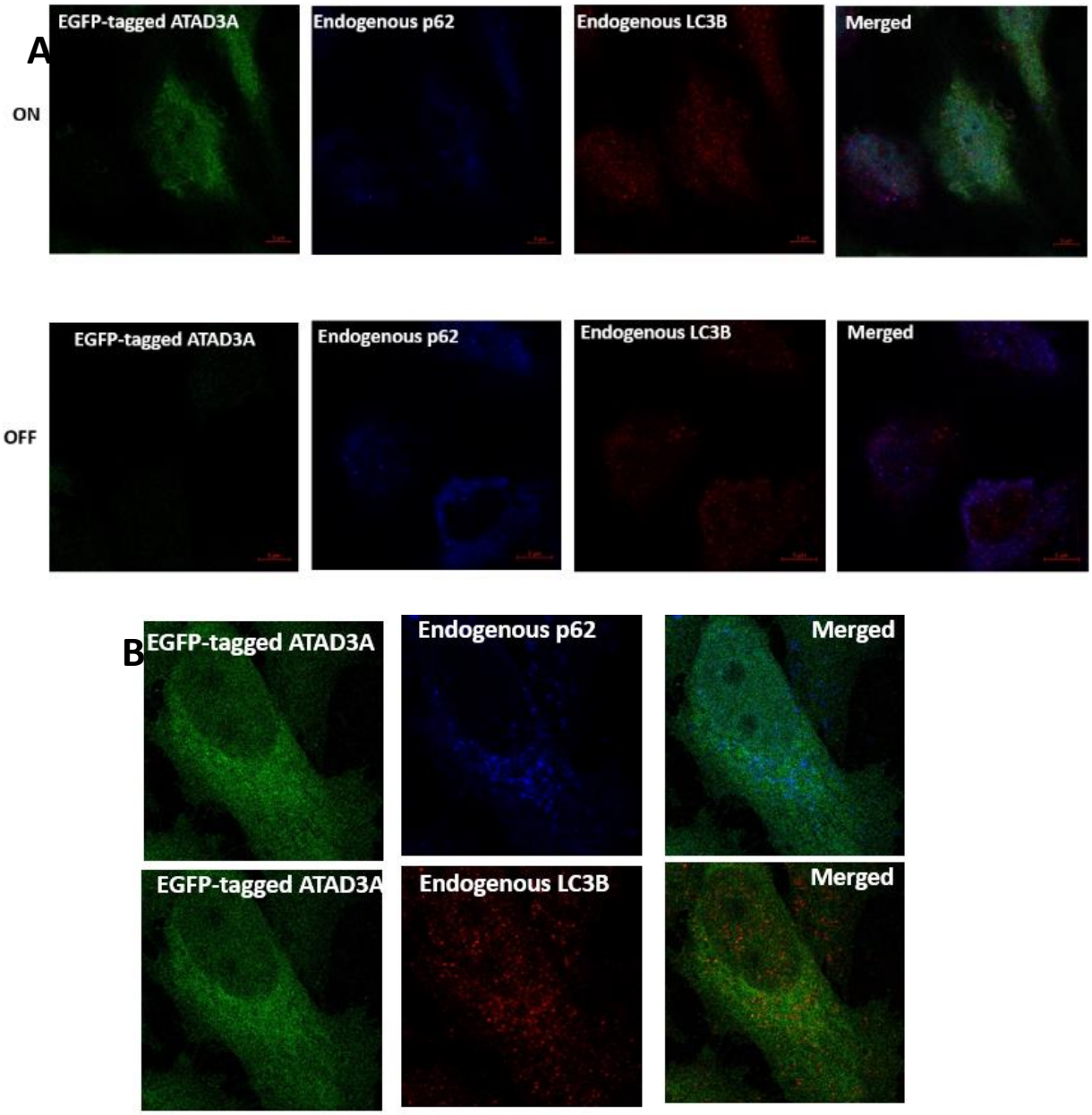

Figure 23: EGFP-tagged ATAD3A do not colocalised with neither p62 bodies or positive LCB.

A. Confocal imaging of flp-in Hela cells stably expressing ATAD3A in growth media. $7.5x10^4$ cells were seeded on coversides in a 24well plate and allow to grow overnight. ATAD3A expression was turned on for 16-24hours with 1µg/ml doxycycline. Cells were fixed with 4% paraformadehde at 37ºC for 10min, and permeabilised with 0.1% triton-x 100, immunostained for LC3B and p62. Images taken using confocal microscope LSM800.

B. Flp-in Hela cells stably expressing ATAD3A were seeded on coverslips in a 24well plate and grown overnight. ATAD3A expression was induced for 16-24hours with doxycycline, and cells were later starved for 6hours with 200ng/ml of bafilomycin A1treatment, then immuno-stained for endogenous p62 and LC3B and visualised by LSM 800 confocal microscope.

It is known that tagging of proteins with GFP may affect their subcellular localisation (110). Thus, the abnormality seen in the staining pattern of EGFP-tagged ATAD3A posed a question whether EGFP-ATAD3A had a wrong subcellular localisation and was therefore not present in the mitochondria. This was verified by checking for its colocalization with endogenous TOM20 and ATAD3A. Thus, EGFP-tagged ATAD3A expression was induced, and cells stained with either anti-TOM20 or anti-ATAD3A antibodies and visualised by the confocal microscope. Unlike endogenous ATAD3A that colocalises with TOM20 as seen above **(Figure 16)**, there was no colocalization seen between the EGFP -tagged ATAD3A and TOM20, or EGFP-tagged ATAD3A and endogenous ATAD3A (**Figure 24A and 24B)**. Thus, confirming that EGFP-tagged ATAD3A was mis-localised and not present in the mitochondria. In addition, TOM20 stains exhibited that the mitochondria were also fragmented, suggesting that overexpression of EGFP-tagged ATAD3A induced fragmentation of the mitochondria.

In search of a suitable tag to use for the overexpression of ATAD3A in cells, the myc-tag was tested. As such, flp-in Hela cells not expressing EGFP-tagged ATAD3A were transiently transfected with myc-tagged ATAD3A. After 48 hours, endogenous ATAD3A and myc-tagged ATAD3A were co-stained with anti-ATAD3A and anti-myc antibodies respectively. Cells were also evaluated for possible co-localisation between myc-tagged ATAD3A and endogenous ATAD3A. It was observed that myc-tagged ATAD3A have a similar staining pattern as endogenous ATAD3A. Moreover, it colocalised with endogenous ATAD3A as evident by the abundant yellow colour in the merged image **(Figure 24C).** Hence, demonstrating that the myc-tagged ATAD3A is in the same subcellular localisation with the endogenous ATAD3A. Unlike the EGFP- tagged ATAD3A that had an abnormal pattern and did not colocalise with endogenous ATAD3A as well **(Figure 23A and 23B)**. This indicates that myc-tag is suitable for overexpressing ATAD3A in cells. Myc tags (12kDa) are smaller than EGFP tags (32kDa), hence the large size of the GFP tag might have caused the proteins to be mis-localised (111). Thus, it was needless making stable cells with EGFP-tagged ATAD3B and the other constructs as planned. Unfortunately, time made it impossible to do further experiments with the myc-tagged constructs.

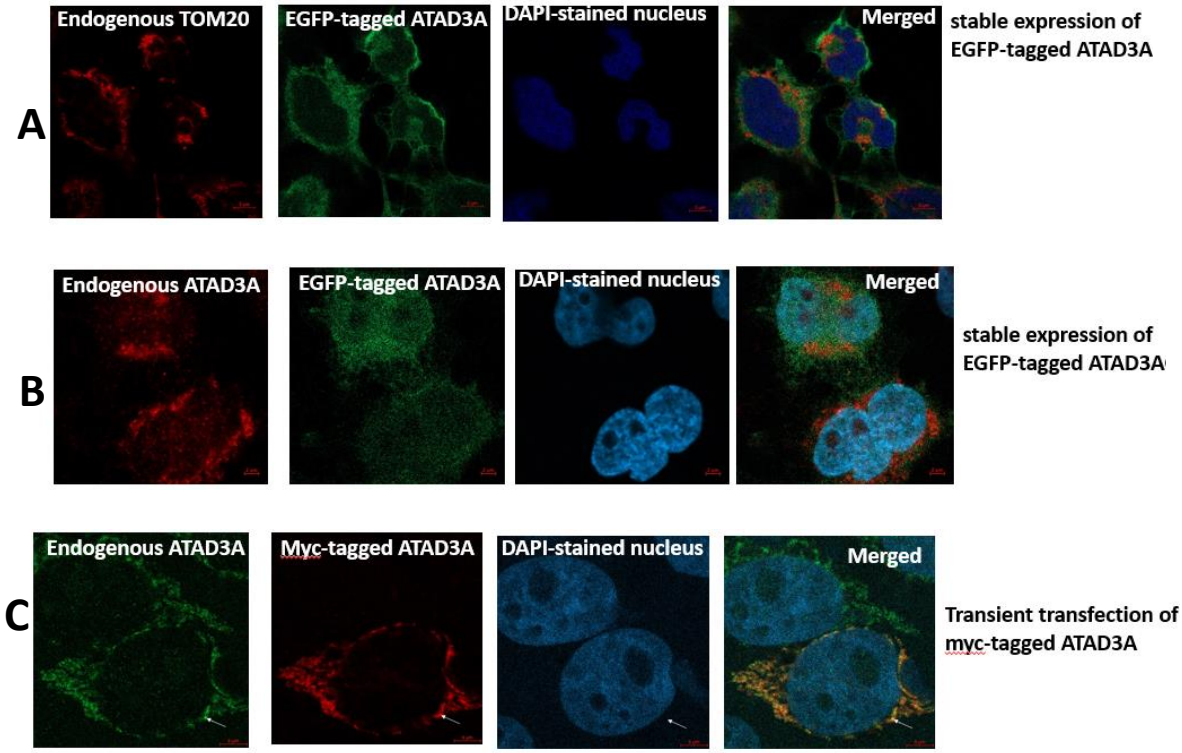

Figure 24: Myc-tag is suitable for overexpressing ATAD3A in cells. Confocal images of Flp-in Hela cells stably expressing EGFP-tagged ATAD3A (image panel A and B) or transiently transfected with myc-tagged ATAD3B (image panel C). Following cell fixation and permeabilization, cells stably expressing EGFP-tagged ATAD3A stained with either ATAD3A antibodies (A), or TOM20 antibodies (B), while cells transiently transfected with myc-tagged ATAD3B plasmids co-stained with myc and ATAD3A antibodies (C) and visualised microscopically. The arrow in image panel C points at areas of colocalization.

Chapter 4

Discussion

4.1. Discussion

ATAD3 proteins are members of the AAA ATPase family that have ATPase activity and are associated with several cellular activities (54, 60, 68). In addition, data obtained from previous studies indicate that ATAD3 proteins may have potential roles in the regulation of autophagy and mitophagy (20, 58, 64). This present study characterised the binding of ATAD3A and ATAD3B to p62, NDP52, CALCOCO1, LC3B and GABARAP. In addition, the colocalization of ATAD3A with p62 and LC3B was assessed and the endogenous levels of ATAD3A during starvation-induced autophagy evaluated. Nonetheless, the relevance of the identified interactions in the process of autophagy or mitophagy could not be addressed. In addition, the anti-ATAD3B antibody available was not good, thus the colocalization between ATAD3B with p62 and LC3B as well as its degradation during starvation-induced autophagy were not evaluated.

I*n vitro* GST analysis show that ATAD3A and ATAD3B interacts directly with the human ATG8 (hATG8) family proteins. Most interaction between hATG8 proteins and several autophagy related proteins is mediated by a short sequence motif known as the LC3 interacting region (LIR) which was first identified in the autophagy receptor p62/SQSTM1 (9, 78). Similarly, hATG8 interaction with LIR containing proteins is mediated by LIR docking site (LDS) (9, 16). To examine whether the interaction between ATAD3 proteins and hATG8 was mediated by a LIR, we used LDS mutant of LC3B (F52A) and GABARAP (Y49A). In vitro GST pulldown assay show no differences in the interaction of ATAD3 proteins with both wild-type (WT) LC3B and GABARAP and their LDS mutants. Thus, this interaction is not mediated by a LIR.

To identify the region on ATAD3 that is responsible for interaction with hATG8 proteins, a combination of deletional mapping and GST pulldown analysis were used. Based on *in vitro* analysis, the binding of ATAD3B to LC3B and GABARAP was completely abolished upon deletion of its mitochondrial embedded ATPase domain (Δ321-518), indicating that this domain is necessary for the interaction. Moreover, the interaction with LC3B or GABARAP was also affected by deletion of the two coiled-coil domains (Δ50-320) of ATAD3B. This suggest that either the coil-coil domain is required to stabilise the interaction

of the adjacent ATPase region or that dimerization of ATAD3 is required for efficient interaction. The latter is supported by earlier studies showing that dimerization of the coiled-coil domain is required to maintain the higher ordered structure of ATAD3 proteins (61). Thus, deletion of the 2 coiled-coiled domains might have resulted in the distortion of the structural conformation of ATAD3B. This conformational change of ATAD3B can alter or affect the orientation of its ATPase binding domain, leading to an interference of contacts between binding sites of the proteins. Hence, accounting for a decreased in the binding capacity of ATAD3B upon deletion of its coiled-coil domain. Another possible reason is that, ATAD3B might have existed as monomers in solution, since the-coiled coil domain that facilitates dimerization of the protein was deleted(57, 59, 61). As such, a lesser amount of ATAD3B monomers were pulled down and detected. Therefore, the interaction is most likely mediated by the ATPase domain which is embedded in the mitochondrial matrix.

Furthermore, the interaction between ATAD3 proteins and the selective autophagy receptors p62, NDP52 and CALCOCO1 was also evaluated. Unlike the ATG8, the interaction with p62, NDP52, CALCOCO1 was not completely abrogated by deleting any one single domain in the N- or C-terminal. Instead, the binding to these proteins is mediated by the C-terminal part of the ATAD3 proteins. The above claim is supported by the fact that the N-terminal construct of ATAD3B (1-224) consistently loss interaction with p62, NDP52 and CALCOCO1. Secondly, the interaction seems to gradually increase as the peptide length increased towards the C-terminal. Therefore, indicating that, the C-terminal part of ATAD3B is required for these interactions. In addition, an increased binding of ATAD3B to p62 and NDP52 was observed when the first 50 amino acid was deleted. This is probably because deletion of this region increases dimerization of ATAD3B as previously reported with the Δ1-50 ATAD3A (36). Moreover, the region of p62 that facilitates its binding to ATAD3 proteins was also mapped. GST pulldown analysis show that the region between 170-257 of p62 mediates the interaction with ATAD3B and ATAD3A. This region which we termed Multiple-interaction region (MIR) also facilitate p62 binding to other proteins such as ALFY(29), HTLV-1 Tax protein(28), TNF receptor associated factor 6 (TRAF6) (112), the LIM protein of Ajuba (30), and TRIM5 alpha (113). Some of which (ALFY and TRIM5 alpha) have been reported to be involved in autophagy (29, 75, 113). Furthermore, it is interesting to note that, ATAD3A and ATAD3B might interact with these proteins (p62, NDP52, CALCOC1, LC3B and GABARAP) in a similar manner, because the truncated ATAD3B (ATAD3B 1-518) without the extended C-terminal did not lose interaction with neither of the autophagic related

proteins. Moreover, the proteins are evolutionary related, having a conserved coiled-coil and the ATPase domain (59, 114).

To study a potential role of ATAD3 proteins in autophagy, the colocalization between ATAD3A and p62 or LC3B under normal physiological conditions was first assessed. Although *in vitro* analysis demonstrated a direct binding of the ATAD3 proteins to both p62 and LC3B, no colocalization between ATAD3A and p62 or LC3B was observed in cells under normal physiological conditions. This might be because the C-terminal part that mediates these interactions is embedded in the mitochondrial matrix (52, 57). Since these proteins are in different subcellular location, they don't seem to colocalize under normal conditions. Notwithstanding, the interaction of ATAD3 proteins with these autophagy related proteins may occur only under certain stress conditions. This theory is supported by a recent study showing that the NIPSNAP proteins, a mitochondrial matrix protein was re-localized to the OMM upon mitochondrial depolarisation and mediate the recruitment of autophagy receptors to the mitochondria during depolarisation to regulate mitophagy (115). Similarly, IMM protein prohibitin 2 has been shown to bind LC3 upon damage to the mitochondrial outer membrane (116). Hence, the C-terminal part of ATAD3 may become exposed during mitochondrial stress or damage, facilitating the recruitment and/or interaction with p62 or LC3B to induce mitophagy.

Unfortunately, the relevance of these interactions in the process of autophagy or mitophagy could not be explored, because the EGFP tag used for the ATAD3A overexpression was not suitable and caused mis-localisation of ATAD3A as well as mitochondrial fragmentation. Hence, they could not be used. However, increased levels of p62 as well as autophagic activities were seen in EGFP-tagged ATAD3A induced cells. p62 is a stressed-induced protein, whose level increases in response to any sort of cytosolic stress (32, 104, 117). Moreover, p62 is involved in the sequestration and autophagic degradation of damaged mitochondria (33). Thus, the increased p62 levels as well as the increased p62 positive punta might have resulted from cytosolic stress exerted by the mis-localised of EGFP-ATAD3A and sequestration of the damaged mitochondria. Autophagy maintains cellular homeostasis and enhances cell survival in response to physiological stress by degrading the deleterious components (104). Thus, upon induction of autophagy, the EGFP-tagged ATAD3A-induced cells exhibited an increase in the rate of autophagic flux to eradicate the increased p62 bodies including the damaged mitochondria.

4.2. Conclusion

Although the aim of this study was not achieved, this study is potentially important. This present study show that the C-terminal ATPase domain may interact with LC3B, and GABARAP and the interaction with p62, NDP52, CALCOCO1 is also dependent on its C-terminal part. Furthermore, it was shown that the translation of ATAD3A is upregulated during starvation-induced autophagy. This observation suggests a potential role of ATAD3 proteins in autophagy or mitophagy. One of the major questions that arose from this study was under what conditions does ATAD3 proteins interact with the studied autophagic-related proteins, provided that the cytoplasmic portion of the proteins does not mediate the interaction? Nevertheless, one cannot exclude the possibility that this interaction can occur under certain stress conditions such as mitochondrial depolarisation or changes in C-terminal environment of ATAD3A possibly regulated by ATAD3B overexpression (59). Which allows ATAD3 proteins to mediate the recruitment of these autophagic related proteins to induce mitophagy. However, further work is required to confirm the interactions between ATAD3 protein and autophagy related protein in cells and to evaluate if these interactions are relevant for autophagy or mitophagy.

Due to time limitations, we could not verify these interactions or test the hypothesis that the ATAD3 proteins are necessary during autophagy or mitophagy. Another major limitation encountered during this study is the absence of sensitive antibodies that can stain endogenous ATAD3B proteins. We established an EGFP-tagged ATAD3 stable cell lines but discovered that EGFP-tagging affects localization of ATAD3A proteins probably due to the size of the tag. Therefore, in the future, it will be necessary to establish myc-tagged stable cell lines of the ATAD3 proteins for further studies. The exact role of each ATAD3 proteins also need to be verified. Finally, CRISPR mediated knockout of the ATAD3 protein will be necessary to evaluate the exact role of the ATAD3 proteins in mitochondrial quality control and mitophagy.

REFERENCE

1. Xu Z, Yang L, Xu S, Zhang Z, Cao Y. The receptor proteins: pivotal roles in selective autophagy. Acta Biochimica et Biophysica Sinica. 2015;47(8):571-80.

2. Johansen T, Lamark T. Selective autophagy mediated by autophagic adapter proteins. Autophagy. 2011;7(3):279-96.

3. Galluzzi L, Baehrecke EH, Ballabio A, Boya P, Bravo-San Pedro JM, Cecconi F, et al. Molecular definitions of autophagy and related processes. Embo j. 2017;36(13):1811-36.

4. Sharma V, Verma S, Seranova E, Sarkar S, Kumar D. Selective Autophagy and Xenophagy in Infection and Disease. Front Cell Dev Biol. 2018;6:147.

5. Leyva-Paredes K, Castrejón-Jiménez NS, Arrieta-Oliva HI, Baltierra-Uribe SL, García-Pérez BE. Choosing Lunch: The Role of Selective Autophagy Adaptor Proteins. Autophagy in Current Trends in Cellular Physiology and Pathology. 2016:391.

6. Zaffagnini G, Martens S. Mechanisms of Selective Autophagy. Journal of Molecular Biology. 2016;428(9, Part A):1714-24.

7. Parzych KR, Klionsky DJ. An overview of autophagy: morphology, mechanism, and regulation. Antioxid Redox Signal. 2014;20(3):460-73.

8. Mancias JD, Kimmelman AC. Mechanisms of Selective Autophagy in Normal Physiology and Cancer. J Mol Biol. 2016;428(9 Pt A):1659-80.

9. Johansen T, Lamark T. Selective Autophagy: ATG8 Family Proteins, LIR Motifs and Cargo Receptors. J Mol Biol. 2020;432(1):80-103.

10. Stanga D, Zhao Q, Milev MP, Saint-Dic D, Jimenez-Mallebrera C, Sacher M. TRAPPC11 functions in autophagy by recruiting ATG2B-WIPI4/WDR45 to preautophagosomal membranes. Traffic. 2019;20(5):325-45.

11. Maeda S, Otomo C, Otomo T. The autophagic membrane tether ATG2A transfers lipids between membranes. Elife. 2019;8:e45777.

12. Valverde D, Yu S, Boggavarapu V, Kumar N, Lees J, Walz T, et al. ATG2 transports lipids to promote autophagosome biogenesis. The Journal of Cell Biology. 2019;218:jcb.201811139.

13. Schaaf MB, Keulers TG, Vooijs MA, Rouschop KM. LC3/GABARAP family proteins: autophagy-(un)related functions. Faseb j. 2016;30(12):3961-78.

14. Xie W, Zhou J. Aberrant regulation of autophagy in mammalian diseases. Biol Lett. 2018;14(1).

15. González-Rodríguez Á, Mayoral R, Agra N, Valdecantos MP, Pardo V, Miquilena-Colina ME, et al. Impaired autophagic flux is associated with increased endoplasmic reticulum stress during the development of NAFLD. Cell Death & Disease. 2014;5(4):e1179-e.

16. Birgisdottir AB, Lamark T, Johansen T. The LIR motif - crucial for selective autophagy. J Cell Sci. 2013;126(Pt 15):3237-47.

17. Furukawa K, Innokentev A, Kanki T. Regulatory Mechanisms of Mitochondrial Autophagy: Lessons From Yeast. Frontiers in Plant Science. 2019;10(1479).

18. Yao N, Wang C, Hu N, Li Y, Liu M, Lei Y, et al. Inhibition of PINK1/Parkin-dependent mitophagy sensitizes multidrug-resistant cancer cells to B5G1, a new betulinic acid analog. Cell Death & Disease. 2019;10(3):232.

19. Sato S, Furuya N. Induction of PINK1/Parkin-Mediated Mitophagy. In: Hattori N, Saiki S, editors. Mitophagy: Methods and Protocols. New York, NY: Springer New York; 2018. p. 9-17.

20. Heo JM, Harper NJ, Paulo JA, Li M, Xu Q, Coughlin M, et al. Integrated proteogenetic analysis reveals the landscape of a mitochondrial-autophagosome synapse during PARK2-dependent mitophagy. Sci Adv. 2019;5(11):eaay4624.

21. Jin G, Xu C, Zhang X, Long J, Rezaeian AH, Liu C, et al. Atad3a suppresses Pink1-dependent mitophagy to maintain homeostasis of hematopoietic progenitor cells. Nature immunology. 2018;19(1):29-40.

22. Yoo S-M, Yamashita S-i, Kim H, Na D, Lee H, Kim SJ, et al. FKBP8 LIRL-dependent mitochondrial fragmentation facilitates mitophagy under stress conditions. The FASEB Journal. 2020;34(2):2944-57.

23. Veljanovski V, Batoko H. Selective autophagy of non-ubiquitylated targets in plants: looking for cognate receptor/adaptor proteins. Front Plant Sci. 2014;5:308.

24. Nezis IP, Vaccaro MI, Devenish RJ, Juhasz G. Autophagy in development, cell differentiation, and homeodynamics: from molecular mechanisms to diseases and pathophysiology. Biomed Res Int. 2014;2014:349623.

25. Putyrski M, Vakhrusheva O, Bonn F, Guntur S, Vorobyov A, Brandts C, et al. Disrupting the LC3 Interaction Region (LIR) Binding of Selective Autophagy Receptors Sensitizes AML Cell Lines to Cytarabine. Frontiers in Cell and Developmental Biology. 2020;8(208).

26. Padman BS, Nguyen TN, Uoselis L, Skulsuppaisarn M, Nguyen LK, Lazarou M. LC3/GABARAPs drive ubiquitin-independent recruitment of Optineurin and NDP52 to amplify mitophagy. Nature Communications. 2019;10(1):408.

27. Puissant A, Fenouille N, Auberger P. When autophagy meets cancer through p62/SQSTM1. Am J Cancer Res. 2012;2(4):397-413.

28. Schwob A, Teruel É, Dubuisson L, Lormières F, Verlhac P, Abudu YP, et al. SQSTM-1/p62 potentiates HTLV-1 Tax-mediated NF-κB activation through its ubiquitin binding function. Scientific Reports. 2019;9:16014.

29. Clausen TH, Lamark T, Isakson P, Finley K, Larsen KB, Brech A, et al. p62/SQSTM1 and ALFY interact to facilitate the formation of p62 bodies/ALIS and their degradation by autophagy. Autophagy. 2010;6(3):330-44.

30. Feng Y, Longmore GD. The LIM protein Ajuba influences interleukin-1-induced NF-kappaB activation by affecting the assembly and activity of the protein kinase Czeta/p62/TRAF6 signaling complex. Mol Cell Biol. 2005;25(10):4010-22.

31. Roodman GD, Windle JJ. Paget disease of bone. The Journal of Clinical Investigation. 2005;115(2):200-8.

32. Bjørkøy G, Lamark T, Brech A, Outzen H, Perander M, Øvervatn A, et al. p62/SQSTM1 forms protein aggregates degraded by autophagy and has a protective effect on huntingtin-induced cell death. The Journal of Cell Biology. 2005;171(4):603.

33. Ding WX, Ni HM, Li M, Liao Y, Chen X, Stolz DB, et al. Nix is critical to two distinct phases of mitophagy, reactive oxygen species-mediated autophagy induction and Parkin-ubiquitin-p62-mediated mitochondrial priming. J Biol Chem. 2010;285(36):27879-90.

34. Okatsu K, Saisho K, Shimanuki M, Nakada K, Shitara H, Sou Y-S, et al. p62/SQSTM1 cooperates with Parkin for perinuclear clustering of depolarized mitochondria. Genes Cells. 2010;15(8):887-900.

35. Geisler S, Holmström KM, Skujat D, Fiesel FC, Rothfuss OC, Kahle PJ, et al. PINK1/Parkin-mediated mitophagy is dependent on VDAC1 and p62/SQSTM1. Nature Cell Biology. 2010;12(2):119-31.

36. von Muhlinen N, Thurston T, Ryzhakov G, Bloor S, Randow F. NDP52, a novel autophagy receptor for ubiquitin-decorated cytosolic bacteria. Autophagy. 2010;6(2):288-9.

37. Lazarou M, Sliter DA, Kane LA, Sarraf SA, Wang C, Burman JL, et al. The ubiquitin kinase PINK1 recruits autophagy receptors to induce mitophagy. Nature. 2015;524(7565):309-14.

38. Vargas JNS, Wang C, Bunker E, Hao L, Maric D, Schiavo G, et al. Spatiotemporal Control of ULK1 Activation by NDP52 and TBK1 during Selective Autophagy. Molecular cell. 2019;74(2):347-62.e6.

39. Fu T, Liu J, Wang Y, Xie X, Hu S, Pan L. Mechanistic insights into the interactions of NAP1 with the SKICH domains of NDP52 and TAX1BP1. Proceedings of the National Academy of Sciences. 2018;115(50):E11651-E60.

40. Ravenhill BJ, Boyle KB, von Muhlinen N, Ellison CJ, Masson GR, Otten EG, et al. The Cargo Receptor NDP52 Initiates Selective Autophagy by Recruiting the ULK Complex to Cytosol-Invading Bacteria. Mol Cell. 2019;74(2):320-9.e6.

41. Viret C, Rozières A, Faure M. Novel Insights into NDP52 Autophagy Receptor Functioning. Trends in Cell Biology. 2018;28(4):255-7.

42. Verlhac P, Grégoire Isabel P, Azocar O, Petkova Denitsa S, Baguet J, Viret C, et al. Autophagy Receptor NDP52 Regulates Pathogen-Containing Autophagosome Maturation. Cell Host & Microbe. 2015;17(4):515-25.

43. Tumbarello DA, Manna PT, Allen M, Bycroft M, Arden SD, Kendrick-Jones J, et al. The Autophagy Receptor TAX1BP1 and the Molecular Motor Myosin VI Are Required for Clearance of Salmonella Typhimurium by Autophagy. PLoS Pathog. 2015;11(10):e1005174.

44. Stefely JA, Zhang Y, Freiberger EC, Kwiecien NW, Thomas HE, Davis AM, et al. Mass spectrometry proteomics reveals a function for mammalian CALCOCO1 in MTOR-regulated selective autophagy. Autophagy. 2020:1-19.

45. Wirth M, Zhang W, Razi M, Nyoni L, Joshi D, O'Reilly N, et al. Molecular determinants regulating selective binding of autophagy adapters and receptors to ATG8 proteins. Nature Communications. 2019;10(1):2055.

46. Lee Y-K, Lee J-A. Role of the mammalian ATG8/LC3 family in autophagy: differential and compensatory roles in the spatiotemporal regulation of autophagy. BMB Rep. 2016;49(8):424-30.

47. Birgisdottir AB, Mouilleron S, Bhujabal Z, Wirth M, Sjottem E, Evjen G, et al. Members of the autophagy class III phosphatidylinositol 3-kinase complex I interact with GABARAP and GABARAPL1 via LIR motifs. Autophagy. 2019;15(8):1333-55.

48. Alemu EA, Lamark T, Torgersen KM, Birgisdottir AB, Larsen KB, Jain A, et al. ATG8 family proteins act as scaffolds for assembly of the ULK complex: sequence requirements for LC3-interacting region (LIR) motifs. J Biol Chem. 2012;287(47):39275-90.

49. Runwal G, Stamatakou E, Siddiqi FH, Puri C, Zhu Y, Rubinsztein DC. LC3-positive structures are prominent in autophagy-deficient cells. Scientific Reports. 2019;9(1):10147.

50. Li S, Lamarche F, Charton R, Delphin C, Gires O, Hubstenberger A, et al. Expression analysis of ATAD3 isoforms in rodent and human cell lines and tissues. Gene. 2014;535(1):60-9.

51. Issop L, Fan J, Lee S, Rone MB, Basu K, Mui J, et al. Mitochondria-Associated Membrane Formation in Hormone-Stimulated Leydig Cell Steroidogenesis: Role of ATAD3. Endocrinology. 2015;156(1):334-45.

52. Hubstenberger A, Merle N, Charton R, Brandolin G, Rousseau D. Topological analysis of ATAD3A insertion in purified human mitochondria. J Bioenerg Biomembr. 2010;42(2):143-50.

53. Hoffmann M, Bellance N, Rossignol R, Koopman WJH, Willems PHGM, Mayatepek E, et al. C. elegans ATAD-3 is essential for mitochondrial activity and development. PLoS One. 2009;4(10):e7644-e.

54. Li S, Rousseau D. ATAD3, a vital membrane bound mitochondrial ATPase involved in tumor progression. Journal of Bioenergetics and Biomembranes. 2012;44(1):189-97.

55. Liu X, Li G, Ai L, Ye Q, Yu T, Yang B. Prognostic value of ATAD3 gene cluster expression in hepatocellular carcinoma. Oncol Lett. 2019;18(2):1304-10.

56. Schaffrik M, Mack B, Matthias C, Rauch J, Gires O. Molecular characterization of the tumor-associated antigen AAA-TOB3. Cell Mol Life Sci. 2006;63(18):2162-74.

57. Gilquin B, Taillebourg E, Cherradi N, Hubstenberger A, Gay O, Merle N, et al. The AAA+ ATPase ATAD3A controls mitochondrial dynamics at the interface of the inner and outer membranes. Mol Cell Biol. 2010;30(8):1984-96.

58. Harel T, Yoon WH, Garone C, Gu S, Coban-Akdemir Z, Eldomery MK, et al. Recurrent De Novo and Biallelic Variation of ATAD3A, Encoding a Mitochondrial Membrane Protein, Results in Distinct Neurological Syndromes. American journal of human genetics. 2016;99(4):831-45.

59. Merle N, Feraud O, Gilquin B, Hubstenberger A, Kieffer-Jacquinot S, Assard N, et al. ATAD3B is a human embryonic stem cell specific mitochondrial protein, re-expressed in cancer cells, that functions as dominant negative for the ubiquitous ATAD3A. Mitochondrion. 2012;12(4):441-8.

60. Peralta S, Goffart S, Williams SL, Diaz F, Garcia S, Nissanka N, et al. ATAD3 controls mitochondrial cristae structure in mouse muscle, influencing mtDNA replication and cholesterol levels. Journal of cell science. 2018;131(13):jcs217075.

61. Zhao Y, Sun X, Hu D, Prosdocimo DA, Hoppel C, Jain MK, et al. ATAD3A oligomerization causes neurodegeneration by coupling mitochondrial fragmentation and bioenergetics defects. Nat Commun. 2019;10(1):1371.

62. Chen D, Yuan X, Liu L, Zhang M, Qu B, Zhen Z, et al. Mitochondrial ATAD3A regulates milk biosynthesis and proliferation of mammary epithelial cells from dairy cow via the mTOR pathway. Cell Biol Int. 2018;42(5):533-42.

63. Miller JM, Enemark EJ. Fundamental Characteristics of AAA+ Protein Family Structure and Function. Archaea. 2016;2016:9294307-.

64. Cooper HM, Yang Y, Ylikallio E, Khairullin R, Woldegebriel R, Lin K-L, et al. ATPase-deficient mitochondrial inner membrane protein ATAD3A disturbs mitochondrial dynamics in dominant hereditary spastic paraplegia. Human molecular genetics. 2017;26(8):1432-43.

65. Tilokani L, Nagashima S, Paupe V, Prudent J. Mitochondrial dynamics: overview of molecular mechanisms. Essays in Biochemistry. 2018;62(3):341-60.

66. McCarron JG, Wilson C, Sandison ME, Olson ML, Girkin JM, Saunter C, et al. From Structure to Function: Mitochondrial Morphology, Motion and Shaping in Vascular Smooth Muscle. Journal of Vascular Research. 2013;50(5):357-71.

67. Hamacher-Brady A, Brady NR. Mitophagy programs: mechanisms and physiological implications of mitochondrial targeting by autophagy. Cellular and Molecular Life Sciences. 2016;73(4):775-95.

68. Goller T, Seibold UK, Kremmer E, Voos W, Kolanus W. Atad3 function is essential for early post-implantation development in the mouse. PLoS One. 2013;8(1):e54799.

69. Fang H-Y, Chang C-L, Hsu S-H, Huang C-Y, Chiang S-F, Chiou S-H, et al. ATPase family AAA domain-containing 3A is a novel anti-apoptotic factor in lung adenocarcinoma cells. Journal of Cell Science. 2010;123(7):1171.

70. Peralta S, Goffart S, Williams SL, Diaz F, Garcia S, Nissanka N, et al. ATAD3 controls mitochondrial cristae structure in mouse muscle, influencing mtDNA replication and cholesterol levels. J Cell Sci. 2018;131(13).

71. Peralta S, Gonzalez-Quintana A, Ybarra M, Delmiro A, Perez-Perez R, Docampo J, et al. Novel ATAD3A recessive mutation associated to fatal cerebellar hypoplasia with multiorgan involvement and mitochondrial structural abnormalities. Mol Genet Metab. 2019;128(4):452-62.

72. He J, Cooper HM, Reyes A, Di Re M, Sembongi H, Litwin TR, et al. Mitochondrial nucleoid interacting proteins support mitochondrial protein synthesis. Nucleic Acids Research. 2012;40(13):6109-21.

73. Kucej M, Kucejova B, Subramanian R, Chen XJ, Butow RA. Mitochondrial nucleoids undergo remodeling in response to metabolic cues. J Cell Sci. 2008;121(11):1861-8.

74. Chen TC, Hung YC, Lin TY, Chang HW, Chiang IP, Chen YY, et al. Human papillomavirus infection and expression of ATPase family AAA domain containing 3A, a novel anti-autophagy factor, in uterine cervical cancer. Int J Mol Med. 2011;28(5):689-96.

75. Princely Abudu Y, Pankiv S, Mathai BJ, Hakon Lystad A, Bindesboll C, Brenne HB, et al. NIPSNAP1 and NIPSNAP2 Act as "Eat Me" Signals for Mitophagy. Dev Cell. 2019;49(4):509-25.e12.

76. Bhujabal Z, Birgisdottir AB, Sjottem E, Brenne HB, Overvatn A, Habisov S, et al. FKBP8 recruits LC3A to mediate Parkin-independent mitophagy. EMBO Rep. 2017;18(6):947-61.

77. Lamark T, Perander M, Outzen H, Kristiansen K, Overvatn A, Michaelsen E, et al. Interaction codes within the family of mammalian Phox and Bem1p domain-containing proteins. J Biol Chem. 2003;278(36):34568-81.

78. Pankiv S, Clausen TH, Lamark T, Brech A, Bruun JA, Outzen H, et al. p62/SQSTM1 binds directly to Atg8/LC3 to facilitate degradation of ubiquitinated protein aggregates by autophagy. J Biol Chem. 2007;282(33):24131-45.

79. Kirkin V, Lamark T, Sou YS, Bjorkoy G, Nunn JL, Bruun JA, et al. A role for NBR1 in autophagosomal degradation of ubiquitinated substrates. Mol Cell. 2009;33(4):505-16.

80. Zhang S, Cahalan MD. Purifying plasmid DNA from bacterial colonies using the QIAGEN Miniprep Kit. J Vis Exp. 2007(6):247-.

81. Desjardins P, Conklin D. NanoDrop microvolume quantitation of nucleic acids. J Vis Exp. 2010(45):2565.

82. Lorenz TC. Polymerase chain reaction: basic protocol plus troubleshooting and optimization strategies. J Vis Exp. 2012(63):e3998-e.

83. Bachman J. Chapter Nineteen - Site-Directed Mutagenesis. In: Lorsch J, editor. Methods in Enzymology. 529: Academic Press; 2013. p. 241-8.

84. Liang X, Peng L, Baek C-H, Katzen F. Single step BP/LR combined Gateway reactions. BioTechniques. 2013;55(5):265-8.

85. Reece-Hoyes JS, Walhout AJM. Gateway Recombinational Cloning. Cold Spring Harb Protoc. 2018;2018(1):pdb.top094912-pdb.top.

86. Costa S, Almeida A, Castro A, Domingues L. Fusion tags for protein solubility, purification and immunogenicity in Escherichia coli: the novel Fh8 system. Front Microbiol. 2014;5:63.

87. Rosano GL, Ceccarelli EA. Recombinant protein expression in Escherichia coli: advances and challenges. Frontiers in microbiology. 2014;5:172-.

88. Sørensen HP, Mortensen KK. Soluble expression of recombinant proteins in the cytoplasm of Escherichia coli. Microbial cell factories. 2005;4(1):1-.

89. Shehadul Islam M, Aryasomayajula A, Selvaganapathy PR. A Review on Macroscale and Microscale Cell Lysis Methods. Micromachines. 2017;8(3):83.

90. Gilquin B, Cannon BR, Hubstenberger A, Moulouel B, Falk E, Merle N, et al. The calcium-dependent interaction between S100B and the mitochondrial AAA ATPase ATAD3A and the role of this complex in the cytoplasmic processing of ATAD3A. Molecular and cellular biology. 2010;30(11):2724-36.

91. Johansen T, Birgisdottir ÅB, Huber J, Kniss A, Dötsch V, Kirkin V, et al. Chapter Nine - Methods for Studying Interactions Between Atg8/LC3/GABARAP and LIR-Containing Proteins. In: Galluzzi L, Bravo-San Pedro JM, Kroemer G, editors. Methods in Enzymology. 587: Academic Press; 2017. p. 143-69.

92. Sandell L, Sakai D. Mammalian Cell Culture. Current Protocols Essential Laboratory Techniques. 2011;5(1):4.3.1-4.3.32.

93. Phelan K, May KM. Mammalian Cell Tissue Culture Techniques. Current Protocols in Molecular Biology. 2017;117(1):A.3F.1-A.3F.23.

94. Wenk MR, Fernandis AZ. A Manual for Biochemistry Protocols. Singapore, SINGAPORE: World Scientific Publishing Co Pte Ltd; 2007.

95. Masters JR, Stacey GN. Changing medium and passaging cell lines. Nature Protocols. 2007;2(9):2276-84.

96. Shi B, Xue M, Wang Y, Wang Y, Li D, Zhao X, et al. An improved method for increasing the efficiency of gene transfection and transduction. Int J Physiol Pathophysiol Pharmacol. 2018;10(2):95-104.

97. Kim TK, Eberwine JH. Mammalian cell transfection: the present and the future. Analytical and bioanalytical chemistry. 2010;397(8):3173-8.

98. Lu H, Khurana S, Verma N, Manischewitz J, King L, Beigel JH, et al. A rapid Flp-In system for expression of secreted H5N1 influenza hemagglutinin vaccine immunogen in mammalian cells. PLoS One. 2011;6(2):e17297-e.

99. Brown RB, Audet J. Current techniques for single-cell lysis. J R Soc Interface. 2008;5 Suppl 2(Suppl 2):S131-S8.

100. Silva RC, Castilho BA, Sattlegger E. A Rapid Extraction Method for mammalian cell cultures, suitable for quantitative immunoblotting analysis of proteins, including phosphorylated GCN2 and eIF2α. MethodsX. 2018;5:75-82.

101. Maity B, Sheff D, Fisher RA. Immunostaining: detection of signaling protein location in tissues, cells and subcellular compartments. Methods Cell Biol. 2013;113:81-105.

102. Donaldson JG. Immunofluorescence Staining. Current Protocols in Cell Biology. 2015;69(1):4.3.1-4.3.7.

103. Vernay A, Cosson P. Immunofluorescence labeling of cell surface antigens in Dictyostelium. BMC research notes. 2013;6:317-.

104. Sánchez-Martín P, Komatsu M. Physiological Stress Response by Selective Autophagy. Journal of Molecular Biology. 2020;432(1):53-62.

105. Mejlvang J, Olsvik H, Svenning S, Bruun J-A, Abudu YP, Larsen KB, et al. Starvation induces rapid degradation of selective autophagy receptors by endosomal microautophagy. The Journal of cell biology. 2018;217(10):3640-55.

106. Bogenhagen DF, Rousseau D, Burke S. The layered structure of human mitochondrial DNA nucleoids. J Biol Chem. 2008;283(6):3665-75.

107. Harper JW, Bennett EJ. Proteome complexity and the forces that drive proteome imbalance. Nature. 2016;537(7620):328-38.

108. Schneider-Poetsch T, Ju J, Eyler DE, Dang Y, Bhat S, Merrick WC, et al. Inhibition of eukaryotic translation elongation by cycloheximide and lactimidomycin. Nat Chem Biol. 2010;6(3):209-17.

109. Zhao J, Zhang B, Li S, Zeng L, Chen Y, Fang J. Mangiferin increases Nrf2 protein stability by inhibiting its ubiquitination and degradation in human HL60 myeloid leukemia cells. Int J Mol Med. 2014;33(5):1348-54.

110. Hanson DA, Ziegler SF. Fusion of green fluorescent protein to the C-terminus of granulysin alters its intracellular localization in comparison to the native molecule. Journal of Negative Results in BioMedicine. 2004;3(1):2.

111. Kaddoum L, Magdeleine E, Waldo GS, Joly E, Cabantous S. One-step split GFP staining for sensitive protein detection and localization in mammalian cells. BioTechniques. 2010;49(4):727-36.

112. Linares JF, Duran A, Yajima T, Pasparakis M, Moscat J, Diaz-Meco MT. K63 polyubiquitination and activation of mTOR by the p62-TRAF6 complex in nutrient-activated cells. Molecular cell. 2013;51(3):283-96.

113. Mandell MA, Jain A, Arko-Mensah J, Chauhan S, Kimura T, Dinkins C, et al. TRIM proteins regulate autophagy and can target autophagic substrates by direct recognition. Dev Cell. 2014;30(4):394-409.

114. Baudier J. ATAD3 proteins: brokers of a mitochondria-endoplasmic reticulum connection in mammalian cells. Biol Rev Camb Philos Soc. 2018;93(2):827-44.

115. Abudu YP, Pankiv S, Mathai BJ, Lamark T, Johansen T, Simonsen A. NIPSNAP1 and NIPSNAP2 act as "eat me" signals to allow sustained recruitment of autophagy receptors during mitophagy. Autophagy. 2019;15(10):1845-7.

116. Wei Y, Chiang WC, Sumpter R, Jr., Mishra P, Levine B. Prohibitin 2 Is an Inner Mitochondrial Membrane Mitophagy Receptor. Cell. 2017;168(1-2):224-38 e10.

117. Jain A, Lamark T, Sjøttem E, Bowitz Larsen K, Atesoh Awuh J, Øvervatn A, et al. p62/SQSTM1 Is a Target Gene for Transcription Factor NRF2 and Creates a Positive Feedback Loop by Inducing Antioxidant Response Element-driven Gene Transcription. Journal of Biological Chemistry. 2010;285(29):22576-91.